Università degli Studi di Torino
Doctoral School of Sciences and Innovative Technologies
PhD Programme in Chemical and Materials Sciences XXXII Cycle

Innovative Syntheses and Applications of Cyclodextrins Cross-Linked Polymers

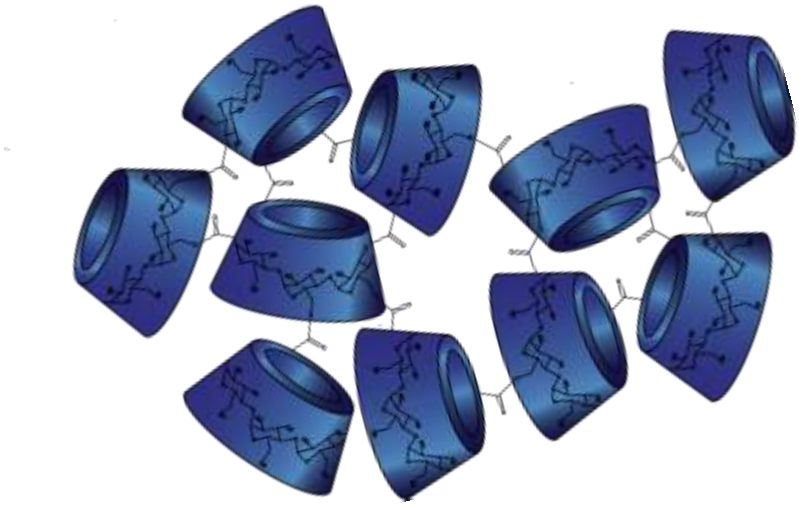

Alberto Rubin Pedrazzo

Supervisor:
Prof. Francesco Trotta

Università degli Studi di Torino
Doctoral School of Sciences and Innovative Technologies
PhD Programme in Chemical and Materials Sciences XXXII cycle

Innovative Syntheses and Applications of Cyclodextrins Cross-Linked Polymers

Supervisor: Prof. **Francesco Trotta**

Jury Members: Prof. **Antonino Mazzaglia**
CNR - Messina
Institute of Nanostructured Materials ISMN

Prof. **Michele Laus**
Università degli Studi del Piemonte Orientale
Dipartimento di Scienze e Innovazione Tecnologica

Prof. **Roberta Cavalli**
Università di Torino
Dipartimento di Scienze e Tecnologia del Farmaco

Head of the Doctoral School: Prof. Massimo Maffei
PhD Programme Coordinators: Prof. Mario Chiesa, Prof. Bartolomeo Civalleri

Torino, 2020

Abstract

Cyclodextrin nanosponges (CD-NS) are nanostructured cross-linked polymers made up of cyclodextrins. The reactive hydroxyl groups of CDs allow them to act as multifunctional monomers capable of cross-linking to bi- or multifunctional chemicals, such as dianhydrides, diisocyanates, diepoxides or dicarboxylic acids etc. The polarity and dimension of the polymer network can be easily tuned by varying the type of cross-linker and degree of cross-linking, influencing final characteristics. Since nanosponges are biocompatible, nontoxic and biodegradable are a powerful tool in the wide field of the nano drug delivery: nanosponges, as a powder, can be used as excipients in in the preparation of tablets, capsules, suspensions and dispersions, or for topical application. Moreover, cyclodextrin nanosponges in last years have been employed, with good results, to encapsulate and release a wide spectrum of drugs and nutraceuticals, showing an improvement in the bioavailability and the release kinetic.
NSs are in this work the common denominator in two different projects.

The first project is focused to the application of NSs as support material for photosensitizers in photodynamic therapy (PDT).
PDT is a clinically approved therapy based on a photochemical reaction between a photosensitizer (a light sensible molecule), light and molecular oxygen. A large and interesting group of photosensitizers are porphyrins or derivatives. However, porphyrins show a number of drawbacks: relatively poor photostability, in some cases weak absorption above 600 nm (tissue transparency window is between 600-900 nm), low solubility in water and very specific (and sometimes undesired) bio distribution. Low solubility in aqueous solutions leads to aggregation and inactivation under physiological conditions, reducing the production of reactive oxygen species, too.
So, the project relates to the synthesis and characterization of innovative nanostructured materials for protection, vehiculation and controlled release of different photoreactive porphyrins and innovative squaraines dyes.

The second part is instead focused on the search for new synthetic ways The most common NS synthetic pathway consists in dissolving the chosen CD and crosslinker in organic polar aprotic liquids (e.g.dimethylformamide or dimethylsulfoxide), which may affect the final result, especially for potential biomedical applications. In this dissertation a new, green synthetic pathway

through mechanochemistry, more in particular via ball milling, is described. The polymer obtained exhibited the same characteristics as a CD-based NS synthesized in a solvent. Moreover, after the synthesis, the polymer was easily functionalized through a reaction between the nucleophilic carboxylic group of three different organic dyes (Fluorescein, Methyl Red and Rhodamine B) and the still reactive imidazoyl carbonyl group of the NS (with the formation of a covalent bond).

Furthermore, new one-step syntheses of NSs functionalized with Folic Acid and PEGylated NSs are reported.

Aknowledgements

I would like to express my gratitude to my supervisor, Prof. Francesco Trotta, for all the things he has taught me and for his continuous encouragement.

I would like to thank Prof. Guido Viscardi, Prof. Claudia Barolo, all the MOF Group and Dott. Enzo Laurenti for supporting and kindly helping me.

I wish to acknowledge the whole polymeric material group of the University of Turin: Prof. Marco Zanetti, Prof. Pierangiola Bracco, Prof. Valentina Brunella, Prof. Dominique Scalarone and Prof. Maria Paola Luda.

I would also like to thank the committee members that will evaluate my work: Prof. Antonino Mazzaglia, Prof. Michele Laus and Prof. Roberta Cavalli.

Thanks to all the people I had the chance to meet in the lab and to work with: Anastasia, Claudio, Nilesh, Giorgia, Enea, Gjylije and Silvia.
Thanks to Roberto and the whole group in Messina.
Special thanks go to Fabrizio for all the patience he had during my storms of absurd ideas.

All this work done wouldn't be possible without the endless support of my parents. Finally, I wish to thank Chiara for all the love and for always being there.

Table of Contents

Table of Contents 9
1 Introduction 1
1.1 Cyclodextrins 1
1.1.1 Structure of CDs 3
1.1.2 CDs inclusion complexes 5
1.2 Cyclodextrins NS 9
1.2.1 CD-based Polyurethane NSs 12
1.2.2 CD-based Polycarbonate NSs 13
1.2.3 CD-based Polyester NSs 14
1.3 Photodynamic therapy (PDT) 16
1.3.1 PDT Principles 17
1.3.2 PDT cellular response and tumor response 19
1.3.3 Photosensitizers 20
1.3.4 Photoreactive squaraines 26
1.3.5 Reactive Oxygen Species Detection 27
1.3.6 Electron paramagnetic resonance (EPR) for the detection of ROS 28
1.4 Mechanochemistry 29
1.4.1 Principles and historical development of Mechanochemistry 29
1.4.2 Planetary Ball Mill 32
1.4.3 Mechanochemistry and organic synthesis 35
2 Photoactivated Therapies 39
2.1 Experimental Methods 40
2.1.1 Materials 40
2.1.2 Synthesis of βNS-CDI 40
2.1.3 Synthesis of βNS-PYRO 42

2.1.4 Squaraine SQ Br-C4 synthesis 43
2.1.5 Synthesis of βNS-CDI+SQ Br-C4..... 44
2.1.6 Synthesis of βNS-PYRO+SQ Br-C4 45
2.1.7 Loading of dyes on synthetized βNS-PYRO and βNS-CDI 47
2.1.8 Preparation and Characterization of TMPyP loaded βNS-PYRO.. 48
2.2 Results and Discussion..... 49
2.2.1 βNS-CDI (1-4) 49
2.2.2 βNS-PYRO (1-4)..... 51
2.2.3 Squaraine SQ Br-C4 characterization..... 53
2.2.4 βNS-CDI+SQ Br-C4 56
2.2.5 βNS-PYRO + SQ Br-C4 58
2.2.6 Reactive Oxygen Species - UV- Vis Measures..... 60
2.2.7 Reactive Oxygen Species – EPR..... 64
2.2.8 βNS-PYRO/ TMPyP (CNR – ISMN Messina) 68
2.3 Conclusions..... 72
3 Mechanochemical Synthesis 75
3.1 Experimental..... 78
3.1.1 Materials 78
3.1.2 Solvent synthesis of Dextrins Nanosponges (for comparison tests) 79
3.1.3 Ball Mill synthesis of Dextrins Nanosponges..... 81
3.1.4 Ball Mill synthesis of Cyclodextrins Carbonate Nanosponges..... 81
3.1.5 Ball Mill synthesis of Cyclodextrins Carbamate Nanosponges.... 82
3.1.6 Ball Mill synthesis of Cyclodextrins Ether Nanosponges..... 82
3.1.7 Functionalization of Carbonate cyclodextrins Nanosponges 83
3.1.8 Ball Mill synthesis of Positively Charged Ether Dextrins Nanosponges..... 83
3.1.9 Ball Mill synthesis of PEGylated NS 83
3.1.10 Ball Mill synthesis of FOLIC ACID NS 84

3.2 Results and discussion 86
3.2.1 Comparison with Solvent Synthesis..... 86
3.2.2 Characterization and Functionalization of CDI Nanosponges..... 92
3.2.3 Characterization of PEGylated CDI Nanosponges 102
3.2.4 Characterization of Folic Acid conjugated CDI Nanosponges (FA βNS-CDI 1:8).....111
3.3 Conclusions.....117
4 Overall Conclusions and Perspectives.....119
5 References 121
Appendix 130

1 Introduction

The work presented in this dissertation comprises two different macro-projects, very different from each other but with the synthesis and application of cyclodextrins (CDs) based polymers as common denominator. Consequently, this thesis will be structured essentially in three part with a long introduction on cyclodextrins and cyclodextrin-based polymers, followed by an in-depth study of the topics addressed during the three years of the doctorate.
The first main project is related with the synthesis and more specifically the characterization of dextrin-based hyper-cross-linked polymers, the so called nanosponges (NS) for photoactivated therapies, with particular attention for the photodynamic therapy and the reactive oxygen species analysis.
The second part will be focused on a mechanochemistry synthesis and derivatization of hyper cross-linked biopolymer with a solvent free approach.

1.1 Cyclodextrins

Cyclodextrins (CDs) are a family of cyclic oligosaccharides with a toroidal structure, composed of α-D-glucopyranose units linked through α -1,4 glycosidic bonds.
The discovery of cyclodextrins dates back to 1891 with Antoine Villiers [1][2] that isolated 3 g of a crystalline substance from the digestion of 1000 g of starch with *Bacyllus Amilylobacter.* He named this product "cellulosine", for the resemblance with cellulose against acidic hydrolysis, but this substance was later proved to be a mixture of α and β cyclodextrins.
In the following years there are many publications on cyclodextrins, with Schardiger and Pringsheim as leading figures [3], but however, none of these included a systematic study, with completely separated systems and adequate methods. Only in the 30s Freudemberg (basing his studies on prior observations of Karrer and Miekeley) described a circular structure made of maltose units and containing only α -1,4 glycosidic bonds.

The first comprehensive review dates back to 1957 with French [4], that worked extensively on the enzymatic production of the so-called "Schardinger Dextrins"[5].
However, they began to attract both academic and industries only in the late 1970s and early 1980s, when the first CDs of pharmaceutical grade purity were produced.
CD (and CD derivatives such as hydroxypropyl-β-CDs, randomly methylated CDs) are nowadays produced industrially and with many commercial applications [4], [6]–[8].
The first International Symposium on Cyclodextrins was in 1981 and from 1984 onward, an International CD symposium is organized every two years to witness the relevance of these molecules.

CDs are obtained from enzymatic conversion of starch: the cyclodextrin transferase enzyme CGT-ase is produced by many microorganisms, like for example the *Bacillus Macerans, Bacillus circulans* [7] and *Klebsiella oxytoca* or specific microorganism modified with genetic engineering [2]. Consequently, CDs are renewable and eco-friendly materials.
The production of CD starts with the high temperature liquefaction of the starch. The viscosity of the solution is then reduced via hydrolyzation, avoiding the formation of oligomers or glucose that can reduce the the final yield in CDs.
The solution is then cooled and the CGT-ase enzyme is added: after this step there is need to separate from the hydrolyzed mixture the formed CDs. By the addition of an appropriate solvent it is possible to discern between the various CDs via the formation of insoluble complexes. Toluene, for example, forms a complex with β cyclodextrins, 1-decanol and cyclohexadecenol are added to achieve the precipitation of α and β, respectively. Insoluble complexes are then filtered, washed, and CDs are recovered by crystallization and filtration.
An alternative route for separating is based on the different relative solubility of CDs: βCD are poorly soluble in water if compared to α and γ (Table 1), so the separation can easily be achieved via crystallization and without solvents.

The purity of the final product, for industrial synthesis of CDs is over 99%[9].

1.1.1 Structure of CDs

The three major and well-known (especially from an industrial point of view) representatives of CDs family are called α-CD, β-CD and γ-CD and are composed of 6, 7 and 8 glucopyranose units, respectively. In Figure 1-1 are reported a simplified structure of a βCD, the cheapest and most used CD and a representation of the toroidal structure with geometric dimensions.
Inside a CD structure, each glucopyranose monomer has 3 hydroxyl groups: in position 2, 3 (secondary OH) and 6 (primary OH), oriented to the external part of the ring providing a hydrophilic character. The inner part of the ring is instead slightly hydrophobic, because of the presence of the glucosidic oxygen and aliphatic hydrogen atoms. The hydroxyl groups in position 6 are the most nucleophilic and reactive (reactivity also due to lower steric hindrance), the OH moieties in position 3 are less accessible and poorly reactive, in position 2 are located the most acidic ones. The reactive hydroxyl groups oriented to the outer side of CDs allows them to react with a variety of chemical permitting derivatizations, functionalization or, as will be extensively explained later, polymerization and/or crosslinking.

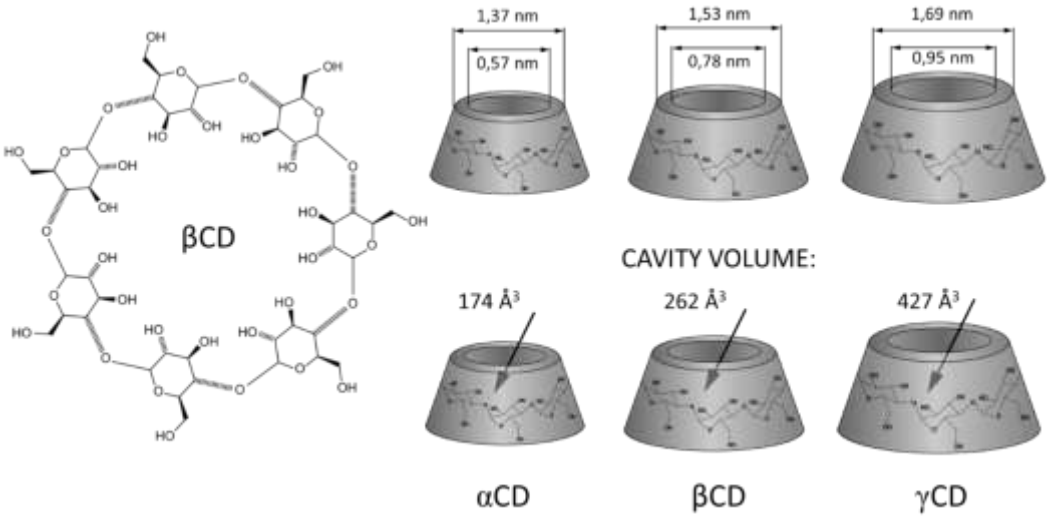

Figure 1-1- Simplified structure of a βCD and dimensions of α, β and γ cyclodextrins

Table 1 – Principal properties of α, β and γ cyclodextrins [2]

	α	**β**	**γ**
Number of glucose units	6	7	8
Molecular Weight [g/mol]	972.84	1134.98	1297.16
Water Solubility [g/100ml at RT]	14.5	1.85	23.2
Cavity Diameter [Å]	4.7-5.3	6.0-6.5	7.5-8.3

In Table 1 is reported the solubility in water of α, β and γ cyclodextrins. As said before βCD exhibit a considerably lower water solubility if compared to α and γ cyclodextrins: in βCD the presence of intra-molecular hydrogen bonds within the structure prevent the formation of hydrogen bonds with the surrounding water molecules. Since the poor solubility is mainly related to the interactions of hydroxyl groups, a way to enhance the solubility of βCDs is to replace one or more hydroxyl groups with different moieties.

The most employed of modified CDs can be divided into three classes: methylated and hydroxypropylated, neutral and sulfobuthylated, negatively charged. In most cases, and especially in the case of βCDs, CDs re randomly substituted [4], [6]–[8] and what is reported is an "average substitution degree" that refers to the number of

substitutions per glucopyranose unit (usually this degree is around 1.8).

1.1.2 CDs inclusion complexes

The peculiar structural features of cyclodextrins, with a slightly apolar cavity and a hydrophilic external part, allow the formation of inclusion complexes.
In
Figure 1-2 the formation of an inclusion complex is represented.

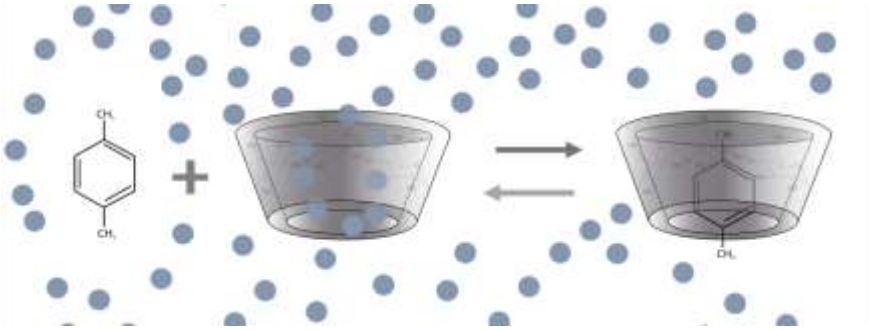

Figure 1-2– Simplified representation of the formation of a CD inclusion complex. In the picture a 1:1 complex, CD:guest is reported. The host molecule is p-Xylene, water is represented with blue dots.

Water molecules inside a cyclodextrin cavity can be replaced by an apolar molecule (or the apolar moieties of complex molecules) leading to the formation of a reversible host-guest complex that can be isolated or separated [7].
Formation and dissociation of inclusion complexes has been attributed to many different forces: the main driving force, in term of thermodynamic, is the expulsion of water from the cavity, then the electrostatic interactions, hydrogen bonds and van der Waals interactions.
The hydrophobic inner space of CDs prevents water molecules from satisfying their hydrogen bonding potentials and the replacement of

these water molecules with less polar molecules leads to a decrease of Gibbs free energy and permit to the system to achieve a higher thermodynamic stability.
The formation of an inclusion complex is regulated by a thermodynamic equilibrium between the free guest (G) and CD molecules (CD):

free CD + free guest (G) ⇆ *CD • G inclusion complex*

$$K_{1:1} = \frac{[CD \bullet G]}{[CD][G]}$$

The constant *K* has different names in literature: *affinity constant* (if describes the affinity of G for CD) *stability constant*, *association constant*, *binding constant*. The value is directly proportional to the stability of the inclusion, the higher the K, the more stable is the complex [7], [10].
Anyway, the equation refers to the 1:1 case, the simplest and most frequent: 2:1, 1:2 or more complicated associations exist.

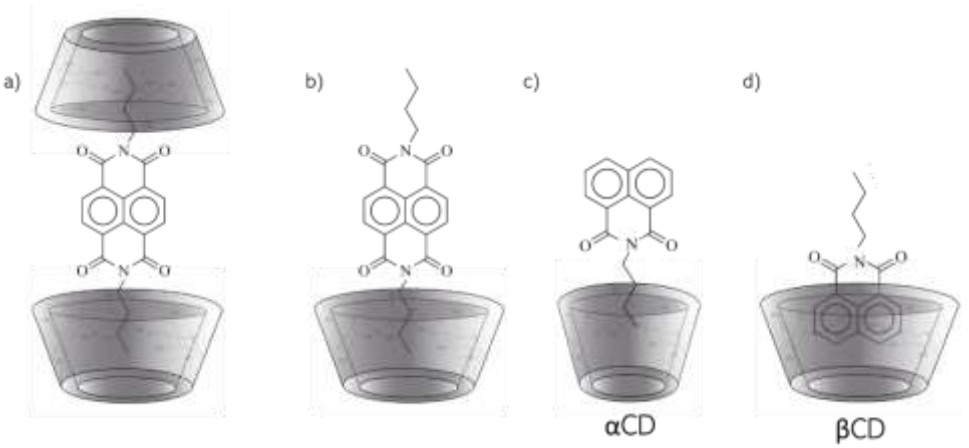

Figure 1-3 – Examples of inclusion complexes. a) Example of a type 1:2 complex b) Example of a type 1:1 complex. c) d) Influence of the cavity dimension on the inclusion complex structure

For large and geometrically complex molecules, two or more CDs might be involved, leading to a different stoichiometry *CD : guest molecule*, schematically represented in Figure 1-3 (adapted from Brochsztain et. al [11]).
The stability of complexes, and so the *K* value, is influenced by many factors.
Among the others there is, of course, the size compatibility between host and guest molecules. The size of CD has to be large enough to permit the guest entrance but if the guest is too small if compared to the cavity, CD-guest interactions will be very weak, and the dissociated form will prevail on the associated one. The same applies for the opposite situation: a molecule larger than the cavity will enter partially or will arrange outside the cavity. In Figure 1-3 are reported some example as shown in inset c) and d) the naphthalimide apolar chain fit preferentially in a smaller α-cyclodextrin cavity, wherein the aromatic moiety of the same molecule will arrange inside a β-cyclodextrin [11].
A key role is also played by the CD derivative substitution, indeed. The substitution can partially hinder the entrance of the guest molecule or increase the interaction between CD and guest.
Another parameter to consider is the reaction medium: if both guest and host are in molecular state the complexation directly depends on the guest intrinsic solubility and on *K* (affinity constant).

The formation an inclusion complex can dramatically modify many features of the guest molecule. For example, there is a variation in the spectral properties: when achiral guest are inserted in CDs they become optically active, the maximum of UV spectra is in some cases shifted of many nm and also the fluorescence is in many cases strongly increasedd [2], [12]–[14].
After the formation of an inclusion complex there is also a variation in the included molecule reactivity: in most cases the reactivity decrease (reactive groups are less reachable) so the guest is protected and stabilized, but in many cases the cyclodextrin can act as an artificial enzyme enhancing the kinetic of the reaction and modifying the reaction pathway [15], [16].

Finally, it is worth to say that the formation of an inclusion complex is not the only possible way of CDs to form complexes: stable interactions are sometimes established between a guest molecule and the external part of CDs.
Indeed, hydroxy group on the outer surface of cyclodextrins can lead to the formation of hydrogen bonds and, consequentially, to water-soluble complexes, in a similar way to what is seen with non-cyclic oligo or polysaccharides [4], [17]. These supramolecular assemblies (since there are no covalent bonds) are called *non-inclusion* complexes. They can, eventually, protect guest molecules from the environment and achieve an efficient increase of solubility. In literature many examples of non-inclusion compounds are reported [18]–[21].

In literature are reported several methods to achieve an enhancement of the complexation ability of CD. Derivatization of CDs as already said, permit to obtain significant results. Another strategy, somehow related with the derivatization, since a chemical reaction is involved, concerns the polymerization of CDs to obtain either soluble or insoluble polymers.
The advantage that derive from the polymerization of cyclodextrins is the formation of a complex three-dimensional network, that permit the complexation not only inside the CDs cavities but also in the free volume between cyclodextrins.
Synthesis and properties of CD-based polymers, so-called Nanosponges, will be extensively discussed in the following paragraphs.

1.2 Cyclodextrins NS

Cyclodextrin Nanosponges (CD-NSs) are a class of insoluble, highly crosslinked dextrin-based polymers, employed in several scientific and technological fields.
The term Nanosponge refers to a class of different organic and inorganic materials with nanometric porosity and efficient adsorption/absorption/complexation properties.
Few examples that can be found in the literature of inorganic nanoporous materials are silicon NS particles [22], titanium dioxide [23] and zeolite NSs.
For what concern organic NSs there are examples with polystyrene [24], polycarbonate and other linear polymer-based NSs and with sugar-based NSs. Some oligosaccharides and polysaccharides, such as CDs but also starches and cellulose, make these materials suitable building blocks for the synthesis of nanosponges [17], [25]–[27].
Starch and starch derivatives are particularly interesting because of the presence of a great amount of reactive hydroxyl groups.
Cyclodextrins are particularly interesting starch derivative for all the many reason described before, furthermore the presence of a nano-sized cavity makes these compounds suitable building blocks for the synthesis of organic NSs.
The reactive hydroxyl group oriented toward the exterior side of CDs, indeed, allows them to act as polyfunctional monomers permitting to cross-link with a variety of chemical (bi or polyfunctional), such as dianydrides, diisocyanates, epoxides, carboxylic acids etc.
The cross-linking process of CDs brings benefits to CD-NSs if compared to native CDs. In general it's possible to say that NSs are able to form complexes with a wider series of molecule [28]: cyclodextrin-based nanosponges can form complexes with different types of lipophilic or hydrophilic molecules and the release of the included molecules can be varied by modifying the structure.
The application of NSs has been widely explored in several scientific and technological fields [28][26][29], but the one of the main area of investigation and research nowadays concern the pharmaceutical and

biomedical, where NSs have been employed as drug delivery systems [30][31][32], thanks to their encapsulation properties and low toxicity. The wide application of NSs in many heterogeneous fields, makes it rather complex to make a list divided by applications or by cross-linkers.

Recently Caldera *et al.* [28] proposed the division of nanosponges in four consecutive generations, grouped by chemical composition, properties and synthesis. This division permit to group the many type of nanosponges in a coherent way.

NSs synthetized by a simple reaction between CDs and a suitable crosslinker can be ascribed to the 1st generation.

A further subdivision in four type can be done, depending on the functional group connecting the CD to the cross-linker: urethane, carbonate, ester and ether NSs. In next paragraphs a more extensive description will be presented.

More complex and functionalized NSs belongs to the 2nd generation: these types of cross-linked polymers are characterized by specific properties, for example electric charge or fluorescence. The 3rd generation deals with stimuli responsive NSs, able to modulate their behavior (for example increasing/decreasing a drug release) according to the external environment.

To the 4th generation belongs a new family of molecularly imprinted CD polymers (MIPs). The molecularly imprinting technique is a synthetic method that permit to induce molecular recognition properties to a tridimensional polymer, through the presence of a template molecule during the formation of a polymer [33]–[35]. The template can be later removed, leaving a cavity with its shape and size or left inside the cross-linked structure, enhancing drug loading capability. In 2016, Trotta *et al.* reported an example molecularly imprinted NSs with the inclusion of an instable and reactive L-DOPA, achieving the aim of shielding its reactive groups and preventing degradation [36]. In the following pictures a scheme of molecular imprinting is reported.

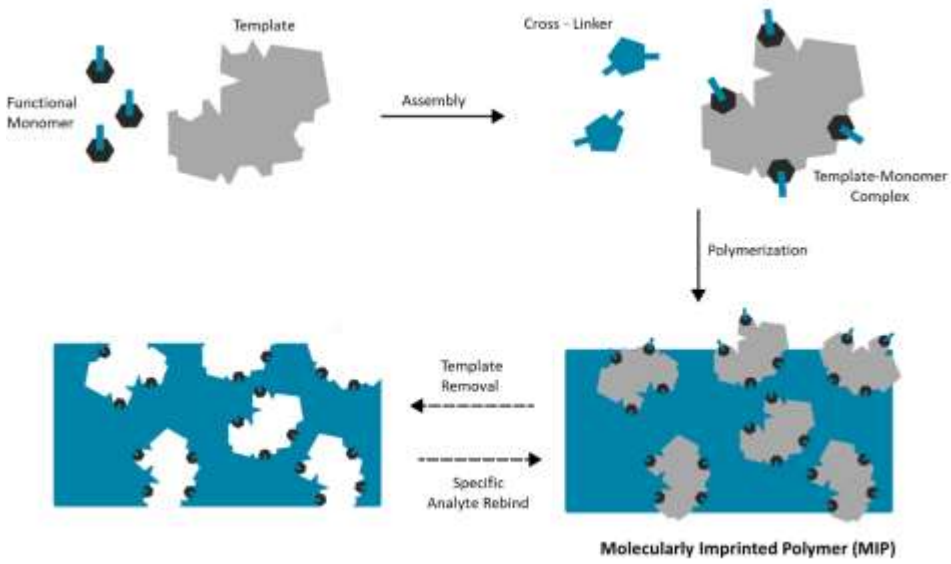

Figure 1-4 – Schematic representation of a Molecularly Imprinted Polymer synhtesis

The most common NSs synthetic pathway consist in dissolving, under continuous stirring, the chosen CD in a suitable solvent, usually organic polar aprotic liquids, for example dimethylformamide (DMF) or dimethylsulfoxide (DMSO), and then adding the crosslinker and, if necessary, a catalyst.

An alternative synthetic route is via interfacial polymerization: two immiscible solution, one of CDs dissolved in an alkaline solution and the other one of the crosslinker in a chlorinated solvent, are mixed and stirred. Crosslinking occurs at the interface between the two solution [37].

Once obtained the polymer, solvent and catalyst (if present), unreacted monomer or crosslinker and byproduct have to be removed: the gel can be washed with an excess of water and, if necessary, heating and under low pressure. At the end of the process a dried powder is obtained.

In this PhD thesis in Part 3 an alternative synthetic method will be presented, via mechanochemistry and without any solvents (neither water nor organic solvents). In this case, since there is no solvent to remove, the whole synthesis is quite simpler. In the next paragraphs

the most common and studied CDs Nanosponges, and relative applications, will be presented.

1.2.1 CD-based Polyurethane NSs

Urethane, or carbamate, Cyclodextrin-NS are usually synthetized by reacting CDs with a suitable diisocyanates as, for example hexamethylene diisocyanate (HDI), toluene–2,4-diisocyanate (TDI). The reaction scheme is reported below (Scheme 1). The resulting NSs are characterized by a rigid structure and a negligible swelling in water and organic solvent and a high resistance to chemical degradation. Carbamate CD-NSs, were originally developed by Li and Ma for the treatment of wastewaters, as a replacement of activated carbon. They obtained with these NSs remarkable performances in the removal of organic molecules such us p-nitrophenol reducing concentration of waste from 10^{-7}-10^{-9} M to ppt level. The surface area is usually lower than activated carbon, (1-2 m2/g, two orders of magnitude): it is supposed that organic molecules can be adsorbed but also can diffuse through the surface and be absorbed inside the bulk of NSs [38]. The good affinity for organic molecules, showed for pollutants [39], is also demonstrated by the application of urethane NSs in the complexation with biologically relevant compounds, such as bilirubin or amino acids. Tang et al. in 2006 evaluated the difference in absorption of aromatic amino acids and branched chain amino acids: the absorption of branched chain amino acids was negligible while NSs absorbed 24% of the aromatic amino acids.
In older works the same polymer was tested for the absorption of bilirubin, reducing the initial concentration of bilirubin (40 mg/l) up to 92.6% after the addition of the NS [40].

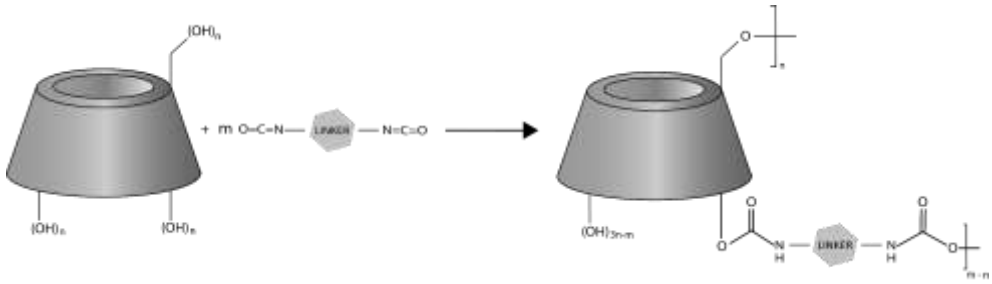

Scheme 1 – Reaction scheme of CD-based Polyurethane NSs

1.2.2 CD-based Polycarbonate NSs

Polycarbonate CD-based NSs are synthesized using active difunctional carbonyl compounds; interesting results have been obtained using 1,1'-carbonyldiimidazole, triphosgene and diphenylcarbonate. Reaction scheme is reported below (Scheme 2). These NSs present short cross-linking bridges, since the resulting CD NSs present carbonate bonds between CD monomers, reduced swelling ability (if compared to polyesters, for example) and a good stability to acidic solutions. The affinity to organic molecules and the surface area is comparable to carbamate NS [26]. The ability of β-cyclodextrin carbonate NS to remove from wastewater chlorinated persistent organic pollutants (also known as POP) was investigated by Trotta and Cavalli in 2009 [31]: the absorption efficiency was higher than the average of activated carbon and for the specific case of hexachlorobenzene, the NS was capable of removing around 99.5% of the pollutant.

An interesting method to evaluate the degree of cross-linking of carbonate β-CD NSs, by means of infrared and Raman spectroscopy, was described by Castiglione et al. [41]. Data from spectroscopic analysis and chemical computation, demonstrated a correlation between the intensity of carbonyl absorption peak and the degree of cross-linking: the degree of cross-linking increased with the content of cross-linker, in total agreement with the stoichiometry. Since we are dealing with sugar-based predominantly amorphous materials, this

method represents a valid and advantageous alternative to x-ray. The crosslinking density, and so the amount of crosslinker, strongly influences stiffness and elastic properties of the NSs, too. Rossi et al demonstrated in their study that the mechanical features of a NS can be easily tuned by changing the molar ratio CD/cross-linker, on the other hand, the cyclodextrin used for the synthesis does not affect the mechanical properties of the final NS [42].

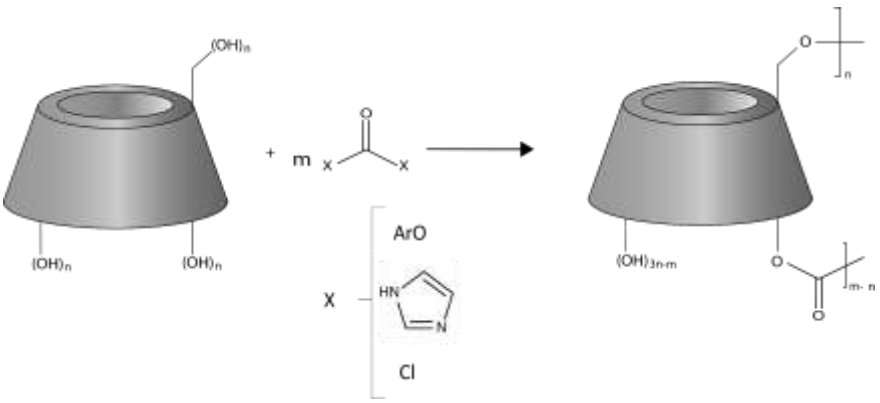

Scheme 2 – Reaction scheme of CD-based Polycarbonate NSs

1.2.3 CD-based Polyester NSs

Ester CD-based NSs are synthesized using dianhydrides or di/polycarboxylic acids, such as pyromellitic dianhydride, ethylenediamine- tetraacetic dianhydride (EDTA dianhydride), butanetetracarboxylic dianhydride, citric acid [26][28].
Reaction scheme is reported in Scheme 3.
Dissimilarly from polycarbonate and polyurethane NSs, polyester NSs are usually able to absorb outstanding amounts of water (up to 25 times their own weight) and form stable hydrogels. In a similar way as seen before with mechanical properties, the swelling capability of these CD-NSs is generally dependent on the degree of cross-linking. The swelling capability is usually inversely proportional to the density of cross-linking: the lower the degree of cross-linking, the higher the water uptake. The structure of the material of course dramatically

influences the chemical stability, in particular Ester NSs are subjected to hydrolysis in aqueous media more easily than polycarbonate and polyurethane NSs. The structure is, on the other hand very interesting because of the presence of free carboxyl groups in their chemical structure, moieties that can be exploited for the absorption of cations, using the material as an ionic exchange resin.

There are in literatures many examples of the formation of complexes with metal cation. The metal ions complexation ability of pyromellitic NSs has been studied by Berto et. al in for different metal cations, such as Al^{3+}, Mn^{2+}, Co^{2+}, Ni^{2+}, Cu^{2+}, Zn^{2+}, Cd^{2+} and Pd^{2+}.

In most cases, pyromellitic NSs were found to be capable of absorbing more than 70% of the tested cation [43].

My research group performed in 2019 a similar test, but in this case with a comparison with citric acid and with the goal of removing heavy metals from wastewaters. At a metal concentration of 500 ppm, the pyromellitate nanosponges (substituted before absorption with Na^{+}, for avoiding a possible modification of the water pH) exhibited a higher retention capacity than the citrate nanosponges. At lower metal concentrations (≤ 50 ppm) both the citrate and the pyromellitate nanosponges showed high retention capacities (up to 94 % of the total amount of metal). While, in the presence of interfering sea water salts, the citrate nanosponges were able to selectively adsorb a significantly higher amount of heavy metals than the pyromellitate nanosponges [44].

For ester nanosponges similar studies of correlation of cross-linking degree and properties had been performed. Surprisingly, the highest cross-linking degree was observed in the sample prepared using molar ratio 1:6 between CD and PYRO [45].

Higher contents of cross-linker, molar ratios like 1:8 and 1:10, led to a decrease of the degree of cross-linking; this is probability related by the steric hindrance generated by the pyromellitic units linked to CDs. Interestingly, by working under limited dilution conditions during the reaction and with an even lower CD/cross-linker ratio (e.g., 1:2 molar ratio), it is possible to obtain a hyper-branched water-soluble polymers [46]. As already described for carbonate NSs, Raman and Brillouin scattering experiments permitted to Rossi et al. to evaluate a relationship between the mechanical characteristics of the polyester

pyromellitic β-CD NS and the molar ratios CD/cross-linker: as seen before, stiffness and elasticity of the polymeric structure can be tuned by varying the amount of cross-linker [42].

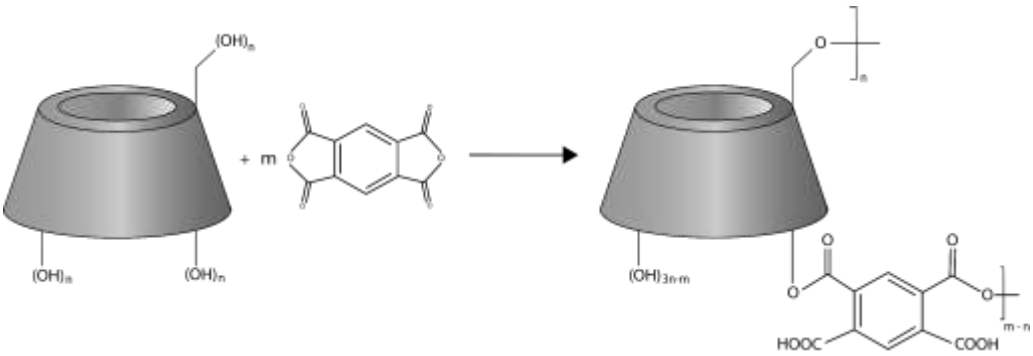

Scheme 3 – Reaction scheme of CD-based Polyester NSs

1.3 Photodynamic therapy (PDT)

Photodynamic therapy (PDT) is a clinically approved therapy based on a photochemical reaction between a photosensitizer (a light sensible molecule), light and molecular oxygen. The combination of these three components leads to the formation of reactive oxygen species (ROS) [47]. ROS can induce inflammatory response and directly damage cells (and vasculature) or induce cellular damage to organelles and cellular membrane.

The photodynamic therapy is a procedure with two different stages: the first stage is the administration of the photosensitizer (or a PS precursor). The administration can be intravenous, intraperitoneal or topical. The second stage is the light exposure of the interested zone resulting in local tissue destruction. The division of the procedure reduces the presence of side effects, allowing a good control of the treated zone: PS alone is harmless indeed, and is activated only via direct illumination.

The history of PDT has widely been described in literature [47]. In the last century photodynamic therapy (PDT) has been developed as we know it today. The first application of chemical and light in humans

was performed with haematoporphyrin (a porphyrin from blood) [48]. Few decades later Diamond et al. [49] used a haematoporphyrin derivative (HPD) to treat cancer in mice, observing a decrease in a glioma growth for few weeks after the treatment. Then Dougherty et al. observed a complete elimination of a mammary tumor in mice after a treatment with a combination of HPD and red light [50]. The first clinical approval of this therapy dates back to 1993 or the treatment of bladder cancer[49].

1.3.1 PDT Principles

Even if the PDT action mechanism is still not completely confirmed (it's in fact an ongoing topic of investigation) [48], its molecular effects are widely accepted to be related with the reaction of a light activated photosensitizer that leads to the production of radicals [51]. The mechanism is the following (Figure 1-5): light illumination of a PS leads to the absorption of a photon, the PS is promoted from S_0 to its excited state S_1. In this state an electron is shifted in a higher-energy orbital. This state is unstable and with a short time life so the PS have to return to the initial state S_0: energy can be converted in heat or fluorescence, depending of course on the structure of the molecule. Alternatively, intersystem crossing can happen, and the result is a population of PS excited to triplet state T_1: in this state energy can be transferred through phosphorescence or through the collision with other molecules, that leads to the creation of chemically reactive species. T_1 can react with organic substrates or solvents and transfer an electron in order to form radical anion or a proton to form cation species. The most common reaction is called a type I: PS reacts with an electron rich substrate forming PS-, that reacts with oxygen to form superoxide anion radicals. Differently, in a type II reaction the PS in state T_1 reacts directly with $^3O_2$ (ground state oxygen) to form singlet oxygen $^1O_2$ through transfer of energy. $^1O_2$ is a highly reactive oxygen species, commonly known as ROS. This molecular mechanism has been described by Foote in 1991 [52].

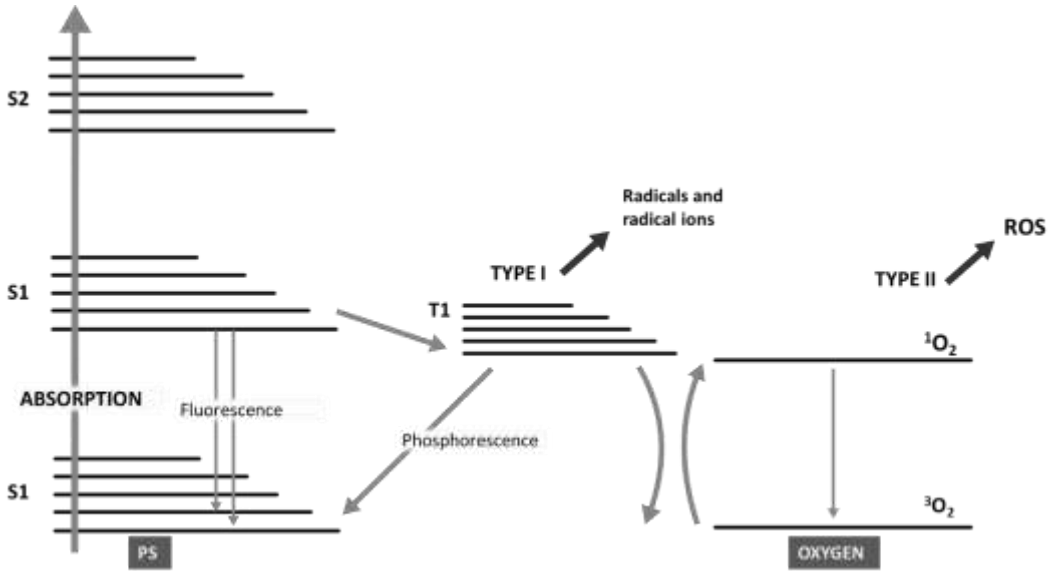

Figure 1-5-Representation of type I and II PS reactions

Singlet oxygen and superoxide anions are, as already said, cytotoxic products: both of them can react e damage many biomolecules such us proteins and nucleic acids. It's worth of say that superoxide anions, from a Type I reaction, do not particularly damage (in a direct way) biological systems, but contributes to reactions that lead to the formation of hydrogen peroxide. Hydrogen peroxide, through a Fenton reaction with superoxide anions, can form very reactive hydroxyl radicals. These radicals can easily react with double bonds in biomolecules, with an addiction, leading to chain reactions.

Most of PSs act through type II reactions: in this case most of the cellular damage is related to singlet oxygen. The $^1O_2$ reacts with membrane lipids and leads to the destruction of the cellular membrane. An alternative reaction is with amino acids, affecting proteins synthesis.

The localized action of the PDT mentioned above is related to the high reactivity of the singlet oxygen: it's lifetime is short (40ns) so the maximum action radius is consequently small (about 20 nm)[53]. Furthermore, the activation of the PS is localized, because related to illumination of target tissue and this, combined with the short action

radius (radius that is smaller than the diameter of most organelles), enhance (in theory) the specificity and controllability of the technique.

1.3.2 PDT cellular response and tumor response

The response of the cells to photodamage related to activated PS depends on multiple factors: a predominant factor is clearly related to the photosensitizer structure and to the amount of radical formed (this aspect will be discussed later) but main role is played by the photosensitizer localization [51]. The photosensitizer can localize near organelles such as lysosomes, plasma membrane, endoplasmatic reticulum and mitochondria. The action of the PS can affect many targets, but the mechanism of cell death induced by photodamage are mainly three: apoptosis, necrosis and autophagy. It is worth of say that these multiple ways of cellular death (different pathways) permit to circumvent the problem of apoptosis resistant cells in tumors, a typical obstacle of most common cancer therapeutics. Differences in mechanism of cells death are the following:

- Apoptosis: controlled mechanism of cell-death, initiated through numerous pathways. Apoptosis can be induced by PDT damage of several organelles but is mainly related to PSs localized to mitochondria (photodamage to mitochondria can result in leak of cytohcrome c into cytosol, that activate the caspase related to apoptosis).
- Autophagy: capability of the cell of "recycle" damaged organelles. Usually seen as a mechanism of cythoprotection, related to PDT can be related to cell death: autophagy function is a protective mechanism with high doses of PS.
- Necrosis: like the apoptotic way, but less controlled and regulated. It is related to an extensive, uncontrolled damage due to a high dosage of PS. Photodamage to the plasma membrane, indeed, results in a leakage of intracellular material that can cause local inflammation.

Unfortunately, the phototoxic effect of PDT, even if current employed, is not selective for tumor cells: PSs can have an effect both on healthy and ill cells. This is clearly a drawback.

However, in general, normal tissue can eliminate PSs after few times, while tumor cells cannot, because the absence of lymphatics. So, there is, in some ways, a retention of the photosensitizer in the tumor tissue, that combined to specific illumination lead to selectivity.
Furthermore, localization of the PS in tumor cells can also be enhanced by the phenomenon called Enhanced Permeability and Retention effect (EPR), well known and accepted in the field of cancer therapeutics: the retention is, in this case, related to the abnormal vascularization of the solid tumor mass, due to the uncontrolled growth of cells.
PDT has three main mechanism of tumor destruction [48], depending on the localization of the PS:

- ROS can directly kill the malignant tumor cells
- PDT can target the tumor vascularization by compromising supply of oxygen and nutrients
- PDT can induce an inflammatory and immune response against malignant cells, activating the immune system

1.3.3 Photosensitizers

Focusing on photosensitizers, as shown in the previous paragraphs, they must satisfy certain characteristics [54].
Preferably, as already said, a photosensitizer is expected to accumulate in tumor tissue and rapidly disappear from the normal tissue.
Then, the amphiphility is a crucial property for a clinically successful PS, which when administered systemically should move to the target tissue (tumor) without hindrances, and so hydrophilicity is needed, and then have to remain inside or near to the target cells, for which it requires some degree of lipophilicity.
Furthermore, a PS must also have a low dark-toxicity, an appropriate triplet lifetime (at least to interact with ground state oxygen or other substrates) and of course high quantum yield of triplet state formation for having a sufficient amount of ROS.
The other properties are essentially light-related. The light irradiation of course dramatically determines the outcome of the treatment.

The parameters that can have an influence are the light wavelength, light power density, light exposure time and how the light is delivered [55].
What is to take in consideration, finally, is how the light interact with tissues: the effective illumination is related to the absorption and scattering properties of the tumoral tissue. In general, the penetration depth is few millimeters, and as shown in Figure 1-6 related to the wavelength [56]. To overcome the poor penetration, it is better to work in the NIR (near-infrared) spectral region, so with wavelength between 600 and 900 nm (the also called phototherapeutic window [57]). In this interval the scattering and absorption are minimized, consequently NIR lasers are widely used and are the most employed in the current research [55]. An alternative are X-ray, since they exhibit a high penetration in soft tissues [58]: they may be promising for the treatment of deep tumors but X-RAY are ionizing radiations.

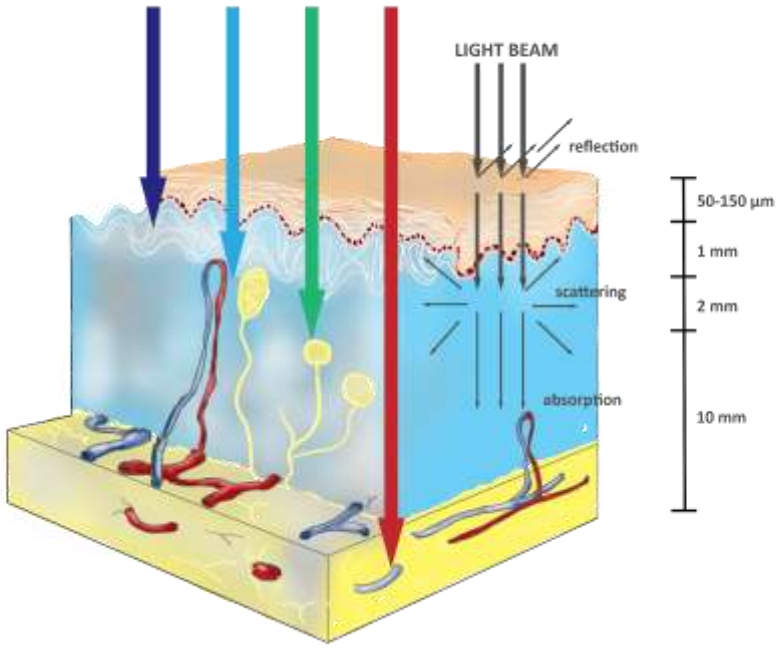

Figure 1-6 – Different wavelengths penetration and light interaction with skin tissues.

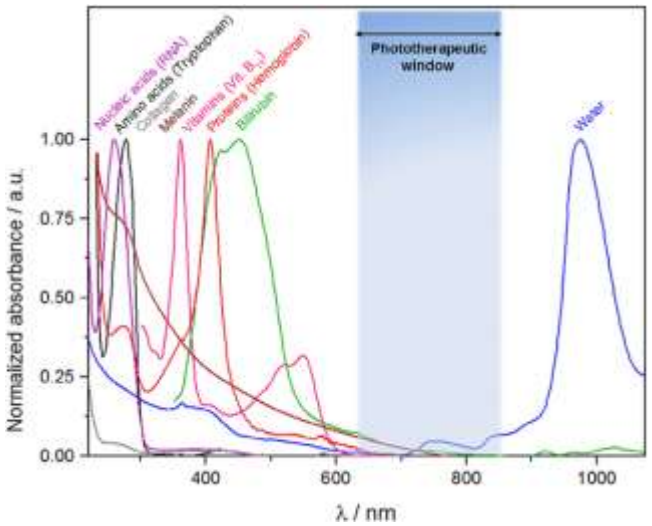

Figure 1-7 Phototherapeutic window and relative absorption of common biological compounds. Adapted from [57]

Many PS, anyway, do not satisfy all reported requirements and do not absorb in the correct range but have been approved for clinical use, since at least one characteristic is satisfied for therapeutic purposes. For the description of the many PS a division in generation, based on time of development and specific characteristics, will be followed, for uniformity with literature and with the reported division in generation of nanosponges [59][54].

The first generation of PS includes usually porphyrin-based photosensitizers usually developed in the 70s or early 80s. in these years research was generally interested in hematoporphyrin derivatives (HpD), that were a mixture of porphyrins monomer, dimers or oligomer or in porfimer sodium. As a matter of facts this first generation was efficient (negligible dark toxicity easily injectable in water formulations) and useful even if the earliest [60], but porfimer sodium exhibit several critical disadvantages. The relatively low absorption of light in the red portion, that as shown in Figure 1-6 is optimal for tissue penetration, significantly reduce the effectiveness of the treatment. Moreover, the low molar extinction coefficient makes necessary the administration of a high dose of drug to obtain a

tangible therapeutic response. The main issue with is the so-called Drug-Light Interval (DLI): DLI is the times between the PS injection and the light administration. In this case the DLI is usually 48-72h: in this time the patient must remain protected from light. Additionally, porfimer sodium tends to accumulate in to be retained in both ill and normal tissues for a long period, even 4-6 weeks. In this period the patient must wear protective clothing and/or and avoid direct sunlight and high energy light. So, briefly, the limitation of the first generation are mainly related to the selectivity and the prolonged photosensitivity, and both are (directly or indirectly) consequences of the high dose of drug needed.

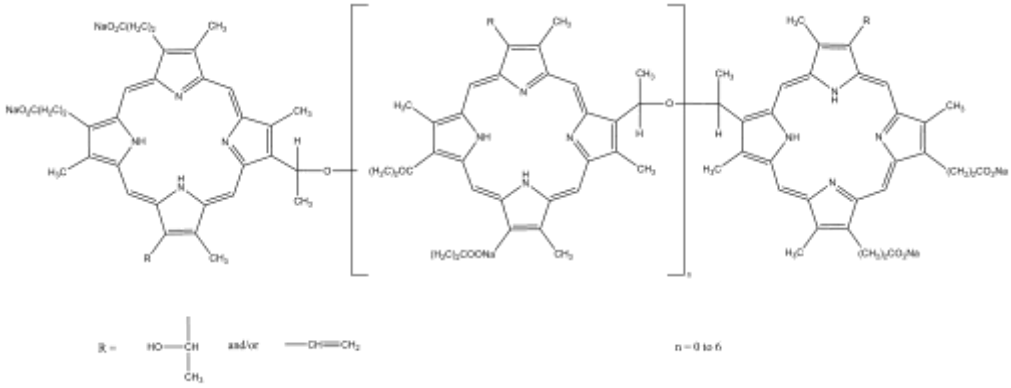

Figure 1-8 Porphimer Sodium polymer molecular structure

The second generation comprises both porphyrinoids (porphyrin and porphyrin based cyclic structures, such as chlorins, phthalocyanines, pheophorbides, texaphyrins) and nonporphyrinoids (cyanines, phenothiazines, anthraquinones, xanthenes, and curcuminoids) [61]. This category also includes metal derivatives of PSs such as zinc C and aluminum phthalocyanine tetrasulfunate.

The majority of these compounds had been developed in the late 80s, overcoming 1st generation PS.

In Figure 1-9 and Figure 1-10 are reported the most common second-generation PSs.

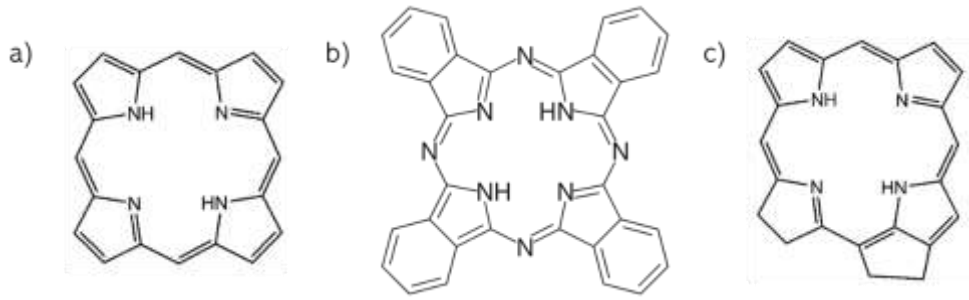

Figure 1-9 Second generation Photosensitizers, Porphyrinoids: a) Porphyrin b) Phtalocyain c) Pheophorbide

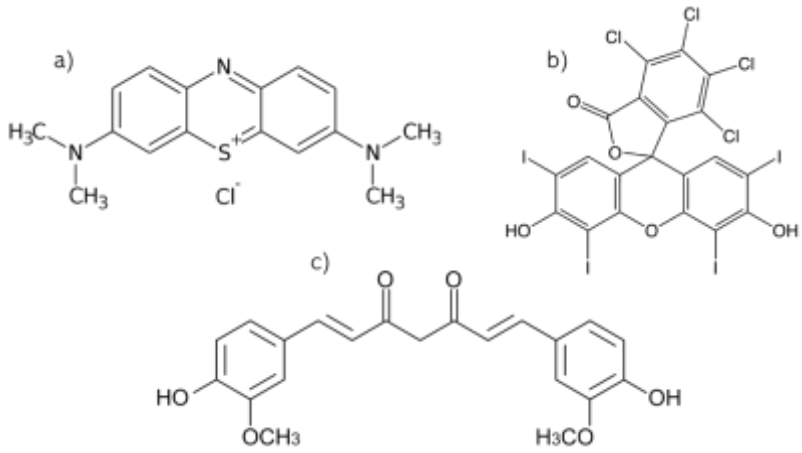

Figure 1-10 Second generation Photosensitizers, Nonporphyrinoids: a) Methylene Blue b) Rose Bengal c) Curcumin

A major, chemically relevant, difference from first generation photosensitizers is that in this case the chemical structure is known (no oligomers).

2nd gen PSs exhibit a high extinction coefficient and, in many cases, absorption maxima at wavelength longer than 630 nm.

In general, PSs from second generation exhibit a better antitumor effect if compared to HpD, thanks to the higher quantum yields of $^1O_2$ and tumor-to-normal tissue concentration.

The main problem of 1st gen, as said, was related to the accumulation time: with these different PSs administration and therapy can be

carried out in the same day (permitting also an out-of-patient approach). Since the variety of structures, final properties of PS depend on physical and chemical parameters such as presence/absence of charged groups, types and number of charged groups and number and types of rings.

Some of 2nd Gen PS are indeed highly hydrophilic but most of them, especially unsubstituted phtalocyanines, are hydrophobic; unfortunately the degree of hydrophobicity affects the administration over and above the pharmacokinetic profile and the biodistribution [62][63]. Anyway, even if hydrophilicity is necessary for penetrating the the cell membrane, hydrophobic molecules tends to aggregate affecting photophysical properties (yield in $^1O_2$) and consequentially photokilling efficiency.

Summarizing, a successful clinical application of PS requires a balance between the degree of lipophilicity and the degree of hydrophilicity.

In a similar way to what said for cyclodextrins in the previous paragraphs, different hydrophilic substituents were introduced within the PSs structures in order to improve solubility and to obtain amphiphilic derivatives. The porphyrin ring possesses 12 positions and, similarly to the 21 hydroxy groups of βCDs, they could be substituted with different groups, such as carboxylic acids, sulfonic acid, quaternary ammonium salts, carbonyl etc. etc. leading to limitless possibilities. PS with anionic substituents (sulfonate for example, more information will be reported in next sections and chapters) are particularly interesting because can localize preferably in the cytoplasm.

Moreover, porphyrin rings can be also modified with oxidation or to carry a central ion, usually a metal, changing dramatically he pharmacological properties. In general PSs with more than 3 charged substituents are considered hydrophilic and with less than 2 groups amphiphilic [58].

3rd generation PSs are now developed with the final goal of having a better tumor selectivity e specificity. This can be reached with PSs that can be activated with longer wavelength and modifying already available PSs with biologic conjugates like peptides or antibodies that can help in targeting specific tissues.

Developing a PS is crucial for PDT: from a synthetic chemist point of view a PS is more interesting if exhibits a delocalized aromatic π system, feature that permits to absorb efficiently light and to tune the absorbance. Unfortunately, at the same time the presence of a π – π leads to hydrophobic interactions so also in this case an equilibrium between efficient absorbance and application in aqueous environment is needed.

1.3.4 Photoreactive squaraines

As seen the search of more effective PS is thus a relevant issue and squaraines dyes are an innovative and interesting classes for photodynamic treatment [64]. Squaraines are the product of the dicondensation between the squaric acid and an electron rich substrate. Squaraines (SQ) are an old class of organic compounds [65] with interesting photochemical and photophysical properties, such as an high extinction coefficient with intense absorption (and fluorescence) in the red/NIR region and easy tunable properties. Substituted squaraines dyes can act as novel sensitizers as demonstrated by Ramaiah et al [66] and are particularly interesting for their strong absorption in the tissue transparency window. Furthermore, squaraines are scarcely cytotoxic in the dark, but after irradiation they promote a strong phototoxic effect.
In the following sections the synthesis and characterization of the halogenated squaraines for PDT, used for my work, will be presented. Like many PS, unfortunately, squaraines have poor water solubility. Low solubility in aqueous solutions lead to aggregation and inactivation under physiological conditions, reducing the production of ROS, too [67].

This research project relates to the synthesis and production of innovative nanostructured materials for protection, vehiculation and controlled release of photoreactive halogenated squaraines. A suitable material for this type of application are the nanosponges previously reported.
In will introduce, moreover, also nanosponges based systems for the encapsulation and the delivering of 2nd generation photosensitizers.

1.3.5 Reactive Oxygen Species Detection

ROS are relatively short-lived molecules, so a precise detection is an issue. Half-lives in aqueous environment (my attention will be focused on aqueous environment because the final application of the delivery system is in physiological conditions) are in the range of nanoseconds to hours, and are usually found in pico/micromolar concentration in environmental systems [68]. In aqueous environment, most free radical ROS undergo self-reaction (such as, for example, dimerization or disproportionation): excited $^1O_2$ rapidly decays through vibrionic coupling with water with a non-radiative decay. H_2O_2 does not react with itself but degrades through catalyzed rapid reactions with trace metal ions and enzymes. Analyses of ROS have proven challenging because their lifetimes, with the exception of the H_2O_2 (less interesting for medical applications than the singlet or the superoxide) are usually too short for an accurate analysis.

Methods for detecting reactive oxygen species are usually divided in direct or indirect, depending on the lifetime of the ROS, on concentration, on environment. Direct observation is only possible on a sub-millisecond timescale. Indirect methods involve the reaction of the ROS with a so-called probe molecule to obtain a more stable, long-lived analyte. The analysis is, consequentially, performed on the more stable new analyte. Indirect detection usually involves specific chemical derivatization (for example trapping in a "spin trap") or competitive kinetics, so there is always the risk of perturbing the system.

Many of the method development for aqueous ROS analysis (for costs, and also for portability in some cases) are focused on UV-Vis light spectroscopic techniques and the use of probe molecules. Most of probes molecule are by their nature reactive, so, especially in water [26], the possibility of probe degradation or competing reactions that may confuse the expected ROS signal. Moreover, some probes are poorly water soluble, so the conditions of their use sometimes require organic solvents such as ethanol or dimethyl sulfoxide (clearly undesired for medical and cellular applications). A large number of

methods and probes have been developed and to measure ROS, these are often times limited by specificity and sensitivity [26].
In my research work I focused my attention on some different probes for UV-Vis detection of ROS production (more details in next sections), than, for a more precise and selective measure and to confirm and cross results, EPR measures were performed.

1.3.6 Electron paramagnetic resonance (EPR) for the detection of ROS

The application of electron paramagnetic resonance (EPR) spectroscopy requires spin trapping techniques and in the detection of transient free radicals shows some advantages over other commonly used methodologies of radical detection, such as a good selectivity on the ROS species (e.g. easily distinguishing superoxide and OH radical).
EPR spectroscopy is the most commonly used method for detection of paramagnetic species [27]: EPR involves absorption of microwave energy by paramagnetic species in the presence of an external magnetic field resulting in the transition of spin states. Unpaired electrons can move between their two spin states and, since there usually are more electrons in the lower state (Maxwell–Boltzmann distribution), there is an absorption of energy, absorption that is converted into a spectrum. The most common way to record and publish a continuous wave EPR spectra is a first derivative of the absorption spectrum.
The principle of spin trapping technique is the reaction between transient radicals, e.g., •OH, $^1O_2$ etc., or relatively stable but not detectable under normal conditions radicals. There is the formation of a covalent bond from the reaction of nitrones and nitroso with reactive radicals, while a coordination bond is formed between NO and Fe^{2+} complexes. For different spin adducts, different and characteristic EPR spectral profiles can be observed and furthermore transient radicals that are otherwise undetectable are observable. The ability of these spectra of recognizing the type of radicals can provide many

information in terms of mechanism, kinetics of radical production in biological systems.

1.4 Mechanochemistry

1.4.1 Principles and historical development of Mechanochemistry

Mechanochemistry (MC) involves the application of mechanical forces (such as compression, shear, or friction) to drive and control chemical reactions, for example using grinding or milling to transfer energy to chemical bonds [69].
The presence of unintentional chemical reactions goes together with many forms of mechanical action and modification, such as grinding and sliding, at laboratory scale and, even more, at industrial scale. The intentional and deliberate application of mechanical energy, on the contrary, provide an interesting method to prepare new and greener materials and to improve the efficiency of many processes. Mechanochemistry is becoming more studied and even if it has been historically a marginal approach to chemical syntheses it could became in future a more mainstream technique because can promote reaction between solids quickly and quantitatively [70].
The current dependence on solvents is nowadays unsustainable for many reasons because depends on fossil derivatives, is environmentally problematic and expensive and energy demanding for what concern solvent production, recycling and disposal.
The term "mechanochemistry" (and consequentially "mechanosynthesis") is commonly used in broad sense, covering any chemical reaction induced mechanically [71]. IUPAC defines a mechanochemical reaction as "*Chemical reaction that is induced by the direct absorption of mechanical energy*" where "*shearing, stretching and grinding are typical methods*". In the specific field of polymers mechanochemistry involve the generation of "reactive site usually macroradicals, in polymer chains that undergo mechano-chemical reactions" [71]. There is a little bit of confusion for what concern the presence of solvent: mechanosynthesis are meant to be

"solvent-free" but actually in some cases the reaction can occur in presence of solvent (or liquid reagents, acting as solvents) for example with hydrated reactants or with polycondensation, where solvent can be a elimination product. So, usually, "solvent free" means that there is no solubilization of reactants for having a reaction [70].

The history of mechanochemistry fade into ancient times.
An early reference point is from Aristotle, that stated (freely translated from Greek) "No reaction proceed in the absence of solvent" [70], effectively laying the foundations for a chemistry inextricably linked to the presence of reaction solvents.
It is worth to say that the chemical effects of mechanical action are different and beyond the effect of heat: this knowledge, and the "intentional" use of mechanical forces for reactions are a watershed in the history of mechanochemistry [69]. First applications of grinding, were of course, for preparing food. Dates backs to pre-history, the intention of using mortar and pestle to reduce size reduction and to obtain eventually physical and chemical changes. The first systematic studies on mechanochemical reactions dates to the end of the 19th century, to the 60s of the 20th century for more "modern" studies [72]. Anyway, unifying principles and methodology for mechanochemistry are not available even nowadays: the main reason is that the late and slow development of mechanochemistry was bounded to a broad variety of areas, and so mechanochemical investigations arose in very different and heterogeneous contexts. This diversity led to a "parallel development" of the subject and Mechanochemistry is becoming only nowadays a unified area of research [69]
I will intentionally skip the early times, because is mostly related to the so called "inadvertent mechanochemistry", because it is beyond the scope of this work. Anyway, the earliest surviving proof of a reaction by grinding is reported by Teophrastus of Eresus, an Aristotle student and successor as helm of Lyceum: he reported the reduction of cinnabar to mercury in a copper mortar with copper pestle, but of course without any awareness of the process.
The first reported (and with scientific method) study is from Faraday in 1820, where he described a "dry way" to obtain a reduction of silver chloride by grinding with zinc, tin, iron and copper [73].

In 1913 Johnston and Adams made a similar assessment saying that "grinding in a mortar will occasionally induce some degree of chemical action between solids" [74]. The first, documented, application of mechanochemistry for organic reactions dates back to 1893 with Ling and Baker, that prepared halogen derivatives of quinhydrone by trituration and dry mixtures [75].

The first investigation of the correlation between mechanical action and chemical reactions was carried out by Wàlthere Spring in the 80s of the 19th century.

Spring performed many syntheses and published different papers, mainly focused on the effect of pressure on phase transformations. One of his results, an observation of recrystallization and amorphous to crystalline transformations under high pressure, was challenged by the eminent organic chemist Friedel, and he proved the efficiency of his method with a public demonstration in Paris. Anyway, the controversy never ended.

The best-known experiment of Spring, confirmed by subsequent studies, is the metathesis reaction:

$$BaSO_4 + Na_2CO_3 \leftrightarrow BaCO3 + Na_2SO_4$$

Obtained via compression and pulverization [76].

Spring's observation on mechanochemistry opened a wide new field of investigation, but of course the open controversy with one of the most famous scientists of the period mined the credibility of his work in the scientific community. Few later examples are in the work of Lea between the 19th and the 20th centuries [77].

Progresses in mechanochemistry were slow in the 20th century. Anyway, more important parallel scientific development, useful for understanding the mechanism, occurred in science: x-ray crystallography was invented and the connection between lattice defects and mechanical properties was described.

In the second decade of the 20th century, moreover, the first motorized mills were developed. The first one dates back to 1923, patented by Retsch [77].

So, between the two world the scientific research on mechanochemistry nearly stopped, but after it could benefit of the general progresses in physical chemistry and technology.

After 1960 the research activities of several groups in Soviet Union and Eastern Europe (east Berlin comprised) was primarily dedicated to mechanochemistry, and the first symposium was organized in 1968, the "All-Union Symposium".
In 1986 Japan joined the symposium. Only in 2009 a section on mechanochemistry was organized in Boston, by the Material Research Society.
As seen, even if with a complicated history, mechanochemistry applied to inorganic chemistry is now well established and easily transferrable to an industrial scale and for what concern mechanochemistry applied to organic synthesis and polymers the development is more recent [78][70].
Thus, mechanochemistry based process appears as safe and efficient activation methods for greener processes, permitting to avoid solvents and to reduce the use of energy. Recently, many examples of modification of starch using ball milling have been reported: there are many examples of esterification and etherification of starch [79] and cellulose [80].

1.4.2 Planetary Ball Mill

The most important operation for the size reduction in industries (from chemical to pharmaceutical) is grinding. Ball mills (BM), and most specifically, planetary ball mills are suitable for grinding wet and dry powders down to the nanometric size range, thanks to the high stress reached. In comparison to others ball mill type, such as mixers or stirred mills, a planetary ball mill exhibits a simpler set up and cleanability, characteristics that makes it very interesting also for reactions.
Planetary ball mills are used for sample processing and colloidal grinding, thanks to the easy handling and the possibility of short times. It is worth to say that today, planetary ball mills and especially high energy planetary BM are built only on laboratory or pilot scales, so for quantities from few milligrams in small jars to 1 litre of material in big jars.
Since the main intended application of a ball mill is processing materials and not conducting reactions, they are not equipped, as a

standard and until now, with perks that a synthetic chemist needs, like temperature control and monitoring (crio cooled mills does exist, but the presence of liquid nitrogen is for cracking rubberish/plastic compounds) or *in situ* monitoring spectroscopic techniques.
A scheme of the movement of a planetary ball mill is reported in Figure 1-11, following:

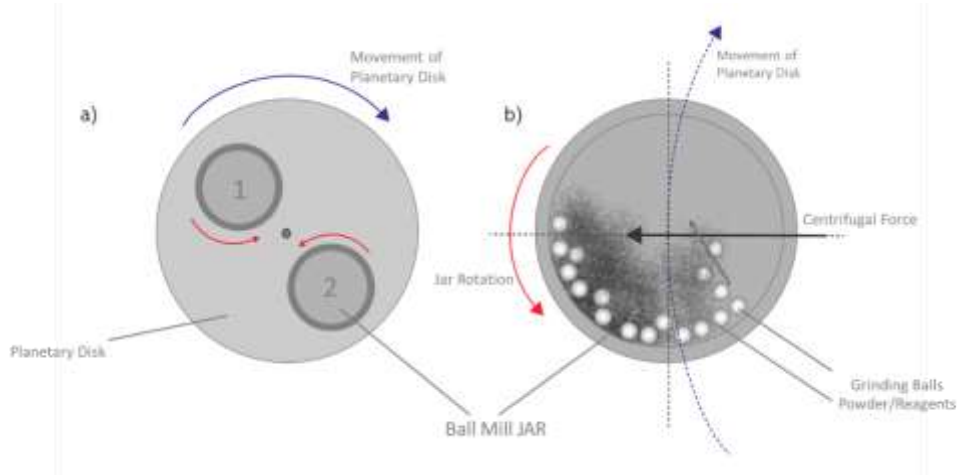

Figure 1-11 – Working principle of a Planetary Ball Mill (Laboratory scale) – a) Overall layout of the rotating planetary disk, top view b) Orizontal section of a grinding jar

A planetary ball mill is based on a rotating disc, with 1, 2 or 4 rotating jars attached on. If there is on 1 jar there is also a counterweight on the opposite side for balancing the weight during the rotation. Jars are fixed on the disk that rotates around a common central axis while the jars are simultaneously rotating around their own axis. The instrument is called "planetary" because the whole rotation reminds to the rotation of planets around the Sun.
The rotation speed of both disk and jars is very high and leads to large impact energies of the spheres inside the pots.
The material inside the jars, during the process, is crushed thanks to the impact and the frictional forces that are caused by collisions.
The powder (or the paste) inside the jars can influence the ball motion as the speed and the direction of rotation.

Since the powder particles are trapped between spheres and the walls of the pots the collisions can became less elastic and the ball motion is slowed down.
The motion of the balls has an influence on the number of collisions and on the balls speed and consequentially on the impact intensity on the powder. The spheres behavior inside the pot is complex and the variation are mostly related to the system and to the operation parameters.

Different variables influence the success of a milling process or mechanosynthesis, and there are many studies that deeply investigated all the possibilities; mechanochemical processes, anyway, are complex and mainly dependent on the milled/processed material so there are no general rules [81].

Anyway, several (and mostly empiric) milling parameters have to be assessed:

- Revolution/rotation speed
- Milling/reaction time
- Filling ratio of milling balls or number or ball (at constant jar volume)
- Milling balls/powder ratio

These parameters are not completely independent of each other and the optimization plays an important role for the obtaining of an high yield or small particles. All these parameters are easy to control at laboratory scale, for large scale processes other milling setup are needed.
Anyway, the parameters assessment is related to the final goal: if we are looking for a size reduction, so a high stress is needed, or if the process depends on the total energy input.
In general, high stress energy can be provided by large ball diameters or high ball densities (more balls, more grinding surface) and high energy speed.
For chemical reaction where the specific energy is crucial the use of small balls permits to achieve a good mixing and, in the meantime, high stress frequencies.

This is anyway not always true: for example, with the reaction that will be reported the use of small ball (high friction surface) impedes a good temperature control. So, condition have to be tuned for each system, trying and optimizing parameters.
The most dominant theory nowadays about the understanding how molecules "receive" the energy for chemical reactivity is the so-called "hot spot theory" [82].
Within this theory the impact of the milling media with the vial wall creates a localized hot-spot of high-intensity energy that is converted in chemically useful energy. So, the temperature is no considered. The practical experience of many research groups and literature anyway demonstrate that the temperature influence and control the reaction [83]. A recent review by Andersen et al. summarizes that the frequency of impact can speed up the reaction, while the temperature can maximize the selectivity [82]. So, shortening the milling time it is possible to achieve more selectivity for a certain product, and so on.

1.4.3 Mechanochemistry and organic synthesis

Even if, as seen, most of the experimentation in mechanochemistry has been empirically driven, few unifying themes and procedures can be discussed.
A typical setup for mechanochemical reaction is easy to prepare, often easier than the solution equivalent [82]. Reactants are weighted and inserted in the vial/milling jar. The milling jar can be made of different materials, usually stainless steel, zirconia or alumina. Then the milling balls must be added: spheres are always made of the same material of the jar. They may be inert but also be sources of catalyst, for example with copper balls.
The vial can now be closed, usually there are safety screws, that permit to have an isolated system. This is a safety improvement as well, because the chemist is isolated from the reaction.
Since no solvent are involved, there is no need of reflux condenser.
Moreover, the absence of solvent permit to avoid completely the presence of water (solvents often are not completely anhydrous), without any purifications.

The time of reaction is usually set directly on the instrument.
When the reaction is concluded, the product can be removed. The fastest approach is using a solvent (also with a short and mild milling for a better solubilization), but the process is not "solvent free" anymore. It of course depends on the application but usually is enough simply scrape out the material.
It is worth to notice that every mechanosynthesis start as a grinding.
In Figure 1-12 is reported a the most probable sequence of event in a mechanochemical reaction.

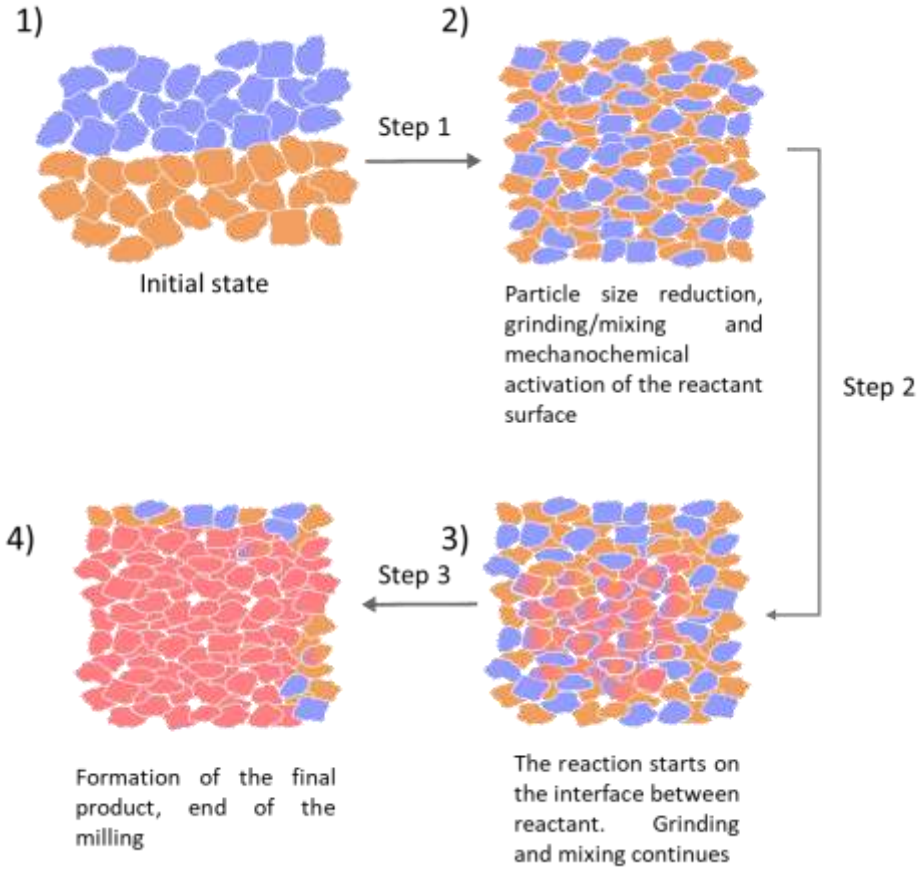

Figure 1-12 – Steps in a solid state mechanochemical synthesis

The steps reported are not dissimilar from a classic solid-state reaction.
The two solid reactants are, in the first step, mixed and in the same time grinded together. Only after Step 1, when reactants are well mixed and there is intimate contact between the finely ground powders, the reaction starts at the interface. The better is the milling in the first step, the higher will be the exposed surface.
After this first step the energy given by the spheres can activate the reaction, giving enough energy for the breaking and formation of new bonds. It makes sense to assume that the reaction starts from the interfaces, to then propagate inside the particles, which in the meantime are continuously minced and reduced in size, offering "new surface" for the reaction.

The reactivity of cyclodextrin in ball mill is a relatively new field.
In 2017, Jicsinszky et al. reported the possibility of obtaining CD derivatives with a solid state reaction, using a planetary ball mill [84], [85] and via other green processes [86].
In my research work, the main goal is to obtain a cyclodextrin nanosponges via a ball milling driven synthesis, with the same physico-chemical characteristics of the same material synthetized with solvents.
The main finality is of course the development of a new, green and safe, synthetic route, but also the possibility of exploiting this new method to obtain functionalized materials more quickly or more easily, or to obtain materials that cannot be obtained otherwise, from reagents that are little or no soluble.

2 Photoactivated Therapies

The following is divided in two different parts, both on materials for photoactivated therapies, but with different approaches and materials.
Moreover, these two different projects were carried out in two different working groups: the first part, mainly focused on synthesis of Nanosponges and on squaraine and organic dyes was performed in Turin, at the Department of Chemistry. The second one was carried out in Messina, at the CNR ISMN, research institute internationally renowned for its activities in the field of nanostructured materials.
Both projects are still ongoing, and most of the work is now focused in the radicals identification and quantification: as seen in Part 1, this is a major issue in analytical chemistry.

The project carried out in Messina, was principally focused on the synthesis of nanomaterial for antimicrobial Photodynamic Therapy (aPDT).
aPDT is a well-known alternative to treat local infection caused by different microorganisms, such as Gram positive and Gram-negative bacteria, viruses, fungi and protozoa. Nowadays, photo antimicrobial systems based on cyclodextrin (and photosensitizer (both as PS eluting fabrics [87] or in aqueous dispersion [20]) have been proposed as drug delivery platforms with high PDT potential [88]. Over the last decade, CD nanosponges research have been boosted the interest of CD scientists thanks to the low preparation costs and high versatility of their use in various field [28] such as drug delivery [89] and driven green chemistry processes.
Here we report on novel nano photosensitizer based on the anionic β CDNS (βNS PYRO) and a cationic 5,10,15,20-tetrakis(1-methyl-4-pyridyl)-21H,23H-porphine TMPyP which currently is utilized in aPDT to photo inactivate Gram bacterial cells. In this respect, in vitro photo antibactericidal studies are in due course to elucidate the aPDT efficacy of these spongly photosensitizers.

2.1 Experimental Methods

2.1.1 Materials

β-cyclodextrins (β-CD), linear Maltodextrins KLEPTOSE® Linecaps (from Roquette) were provided by Roquette Italia SpA (Cassano Spinola, Italy). 1,1-Carbonyldiimidazole (CDI), Pyromellitic Dianhydride, dimethylformamide (DMF), Dimethyl sulfoxide (DMSO), acetone and ethanol were purchased from Sigma Aldrich (Munich, Germany) and used with no further purification. Dextrins were dried before use, in oven at 100°C until constant weight.
5,10,15,20-tetrakis(1-methyl-4-pyridyl)-21H,23H-porphin was purchased from Sigma Aldrich and maintained in freezer.
Thermogravimetric Analysis were carried out on a Hi-Res TGA Q500 Thermogravimetric Analyzer from TA Instruments.
IR spectra on dried powders were recorded on a PerkinElmer Spectrum 100 FT-IR Spectrometer with 8 scans.
NMR Characterization was driven on a Bruker Avance 200
Steady-state fluorescence measurements were performed on a Jasco FP-750 spectrofluorimeter at r.t. ≅ 25 °C. Fluorescence emission spectra were not normalized by extinction at excitation wavelength.
Time resolved fluorescence emission measurements were performed on a Jobin Yvon-Spex Fluoromax 4 spectrofluorimeter using time-correlated single-photon counting technique. A NanoLED (λ = 390 nm) was used as the excitation source.

2.1.2 Synthesis of βNS-CDI

Polycarbonate βNS-CDI(1-4) (1:4 is the molar ratio between βcyclodextrins and crosslinker), NSs based on βCD monomers (the numbers in brackets indicate the molar ratio between β-CD and the cross-linker, respectively), were synthesized by reacting β-CD with 1,1'-carbonyldiimidazole (CDI) as cross-linker (Figure 1-13). The procedure for the preparation is the following: 787 mg of β-CD (desiccated in oven at 120°C for at least 2-3 days) is dissolved in 4,70 ml of anhydrous dimethylformamide (DMF) under vigorous stirring, then 449 mg of CDI is added. The solution, after complete solubilization is heated, under reflux, to 80-90°C. After 30 minutes the gelation process occurs.
The following day the already formed NS is ground in a mortar and cleaned, on Buchner filtration, with deionized water (a cross-linked NS is water insoluble), in

order to remove the DMF (water miscible) and unreacted monomers and imidazole. The imidazole is formed as a byproduct of the polycondensation reaction.
Usually a further purification is performed by Soxhlet extraction with ethanol and/or acetone (at least a week of Soxhlet).

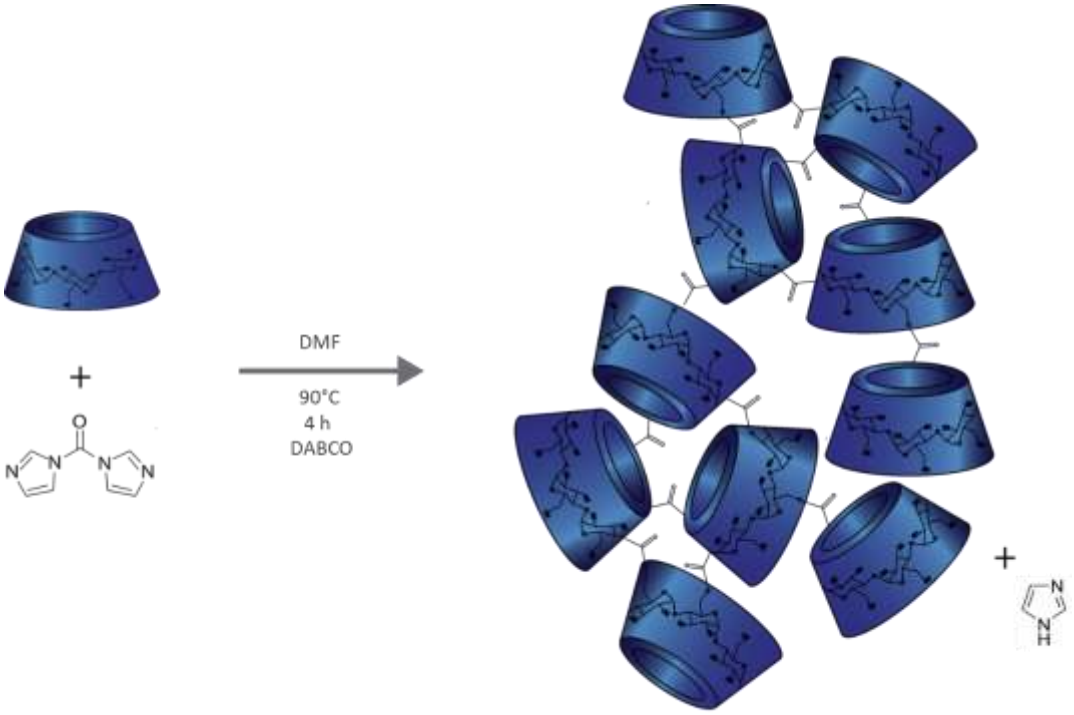

Figure 1-13 Synthesis of βNS-CDI and representation of the NS structure

2.1.3 Synthesis of βNS-PYRO

Polyester βNS-PYRO(1-4), NSs based on βCD monomers with the same molar ratio of βNS-CDI but by reacting β-CD with pyromellitic dianhydride as cross-linker (Figure 1-14).
The procedure for the preparation of the polymer is the following: 769 mg of β-CD (desiccated in oven at 120°C for at least 2-3 days) are dissolved in 4,00 ml of anhydrous dimethyl sulfoxide (DMSO) under vigorous stirring.
After complete solubilization of cyclodextrin, triethyl amine (0,100 mL) are added. Triethylamine (Et_3N) or other organic bases, acts as co-reagent has also a catalytic activity role (helping in the opening of the dianhydride rings and partially balancing the negative final charge).
After few minutes 659 mg are added: the crosslinking reaction is very fast and carried out at room temperature.
Reaction is exothermic and takes few minutes to complete.
The following day the already formed NS is ground in a mortar and cleaned, on Buchner filtration and in Sohxlet as seen before for βNS-CDI (1:4).

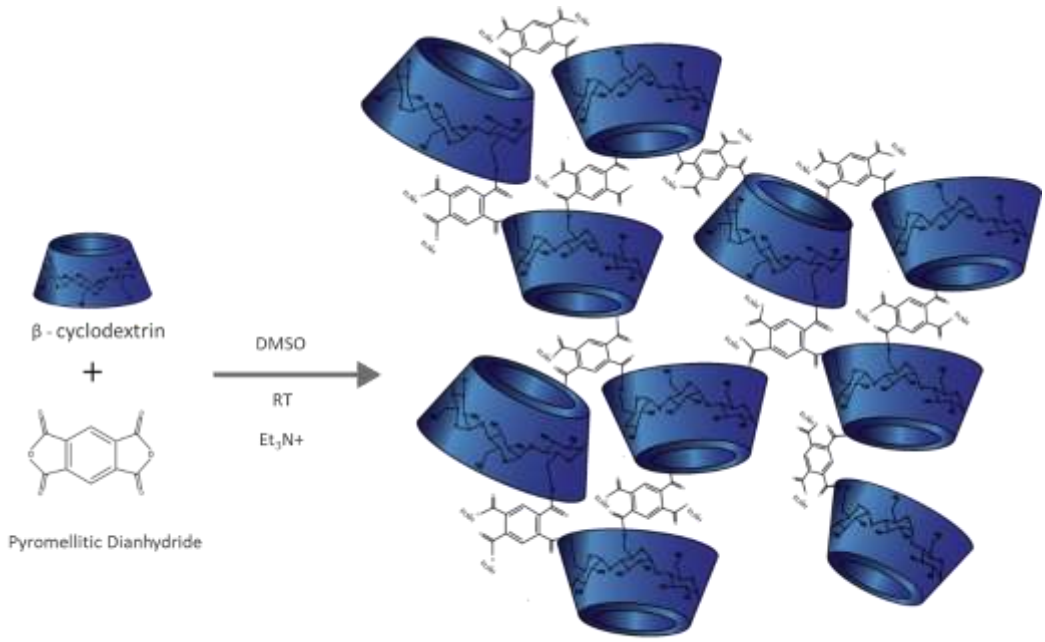

Figure 1-14 Synthesis of βNS-PYRO and representation of the NS structure

2.1.4 Squaraine SQ Br-C4 synthesis

The synthetic steps for the Halogenated (Br) Squaraine bearing C4 chain (SQ Br-C4) are showed below. Synthesis are carried out with the use microwave heating to accelerate chemical reaction. Details on the synthesis and on the characterization are reported in literature (Barbero et al. Org.Lett. 2015 [90] and Serpe et al. Org.Lett. 2016 [64]).
The procedure starts with the synthesis of 5-Bromo-2,3,3-trimethyl-3H-indole and the quaternarized indolenine ring, as showed in Figure 1-15, below.

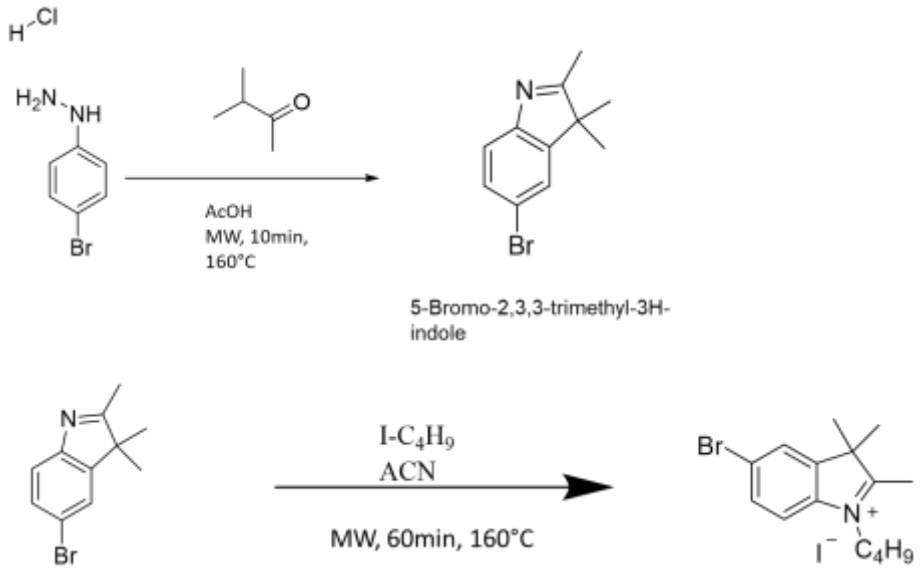

Figure 1-15 Quaternarization synthesis of indolenines

In the third and final step, squaric acid is microwave overheated in a closed vessel with a 2-fold excess of the quaternarized indolenine in 1-butanol: toluene mixture (1:1, v/v), giving the desired symmetrical squaraine dyes. Further details are reported in Figure 1-16.

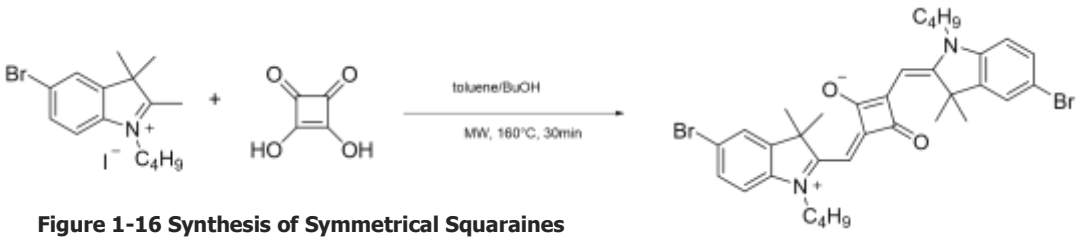

Figure 1-16 Synthesis of Symmetrical Squaraines

2.1.5 Synthesis of βNS-CDI+SQ Br-C4

βNS-CDI (1:4) was loaded with SQ Br-C4, by adding a 1 % of dyes respect to the wt. of CD directly in synthesis, before the addition of the cross-linker.
The synthetic procedure is similar to a Molecularly Imprinted Polymer, but in this case the organic dye is not removed. In Figure 1-16 the synthetic procedure is reported.
The syntheses are different from plain βNS-CDI, covering the solutions from light using an amber vial, to preserve the Squaraine. TGA measures of dye (see later) showed degradation only after 200°C so a high temperature is permitted. Besides this first synthesis was carried out at a lower temperature, 65°C, and with the help of a catalyst (DABCO).
Longer times, in this case permit a better mixing and inclusion of the "template" molecule.
After the synthesis, the NSs were washed with an excess of water: the aim is to remove only the solvent, imidazole byproduct and possible unreacted monomers leaving however the squaraine dye inside the material bulk (SQ Br-C4 is almost insoluble in water). The obtained cross-linked material was freeze-dried for 5 days to eliminate residual water. The final blue colored powder was ball-milled for 2h at 600 rpm, obtaining particles around 400 nm.
βNS-CDI+SQ Br-C4 was then stored, covered from light with aluminum.

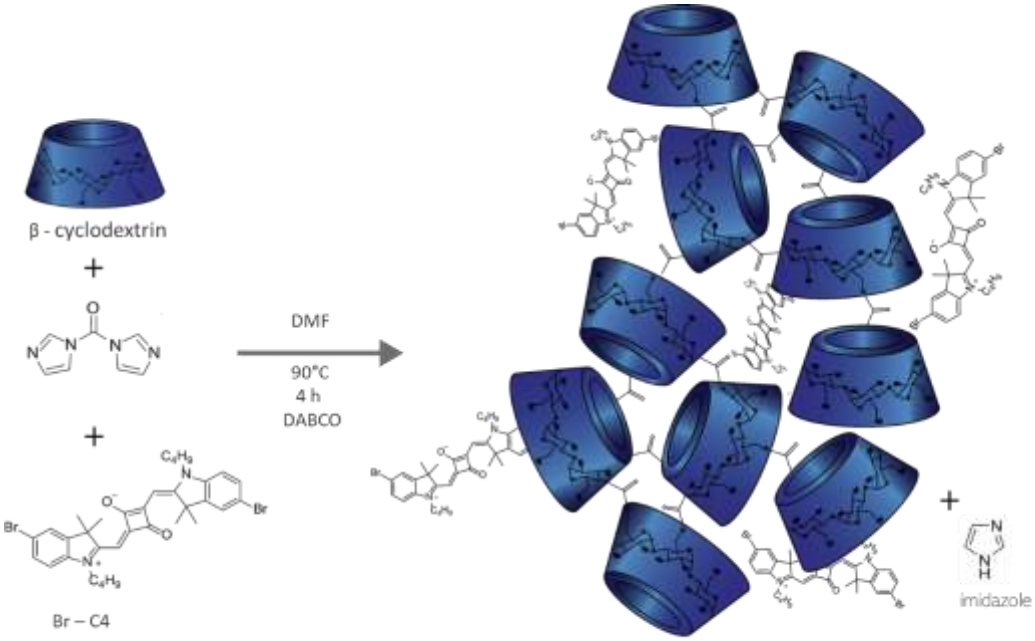

Figure 1-17 Synthesis reaction and schematic representation of the βNS-CDI loaded with SQ Br-C4

2.1.6 Synthesis of βNS-PYRO+SQ Br-C4

Same as for βNS-CDI (1:4) +SQ Br-C4, βNS-PYRO+SQ Br-C4 was obtained by a synthesis with SQ Br-C4, by adding 1% of dyes respect to the wt. of CD. Squaraine is easily soluble in DMSO, so there is complete solubilization. All the synthesis is carried out by protecting the solution from light using an amber vial, to preserve the Squaraine structure.

The cross-linking reaction in this case does not occur immediately, as for a plain βNS-PYRO because the molecule of squaraine occupies the space between the CDs and the crosslinker, slowing down the crosslinking process (that literally form a "cage" of polymer around the molecule of dye) . After few hours the bulk is formed.

After the synthesis, the obtained insoluble NS was cleaned in buchner, with an excess of water, removing the solvent, unreacted monomers and crosslinker (and leaving the squaraine dye inside the material). The swollen material (light green colored, different from the CDI nanosponges with the same dye) was freeze-dried for 5 days to eliminate residual water. The obtained powder was

then grinded using a ball-mill. The βNS-PYRO+SQ Br-C4 was then stored in dryer, covered from light with aluminum.
In Figure 1-18, reported below, the synthesis and a representation of the structure of the βNS-PYRO+SQ Br-C4.

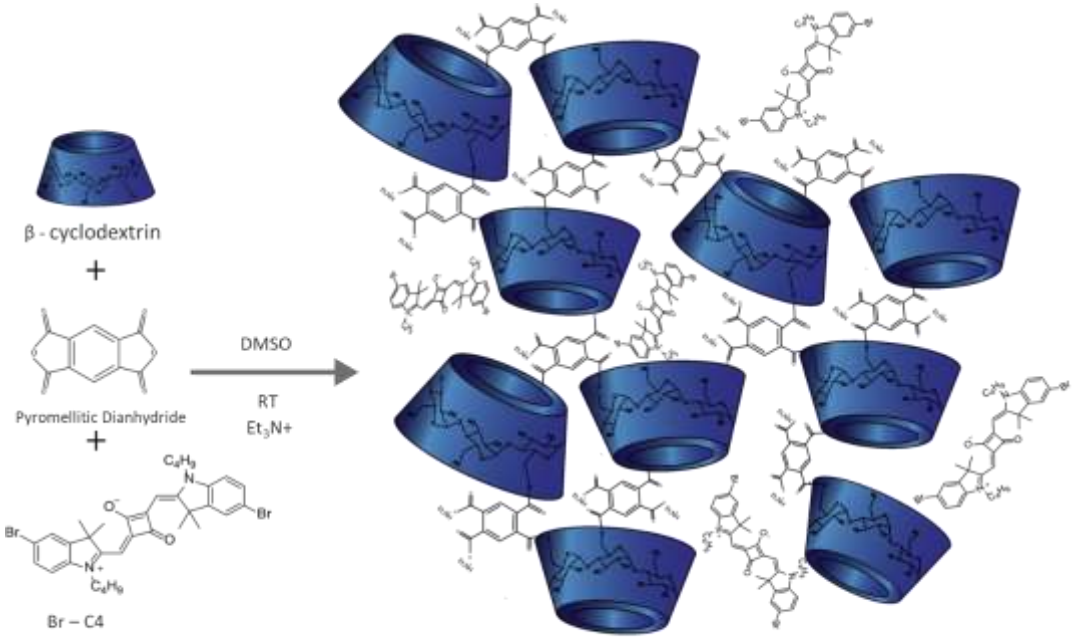

Figure 1-18 Synthesis reaction and schematic representation of βNS-PYRO loaded with SQ Br-C4

2.1.7 Loading of dyes on synthetized βNS-PYRO and βNS-CDI

Before starting with the ROS tests, different samples with well-known water soluble and ROS-generator dyes were prepared.
The chosen dyes are the following:
Methylene blue: common extensively studied organic dye, that can generate a great amount of different ROS species, often used in comparison as a reference [91]. Methylene blue (MB) has been purchased from Sigma Aldrich. The structure is reported in Figure 1-19 below.

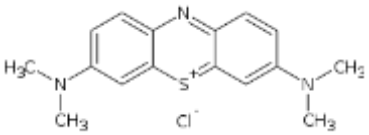

Figure 1-19 Methylene Blue structure

Bengal rose organic dye that under irradiation can produce singlet oxygen, useful for testing a probe sensibility for a specific ROS. Rose Bengal has also been purchased from Sigma. The structure is reported in Figure 1-20 below.

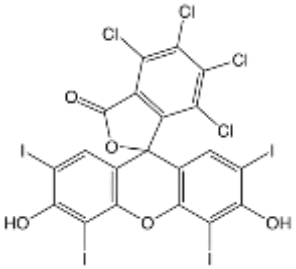

Figure 1-20 Rose Bengal structure

Both dyes are reported in Part 1, as representative of 2nd Generation of PS.
For the preparation of the following samples a different, but simpler, approach is used; a finely minced powder (ball mill, for at least one hour at 600 rpm) of two different types of nanosponges, polyester and carbonate, is added to an aqueous solution of the dye. NSs work, as the name can suggest, as "sponges", swelling and adsorbing water and, of course, the solubilized dye. After few minutes of swelling (NSs swell in a different way, depending on structure and crosslinker[26]), the obtained dispersion is freeze dried. The result is a colored powder. Since the powder is not washed there is no loss of dye, all dye is absorbed or adsorbed on the surface of the NS.

The loaded quantity is 3% wt./wt. dye/NS for all samples.
The prepared samples are the following:

- **βNS-PYRO – Rose Bengal**
- **βNS-PYRO – Methylene Blue**
- **βNS-CDI – Rose Bengal**
- **βNS-CDI – Methylene Blue**

2.1.8 Preparation and Characterization of TMPyP loaded βNS-PYRO

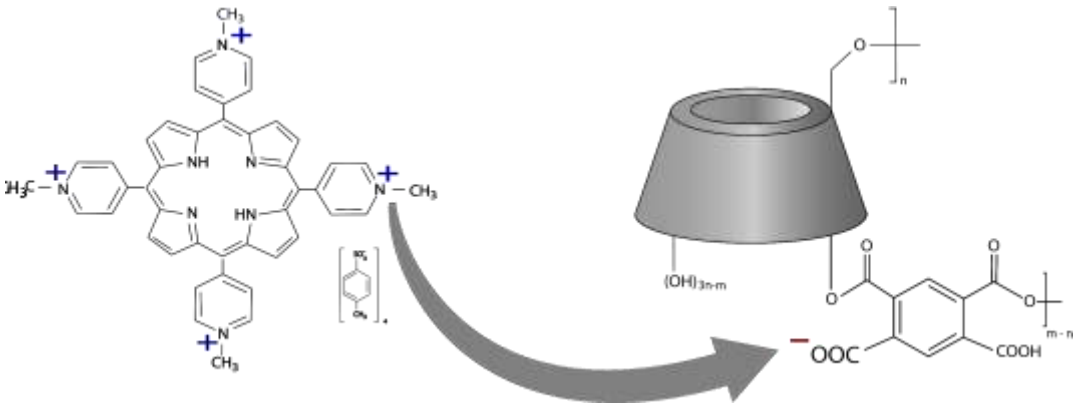

Figure 1-21 Interaction between TMPyP and βNS-PYRO (1:8)

The base principle of the preparation of this sample is to take advantage of the interaction between the positive charges on the four N-methyl-4-pyridyl moieties and the negative charges of the carboxylic group of the pyro nanosponge (Figure **1-21**). The preparation is the following: 50 mg of βNS-PYRO (1:8) are added in 10 mL of ultrapure water after complete dissolution of 2 mg of TMPyP. After 3h under stirring, the dispersion is centrifuged for 3 times, for removing the supernatant and washing the dispersed powder, removing the non-complexed porphyrin (adsorbed on surface, for example). After freeze-drying a red/brown powder is obtained (in Figure 1-42 the interaction between βNS-PYRO and porphyrin).

2.2 Results and Discussion

2.2.1 βNS-CDI (1-4)

Detail and parameter of synthesis have already been reported before.
If the reaction of crosslinking occurred, NSs shows a rigid and compact structure and then, fundamental characteristic, insolubility in water and organic solvents. Since primary hydroxy groups are involved in the formation of a network, there is a clear difference in ATR spectra of β-CD and cross-linked β-NSs [89]. The reaction is easily monitored by the appearance of a band around 1750 cm^{-1} in FTIR spectra related to the carbonyl group of the carbonate bond. This peak at 1750 cm^{-1} is missing from the IR spectrum of the plain β-CD [26]. In is worth to say that there is anyway necessity of further characterizations for knowing degree of cross-linking, such as Raman and solid-state NMR analyses. This syntheses and the followed procedures are anyway well known, so in this case the no further characterization where driven on the materials.
Compared spectra of βNS-CDI and native β-CD are reported in Figure 1-22:

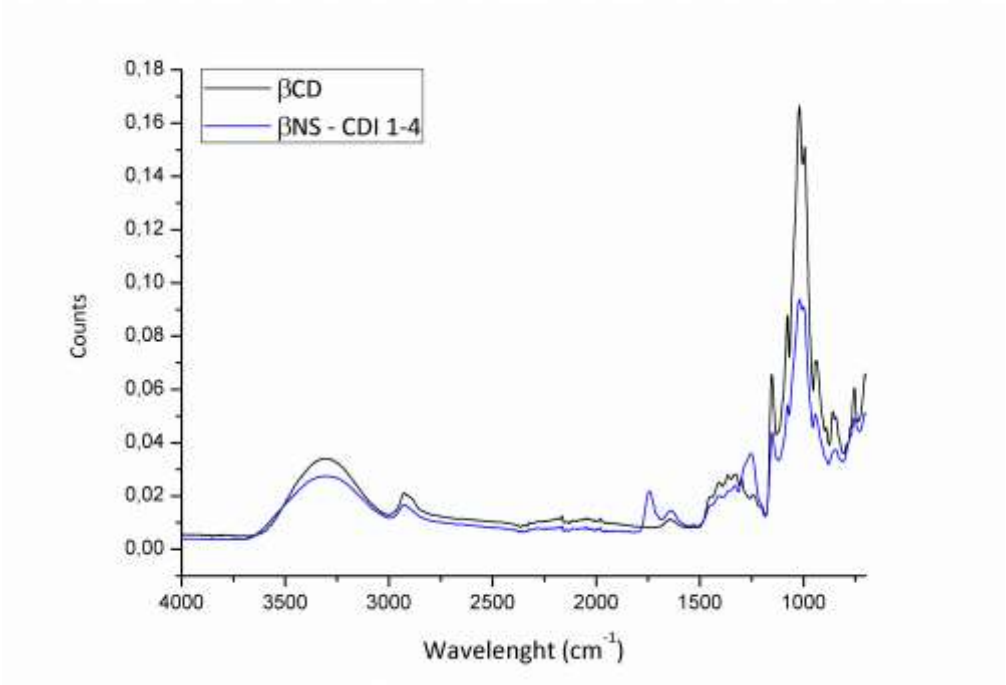

Figure 1-22 Comparison of ATR spectra of β-CD and cross-linked β-NS CDI. The peak of interest is the one at 1741 cm^{-1}, due to the carbonyl group of the carbonate bond

Thermogravimetric analysis, comparing the degradation path with a plain beta-cyclodextrin are reported in Figure 1-23, below.
The βNS-CDI(1-4) shows a higher degradation temperature than the non-crosslinked cyclodextrin: degradation, in N_2, starts at a temperature about 100° degrees higher (as reported in literature [92]).

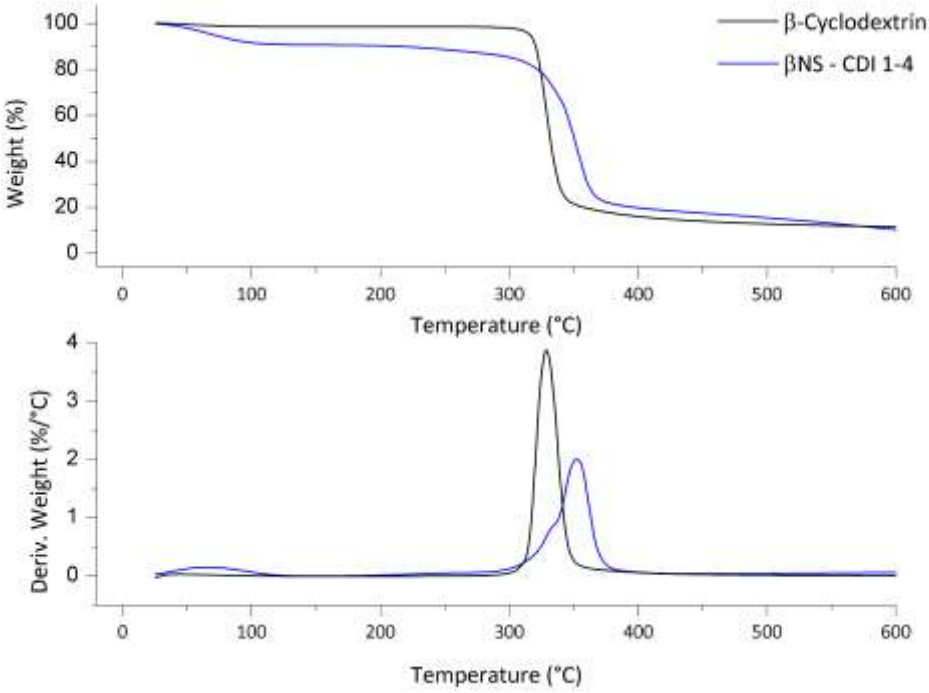

Figure 1-23 TG analysis of βCD and cross-linked βNS-CDI (1-4)

2.2.2 βNS-PYRO (1-4)

As already seen before for carbonate nanosponges (CDI), after crosslinking, mincing and purification, an insoluble powder is obtained. Since this type of NS contains a polar free carboxylic acid group, it can host boot apolar organic molecules and cations [26] and, furthermore, pyromellitic nanosponges swell considerably more than a carbonate NS in presence of water. This is significant for many reasons: every time we deals with this type of NS, must be taken into consideration the presence of water, adsorbed from the environment, and this is particularly significant with FTIR and TGA analysis (the signal of the water can interfere).
A FTIR spectrum of a NS-PYRO (in comparison with plain beta cyclodextrins) is showed below, Figure 1-24.

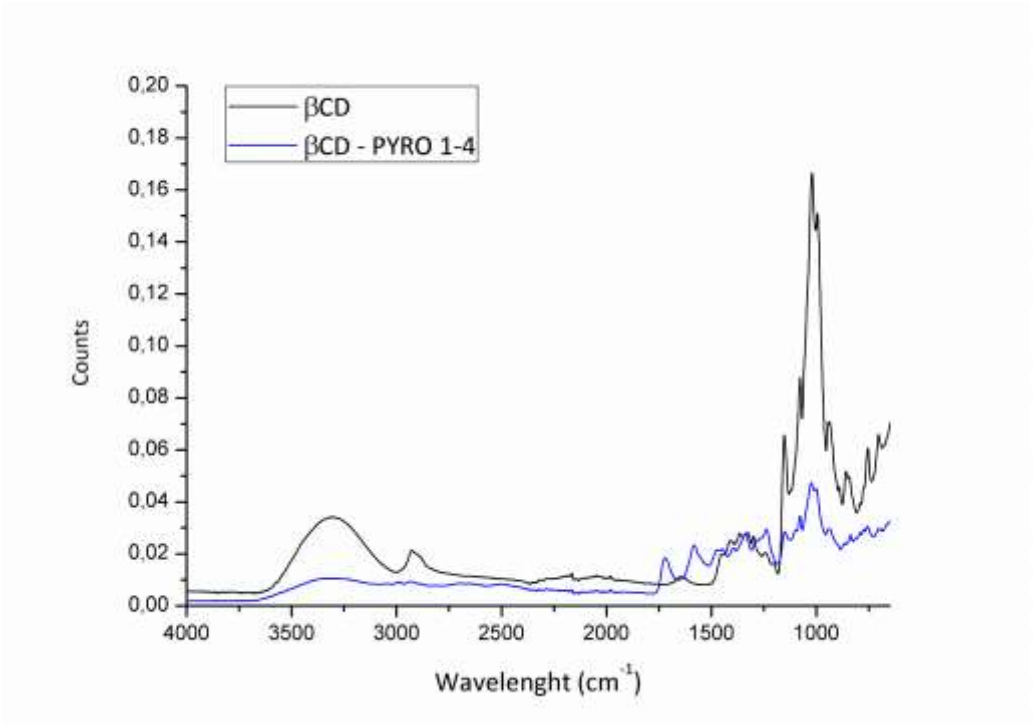

Figure 1-24 Comparison of ATR spectra of β-CD and cross-linked β-NS-PYRO

What is significant here is the clear band at 1727 cm^{-1}, relative to the ester carbonyl group (missing in the plain βCD).
As for CDI nanosponges, a TG analysis has been performed (Figure 1-25). The behavior is similar that seen previously and to examples in literature [92].

An interesting difference is in the quantity of residue: pyromellitic nanosponges exhibit a noticeably higher quantity of final residue, up to 40% (carbon char residue).

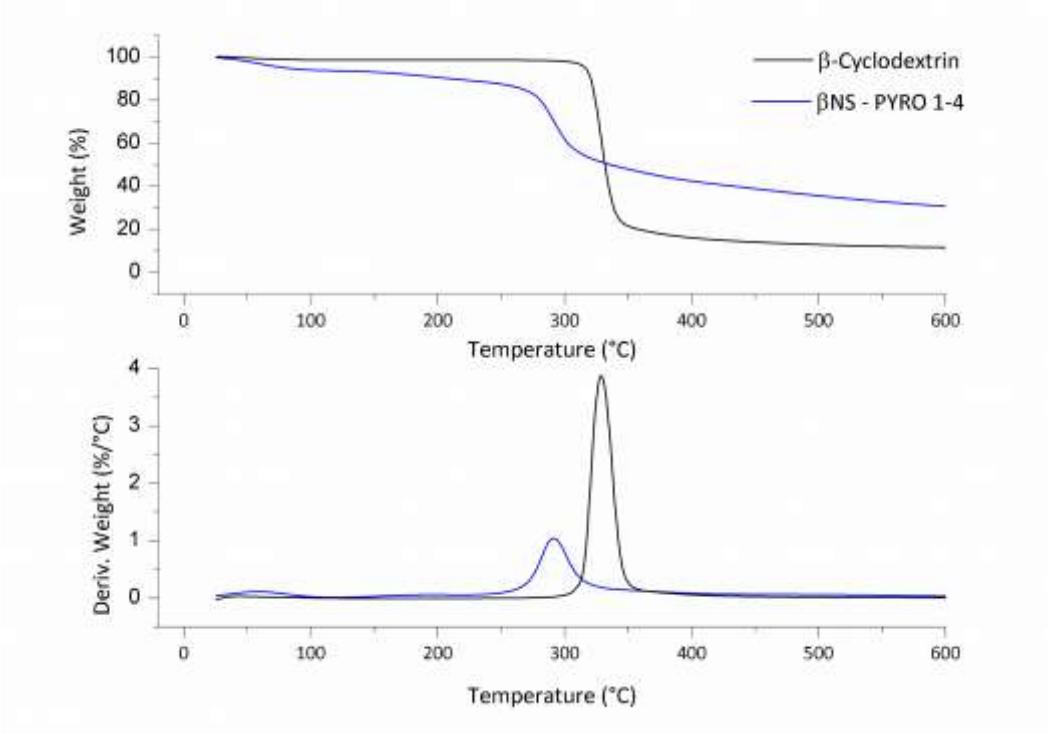

Figure 1-25 TG analysis of βCD and cross-linked βNS-PYRO (1-4)

2.2.3 Squaraine SQ Br-C4 characterization

Since the synthesis of the squaraine dye has already been discussed, most of this sub chapter will be dedicated to the characterization's techniques, on the final product and on the intermediates.
2,3,3-Trimethylindolenine and 5-carboxy-2,3,3-trimethyl-3H-indolenine are commercially available, the synthesis of the other derivatives was carried out with a Fisher indole synthesis using microwave instead of classic heating methods. Compared to traditional method of synthesis, MW assisted quaternarization (the nitrogen quaternarization increase the acidity of methyl group, enabling the bridge formation) permit to achieve higher yields and to shorten reaction times: time is decreased from 24h to about 9 minutes. Furthermore anhydrous condition are uninfluential with a MW performed reaction, as described by Barbero et al [90].
The ^{1}HNMR spectrum of the synthesized quaternarized indolenine ring is shown (Figure 1-26):

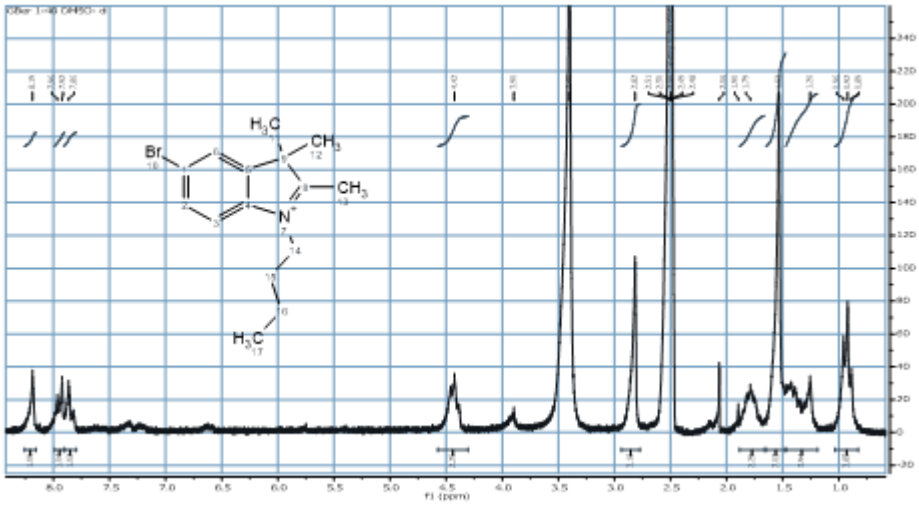

Figure 1-26 ^{1}HNMR of quaternarized indolenine

Reaction time is considerably shorter in the synthesis of the symmetrical squaraine dye, too: the last step takes about 30 minutes instead of 18-20 hours. In theory, by choosing a right amount of solvent it's possible to obtain direct crystallization of the dye inside the vessel, with high purity and no need of purification. In this synthesis the final squaraine dye needed a chromatographic purification in column. A preliminary 1HNMR measures showed the presence of

impurities, so purification was necessary. After column, the analysis HNMR on a first batch (used for the MIP syntheses) confirmed the structure through a comparison with spectra in literature.
1HNMR spectrum of SQ Br-C4 used for all MIP is showed in Figure 1-27 below:

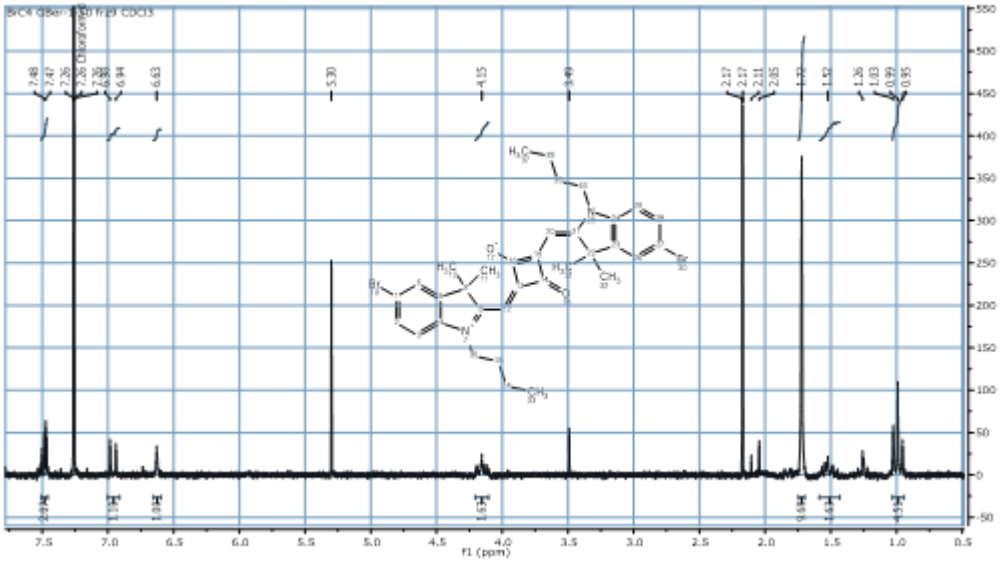

Figure 1-27 ^{1}HNMR of SQ Br-C4

The thermal stability of SQ Br-C4 was investigated using thermogravimetric analysis (Figure 1-30 inset B). As it can be observed there is no weight loss until almost 300°C. The TGA program for this measure is the following: 10°/min up to 800°C, in nitrogen. So SQ Br-C4 is not affected by the thermal treatments used during the synthesis procedure of the polycarbonate NSs, carried out at considerably lower temperatures.

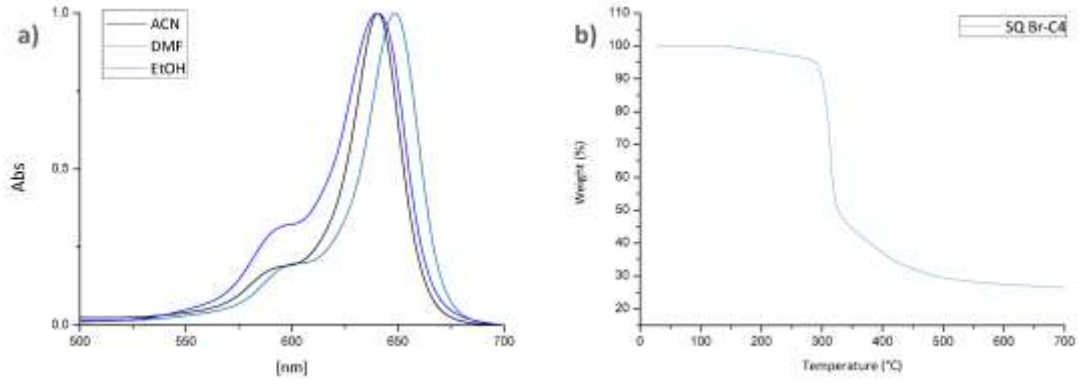

Figure 1-28 A) UV-VIS of SQ Br-C4 in different solvents: black for Acetonitrile, red for N,N-Dimethylformamide, blue for Ethanol B) Thermogravimetric Analysis for SQ Br-C4

In Figure 1-30, inset A, are reported the normalized UV-Vis spectra of the squaraine dye in different solvents: there is correspondence with spectra found in literature [90], showing a narrow peak at 650 nm for DMF and at around 640 nm for ACN and ethanol and a shoulder at 600 nm.

2.2.4 βNS-CDI+SQ Br-C4

FTIR-ATR analysis of the first MIP NS loaded with SQ Br-C4 is shown in Figure 1-29. As described before, MIP synthesis is quite similar to a traditional synthesis, but the presence of the template molecule can be an obstacle during the cross-linking process, because of the steric hindrance. This effect is particularly significant with guest molecule in the scale of cyclodextrins or larger (as reference: βCDs diameter ≈ 1.53 nm, with a cavity ≈ 7 Å) and in presence of large quantities of "charge". After the synthesis, a blue powder was obtained; the molecular structure of this powder is slightly similar to the "plain" βNS-CDI and this is demonstrated by the spectrum in Figure 1-29:

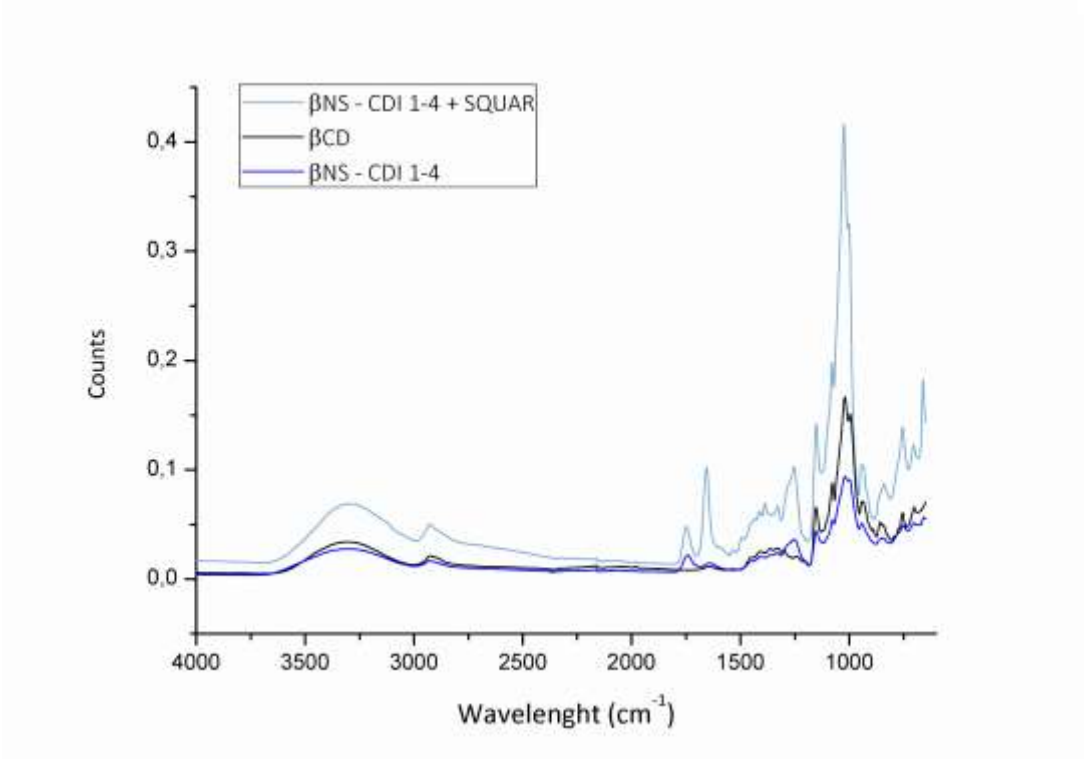

Figure 1-29 Comparison of ATR spectra of β-CD, cross-linked β-NS CDI and β-NS CDI+SQ. The peak of interest is the one at 1741 cm^{-1}, due to the carbonyl group of the carbonate bond

The peak at 1750 cm^{-1} shows the presence of a carbonate bond, as seen before. The main difference in the two spectra is the high e narrow peak at 1658 cm^{-1}: This peak can be related to the unreacted CDI, entrapped within the NSs bulk and not washed away. The presence of CDI is probably related to an incomplete cross linking, that lead to the presence of oligomer and not to a tridimensional

structure. Anyway, physico-chemical properties of the freshly prepared βNS-CDI+SQ Br-C4 are similar to a plain βNS-CDI: the material is insoluble in water and organic solvents (the powder is washed with deionized water during the synthesis).
Before proceeding in further characterization, a particle size distribution, via DLS, was carried out, evidencing a mean diameter around 700 nm.
Dealing with nanoparticles for drug delivery in aqueous solution, size distribution has a crucial role in obtaining a stable dispersion. According to the report, in this case there is an average diameter of 700 nm, but the presence of larger particle is assumable; what we can imagine it's that a consistent part of small particles can form a stable dispersion, but some relatively big particles will precipitate. The presence of two families can also be related to aggregation; all measures had been carried out, for limiting the problem, after sonicating for 10 minutes the NS/water dispersion.
Another crucial measure for colloid and water suspension, performed on βNS-CDI+SQ Br-C4, it's the ζ-potential, whose results are shown in Figure 1-30.

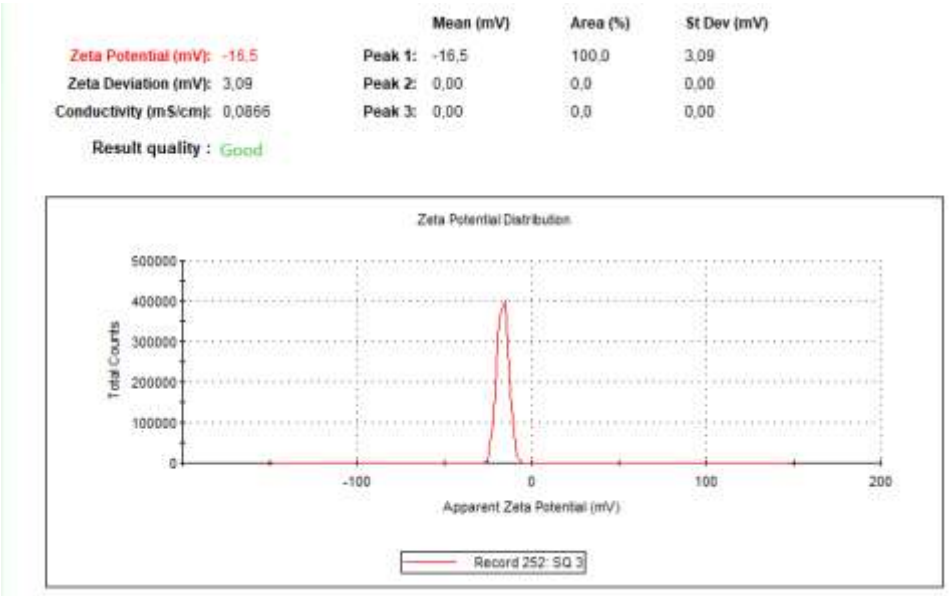

Figure 1-30 Zeta potential [mV] for βNS-CDI+SQ Br-C4

In theory, for small particles, a high (+ or -) zeta potential will confer stability, and the solution or dispersion will resist aggregation. When the potential is small,

attractive forces exceed this repulsion and the dispersion may break: colloids with high (negative or positive) ζ-potential are electrically stabilized while colloids with low zeta potentials tend to coagulate and/or flocculate. A colloidal is considerable as stable with a ζ-potential higher (+ or -) than 30-40 [93]. The examined dispersion presents a ζ-potential of -16,5, so only slightly negative, and this confirm the previous size results and the possibility of formation of aggregates.
Anyway, dimension and dispersion are acceptable for tests of ROS.

2.2.5 βNS-PYRO + SQ Br-C4

FTIR-ATR analyses of the second MIP NS loaded with SQ Br-C4 are reported in Figure 1-31. As described before, MIP synthesis is quite similar to a traditional synthesis, with a dye molecule during the crosslinking.

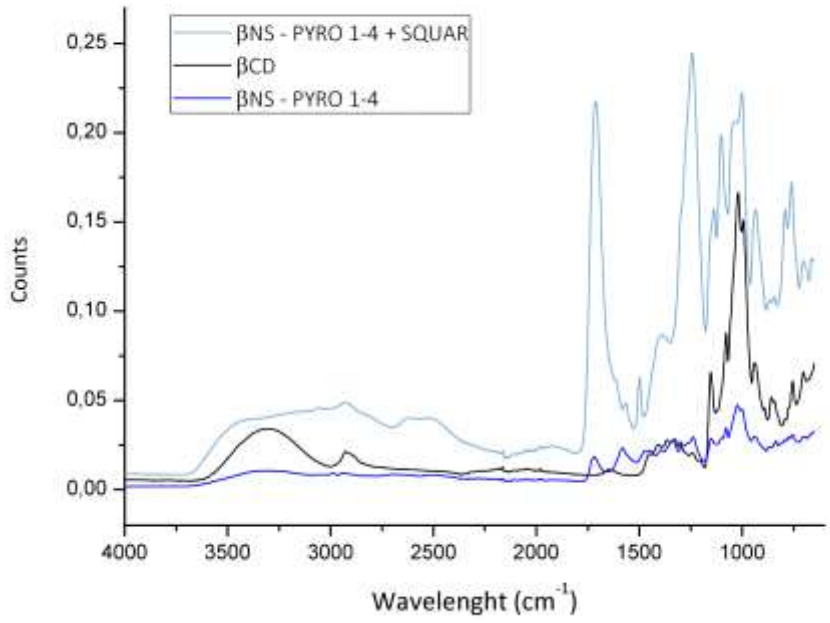

Figure 1-31 Comparison of ATR spectra of β-CD, cross-linked β-NS PYRO and β-NS PYRO+SQ

A clear band at 1727 cm^{-1}, relative to the ester carbonyl group, and a similar spectrum to the plain NS-PYRO in shown. From the FTIR spectrum is not possible to understand more than some qualitative information, the higher intensity of peaks relative to the SQ MIP nanosponges is probably related to the smaller dimension of particles (longer ball milling).
As for the carbonate sample, the particle size distribution and the ζ-potential were tested (Figure 1-32).

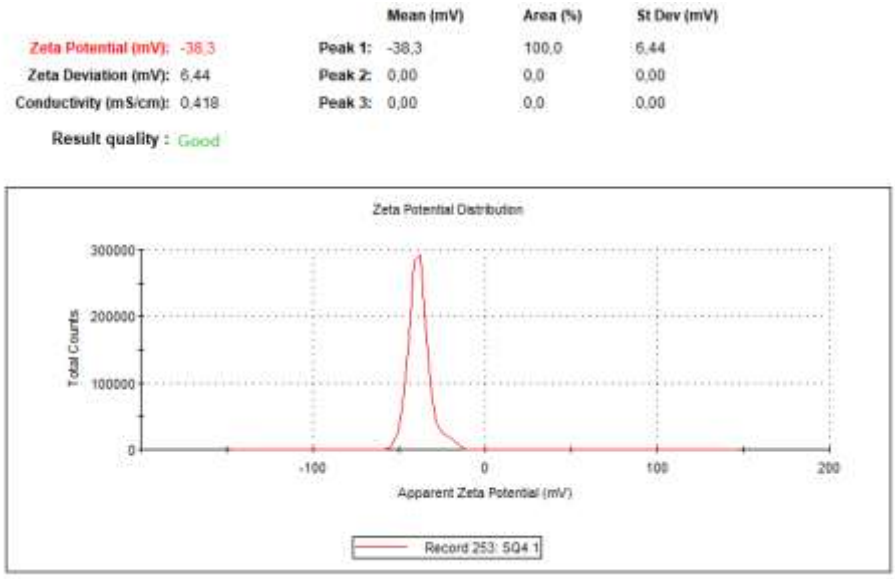

Figure 1-32 Zeta potential [mV] for βNS-CDI+SQ Br-C4

For the βNS-PYROI+SQ Br-C4, there are more interesting results: the ζ-potential is considerably higher (more negative). The molecular structure permits a better dispersion in water, because of the water affinity of the cross-linker itself. Furthermore, the high negative charge it's clearly due to the carboxylic group. Besides, the βNS-PYRO, if compared to a carbonate nanosponge, is usually not so resistant in a protic environment because of the ester bond (that can give hydrolysis). For what concern the average dimension: the mean diameter from DLS is around 450 nm, smaller than what seen for CDI.

These results led us to very interesting analysis: both samples were treated with the same ball mill, in the same way.
Of course, a different cross-linker gives different physical properties to the polymer bulk, but surprisingly when we measured the average particle

dimension for CDI, we found unexpected results: after different cycles of milling the dimension of CDI NSs was increasing.
Since was clear that a long high energy milling was modifying the molecular structure, we started a series of tests, that led us to all mechanochemistry related projects (Part 3). The carbonyl diimidazole inside the structure was indeed still able to react, forming new bonds within the nanosponge structure and increasing the particle size.
More details are reported in Part 3.

2.2.6 Reactive Oxygen Species - UV- Vis Measures

At experimental level, it's usually not simple to find a good probe molecule for ROS detection: there are many criteria to satisfy, such as stability in the appropriate solvent before irradiation, reproducibility, compatibility. An important limitation in case of UV-Vis analysis is the position in the spectra of the absorbance band of the photosensitizer: the squaraine dye in NS, for example, present a maximum peak of absorbance between 650 nm and 800 nm, so the probe for ROS must have a maximum (or a shoulder, a relevant peak) between 300-450 nm for avoiding any possible interferences with the photosensitizer signal.
Then solubility in water and/or in PBS (pH 7.4), to mimic physiological conditions, is necessary for this type of applications.
One of the first UV-Vis probes tested for my materials is the 1,3-Diphenylisobenzofuran (DPBF), one of the most used molecules in literature for this purpose [68] and used in previous work with the same halogenated squaraine [64].
Surprisingly, and unfortunately, since first tests on photostability without PS, the DPBF showed low stability at light (even for few minutes) and low reproducibility.
In Figure 1-33 and Figure 1-34 are shown preliminary tests in ethanol (DPBP is not soluble in water, but is also necessary to solubilize in an appropriate organic solvent and then dilute in water or PBS) and PBS. All spectra are collected after a minute since the dilution of the probe molecule in the appropriate solvent.

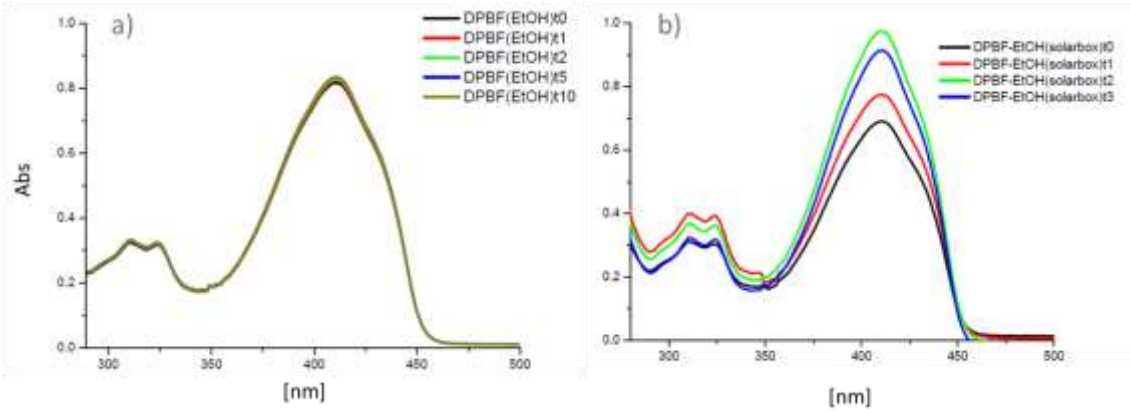

Figure 1-33 Absorption spectra of DPBP in EtOH A) without irradiation B) after irradiation sequences of 1 minutes in solar box

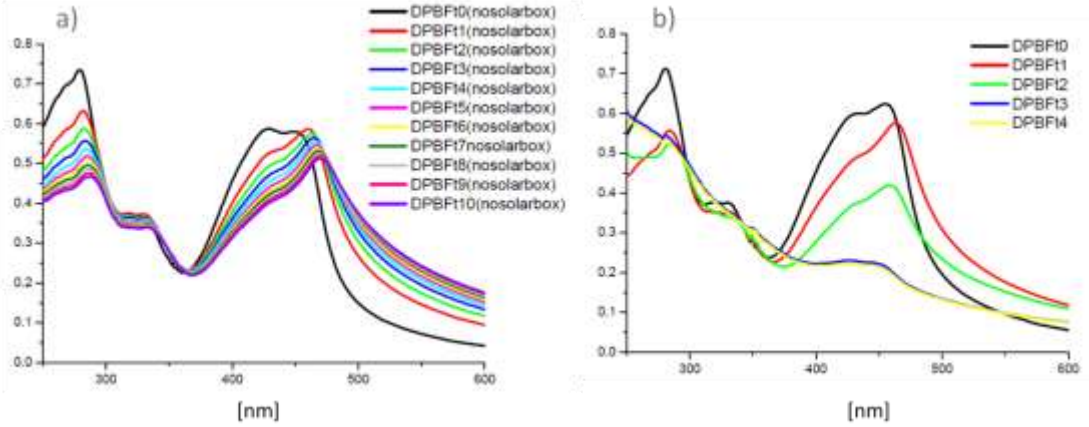

Figure 1-34 Absorption spectra of DPBP in PBS A) without irradiation B) after irradiation sequences of 1 minutes in solar box

As shown, the UV-Vis spectra of the probe molecule, even if not irradiated or if irradiated without a PS decrease in intensity. In PBS, moreover, is clear a shift in the peak maximum after irradiation.

Further tests were carried out using as probe molecule the 9,10-Dimethylanthracene, DMA (Figure 1-35 and the 9,10-Anthracenediyl-bis(methylene)dimalonic acid, ABDA (Figure 1-36), probe molecules more sensible to singlet oxygen and not for a wide range of ROS [68]. Results are shown in the following pictures:

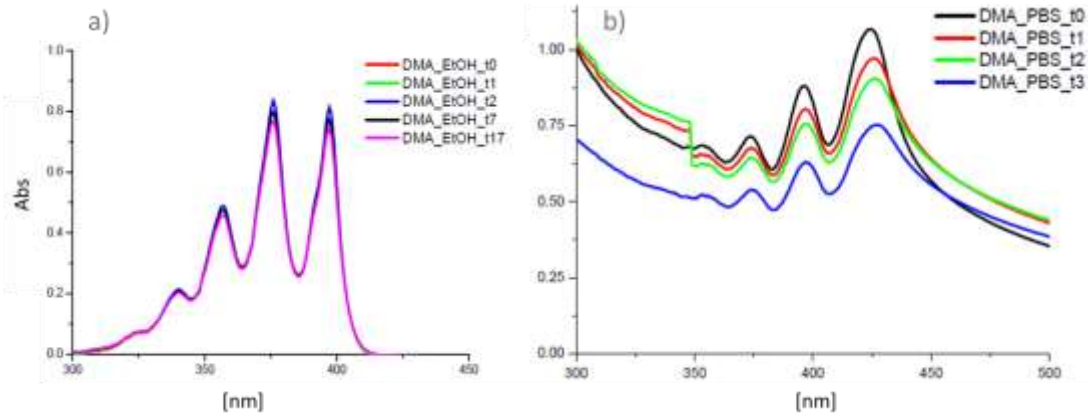

Figure 1-35 Absorption spectra of DMA A) in EtOH B) in PBS both with irradiation sequence of 1 minutes in solarbox

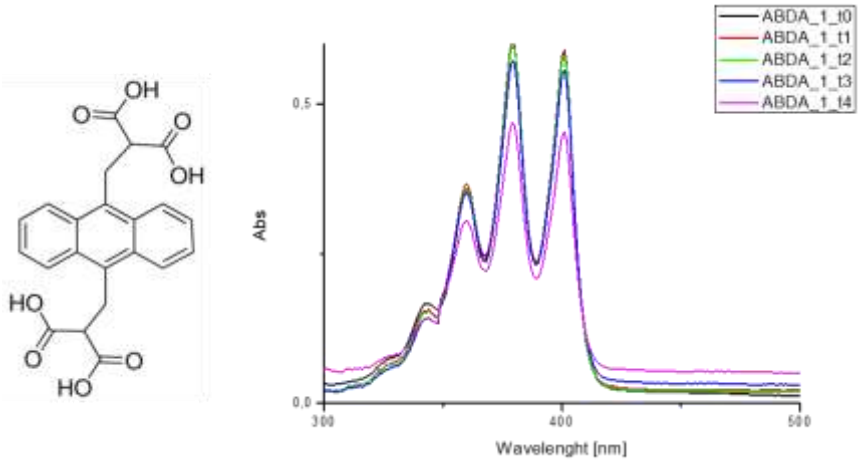

Figure 1-36-Absorption spectra of ABDA in PBS. t4 spectrum is collected after 20 min of irradiation.

As is possible to see, the DMA exhibits good stability even after irradiation in EtOH, but the situation is completely different in phosphate buffer: the spectra intensity decrease fast and as is possible to see in Figure 1-35, inset B, there is also some scattering. The scattering phenomenon is usually related to the presence of non-solubilized reagent or nano-microparticle, so can be related to the low water solubility of DMA. A different probe must be used.

A totally different situation is shown in Figure 1-36: ABDA is water soluble (and this is also presumable from the structure) and in PBS, after irradiation is stable.

Only after 20 min of continuous irradiation in solar box (250 W/cm^2) there is an evident lowering in the absorption spectrum.
After preliminary tests, ABDA had been used for tests with different dyes, and for molecularly imprinted polymers with halogenated squaraine and NS with encapsulated dyes.
In following picture (Figure 1-37) a comparative study of the ability in generate singlet oxygen of the samples previously described. The tests are carried out by trapping $^1O_2$ with 9,10-Anthracenediyl-bis(methylene)dimalonic acid and monitoring at different time the disappearing of the band at 328 nm.

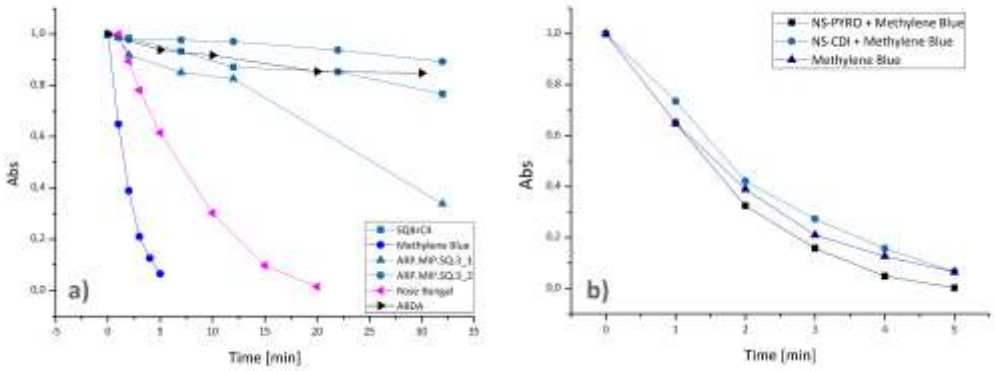

Figure 1-37 A) Singlet oxygen generation of synthetized Squaraine Br-C4, βNS-CDI+SQ and Bengala Pink using Methylene Blue as standard reference B) Comparison of singlet oxygen generation between Methylene Blue and methylene blue loaded on ester and carbonate NS

As is clear in Figure 1-37, inset A, using the methylene blue as reference, the squaraine dye BrC4 (2 tests, with a repetition of the NS test) shows surprisingly a totally different behavior if compared with studies with DMA in literature [64]. This is probably related to the different species of reactive oxygen generated by different dyes ant to the different probes reactivity: methylene blue generates ROS of many type, singlet $^1O_2$ and $O_2^{-\cdot}$. ABDA is selective for singlet oxygen a this is also confirmed by the test with Bengala Rose, known as a selective $^1O_2$ generator [68].
So, the conclusion is that halogenated squaraine BrC4 may only generate O_2-·, so is not detected by the ABDA instead reacting with the DMA.
Since the priority of my study is to develop an efficient drug delivery system for photoreactive species, a major doubt was the influence in ROS generation of the nanosponges.

In Figure 1-37, inset B, there is a preliminary study of the influence of the crosslinked polymers in singlet oxygen (all tests carried out with ABDA) with methylene blue, since this dye gave good results and reproducibility.
As is possible to see, the nanosponge not only does not prevent production of $^1O_2$ but using a pyromellitic nanosponges, the signal of the probe decay even faster than with the dye alone.
New tests with different dyes and different NS are needed to confirm the trend.

2.2.7 Reactive Oxygen Species – EPR

Since the results with UV-Vis measures and probe are only partially encouraging and there is a lack of specificity in reactive species detection [68] we performed also EPR measures to cross results and to confirm what seen with a completely different technique. All measurement reported in this work were performed by Dott. Enzo Laurenti in the Department of Chemistry in Turin.
All this work is at a preliminary stage and some test were just carried out at sunlight and not in solar box, only for determining if a dye is a specific ROS generator or not.
Following images present results of tests on methylene blue in water solution (as seen for tests in

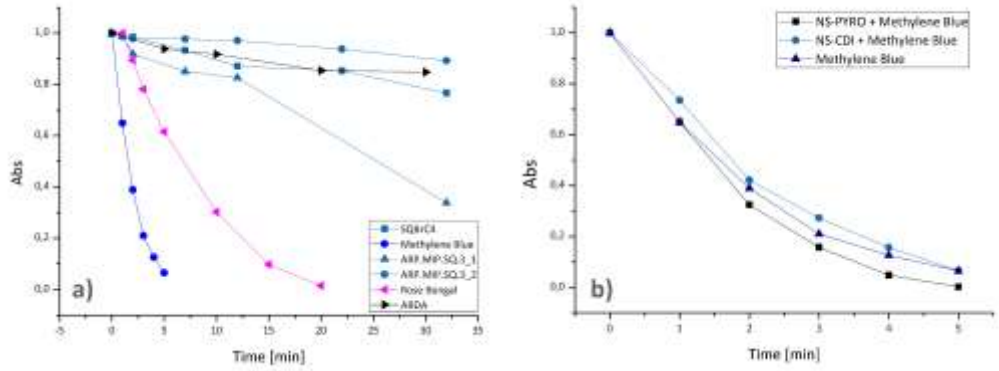

, B) with and without the support of an ester nanosponges (since the pyromellitic NS gave interesting results).
Preliminary tests were carried out using two different spin traps (already available in laboratory):

- 5,5-Dimethyl-1-pyrroline N-oxide (**DMPO**), that form spin-adduct with ·OH and can partially detect superoxide (difference in the shape of derivative spectrum)[94]
- 3,3,5,5-tetramethyl-1-pyrroline-1-oxide (**TMPO**)), that form spin-adduct with singlet oxygen $^1O_2$

I will report here only first tests, with methylene blue and DMPO as spin adduct (Figure 1-38 and Figure 1-39):

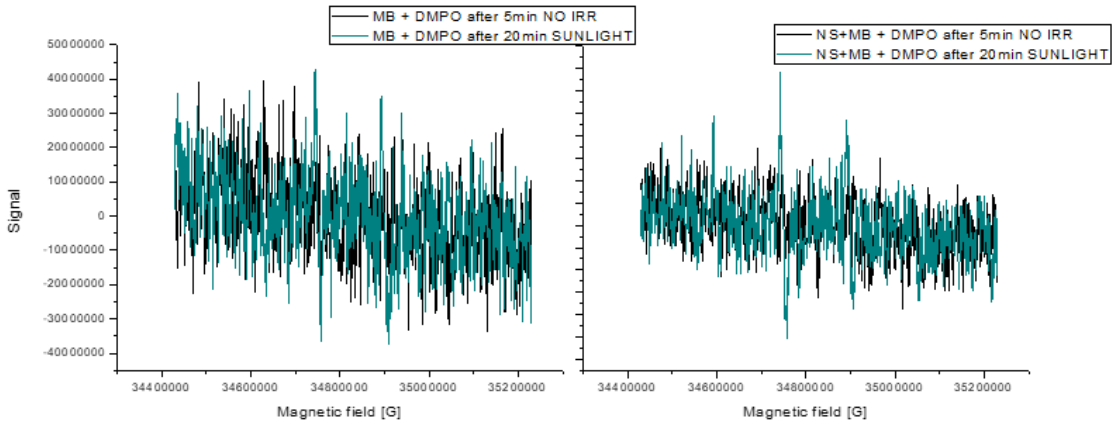

Figure 1-38 DMPO spin trap EPR analysis of methylene blue and methylene blue+ βNS-PYRO, in water solution

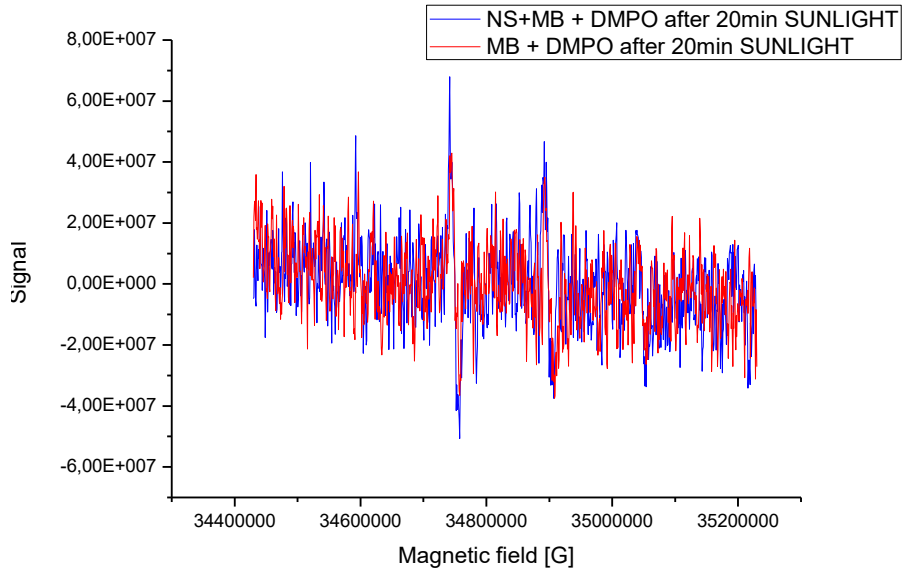

Figure 1-39 Comparison of EPR spectra of MB and βNS-PYRO + MB

The signal relative to the spin adduct is, in all pictures, not intense but still visible.
Characteristic EPR spectral profiles can be observed, with 2 major peaks in the center and 2 lower peaks at the sides [94].
What it is worth to highlight is in Figure 1-39 as seen with UV-Vis measures, so with a completely different technique, ester nanosponges with methylene blue seem to enhance the ROS production.
After these preliminary results new tests were carried out with more specific and refined experimental conditions.
Sunlight was substituted by a solar box set at 250 W/cm^2 and the exposition at light is limited to 5 minutes.
Condition were chosen after several tests at different irradiation times and light intensity. The two samples reported here (Figure 1-40 and Figure 1-41) refers respectively to a PBS solution of methylene blue 10^{-6} M and to a dispersion of βCD NS-PYRO loaded with methylene blue. Spectra are recorded using a flat cell, to decrease the signal-noise ratio.
The concentration of the dye in the solution and dispersion is the same. In the next pictures, the EPR spectra:

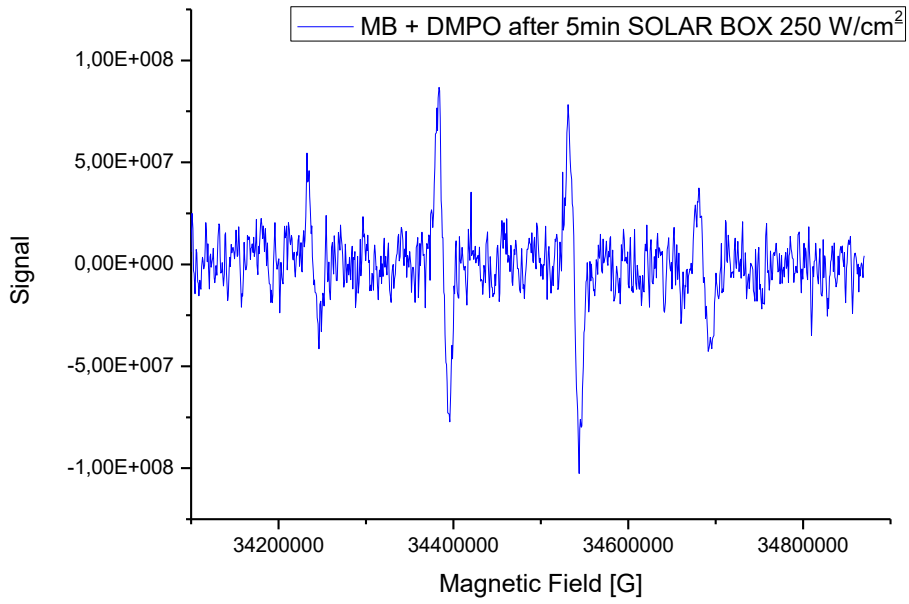

Figure 1-40 DMPO spin trap EPR analysis of plain methylene blue in PBS solution

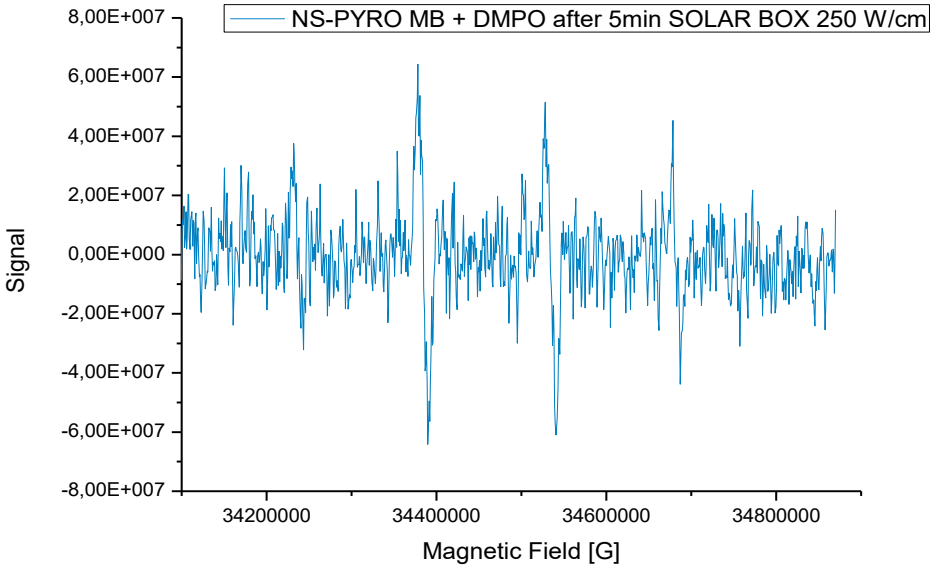

Figure 1-41 DMPO spin trap EPR analysis of βNS-PYRO +methylene blue

In this case too, the signal of the DMPO is clearly visible in both samples.
Further tests are now ongoing with different organic dyes and cross-linked material.

2.2.8 βNS-PYRO/ TMPyP (CNR – ISMN Messina)

The supernatant and the washing solution were characterized with UV-Vis spectrophotometer to quantify the NON encapsulated TMPyP.
The percentage of captured porphyrin is so determined by difference.
30,5 % of the porphyrin is inside the βNS-PYRO (1:8) structure, so the weight percentage of load is 1,3% (wt. TMPyP /wt. βNS-PYRO (1:8)).
In the following picture, a probable structure of βNS-PYRO/ TMPyP is reported.

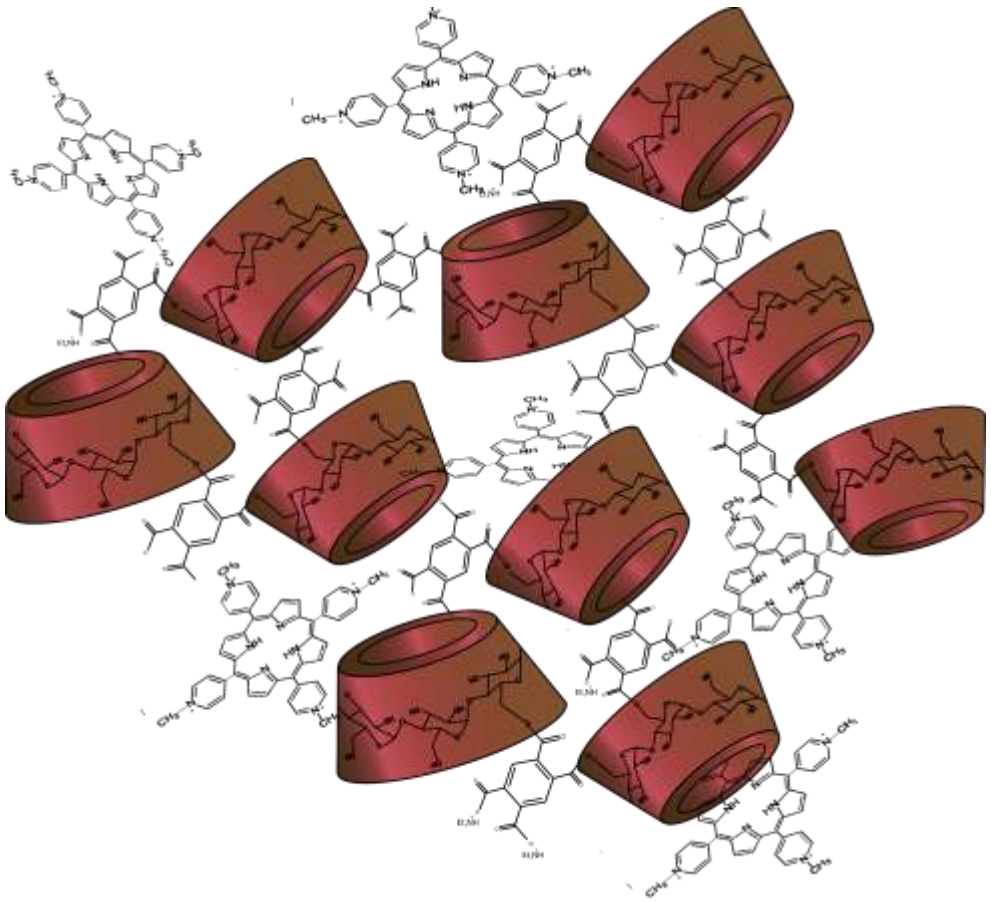

Figure 1-42 Representation of probable structure of βNS-PYRO/ TMPyP.

A calibration curve for TMPyP was built, using a solution with a known concentration of TMPyP and as solvent, the supernatant water of a blank βNS-PYRO (1:8) dispersion.
The results are the following, shown in Figure 1-43:

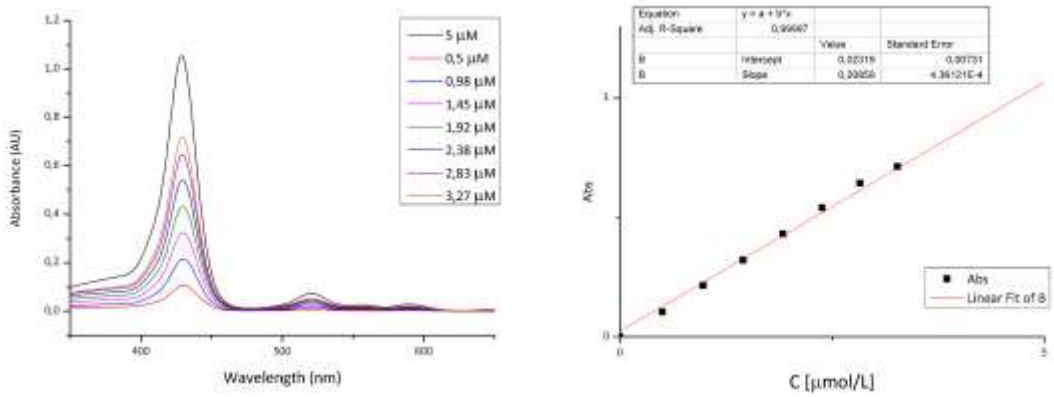

Figure 1-43 UV-Vis spectra and calibration curve for βNS-PYRO/ TMPyP

The obtained powder dispersed in water, 1mg in 5mL, displayed a hydrodynamic diameter around 300 nm and a still negative zeta potential (-45 mV, Figure 1-44). The obtained dispersion is stable and shows no aggregation or changes in ζ-pot after 3 days.
The UV spectrum of the dispersion is shown in the following picture:

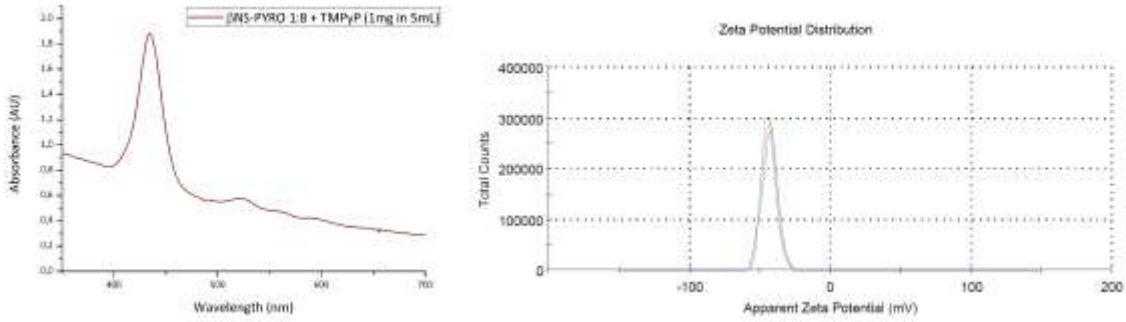

Figure 1-44 UV-Vis spectrum and ζ potential distribution of a βNS-PYRO/ TMPyP water dispersion (1mg in 5 mL).

On the same dispersion fluorescence measure of emission and excitation have been carried out, results are in the following pictures (Figure 1-45).

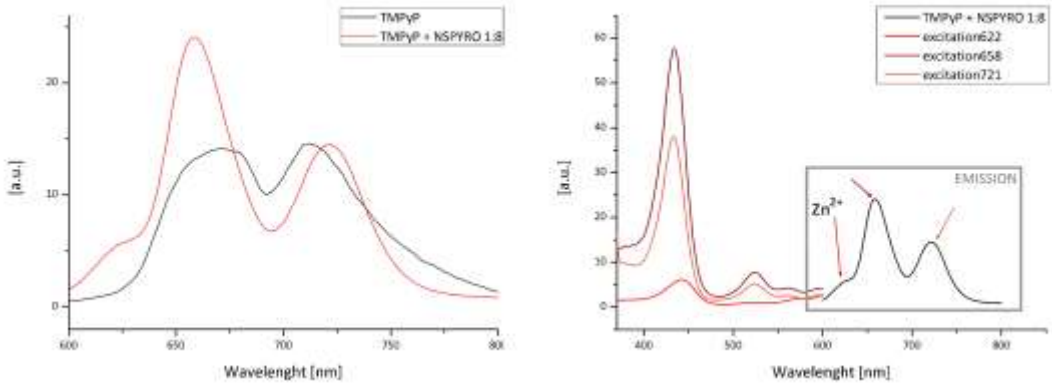

Figure 1-45 Steady state fluorescence emission (λexc = 448 nm, left) and excitation (right) of TMPyP (a) and TMPyP/βNS-PYRO in aqueous solution; [TMPyP] = 8 μM, r.t = 25°C.

As shown in Figure 1-45 on the left, the shape of the emission spectra dramatically changes.

Excitation spectra (excitation respectively at 622 nm on the shoulder, and 658 and 721 nm) show the presence of different species, one probably related to the presence of Zn^{2+} in the porphyrin.

On the same sample time-resolved fluorescence characterizations were carried out.

The time-resolved fluorescence lifetime measurements are a steady state, absolute (independent of concentration) measurement of the fluorescence emission decay. The emission of a fluorophore is influenced by its environment or the presence of other interacting molecules.

Fluorescence anisotropy or fluorescence polarization is the phenomenon where the light emitted by a fluorophore has unequal intensities along different axes of polarization. Fluorescence anisotropy is a measure of the depolarisation of the fluorescence emission. The main reasons for depolarisation include the energy transfer to another molecule with a different orientation or molecular rotation caused by Brownian motion. Molecular motion depends on local environmental factors, such as viscosity and molecular confinement, and the size of the molecule. Thus, a measurement of fluorescence anisotropy is useful in obtaining information concerning molecular size and mobility.

In Figure 1-46, results of time-resolved fluorescence lifetime and anisotropy on sample βNS-PYRO/ TMPyP are shown:

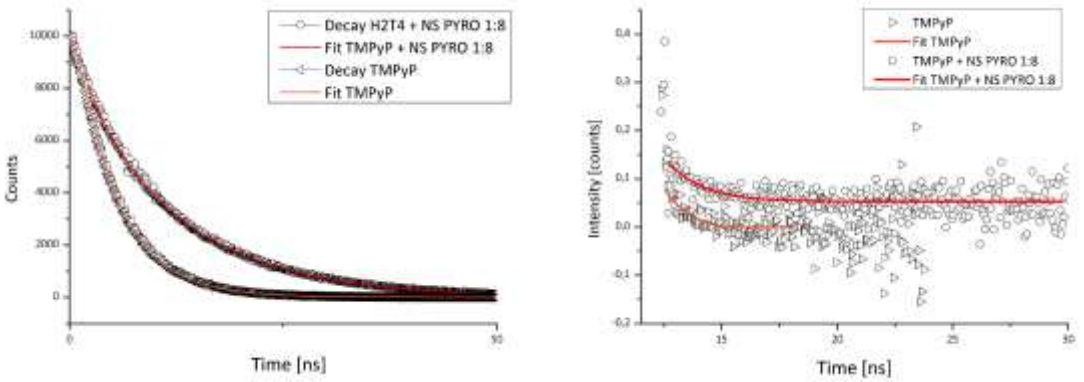

Figure 1-46 (Right) Time-resolved fluorescence anisotropy: comparison of free TMPyP (orange, triangles) and βNS-PYRO/ TMPyP (Left) Time-resolved fluorescence lifetime measurements of TMPyP: comparison of free TMPyP (orange, triangles) and βNS-PYRO/ TMPyP.

Both analyses presented in Figure 1-46 clearly shows an interaction between the molecule of TMPyP and the structure of the NS. The NS seems to avoid the aggregation of TMPyP, extending the fluorescence lifetime and the fluorophore is not fully free to rotate, showing a non zero limiting anisotropy in the anisotropy decay. Spectroscopic evidences indicate the good dispersion of the PS in aqueous solution, related to the entrapment in βNS-PYRO.

2.3 Conclusions

New cross-linked biopolymers with squaraine dyes were synthesized, and different dyes and porphyrins have been loaded on cross-linked biomaterials. Obtained materials showed a different behavior compared to traditional analogue nanosponges.
Nanosponges, furthermore, showed an influence in the ROS production, measured with different techniques (UV-Vis, EPR).
A novel nano photosensitizer has been successfully prepared based on electrostatic interaction between an anionic cyclodextrin nanosponge and a cationic porphyrin as photosensitizer.
The formation of CD nanoconstruct was confirmed by the use of complementary spectroscopic techniques and a photosensitizer loading of 1,3 % wt was obtained.
In vitro photo antibactericidal studies are in due course to elucidate the aPDT efficacy of these new photosensitizers.

The planned experiments regarding this macro project are the following:

- To study on the ability of the βNS-CDI+SQ Br-C4 and βNS -PYRO+SQ Br- C4 ability to generate reactive oxygen species, both with UV-Vis and EPR, with more experiments
- To complete βNS-PYRO/ TMPyP characterization with: release tests, singlet Oxygen measures, stability tests in PBS, H2O, BSA, FBS
- Synthesis and characterization of a NanoSponges-MIP (molecular imprinted polymer) with ZnPC
- A study, both *in vitro* and *in vivo,* of the photodynamic activity of these new materials

3 Mechanochemical Synthesis

Since NS are biocompatible and nontoxic are a powerful tool in the wide field of the nano drug delivery[32], [36], [89] but as seen the preparation of nanosponges involves the presence of organic and often toxic solvents.
As seen, the most common NSs synthetic pathway consist in dissolving, under continuous stirring, the chosen CD in a suitable solvent and then adding the crosslinker and, if necessary, a catalyst. The solvents are usually organic polar aprotic liquids, for example dimethylformamide (DMF) or dimethylsulfoxide (DMSO).
An alternative synthetic route is via interfacial polymerization: two immiscible solution, one of CDs dissolved in an alkaline solution and the other one of the crosslinker in a chlorinated solvent, are mixed and stirred. At the interface between the two solution, crosslinking occurs [37].
The presence of solvent of course affects the whole synthesis, because, especially for biomedical application, the final material has to be accurately cleaned by an extraction procedure with an excess of water or volatile solvents, for removing all the solvent inside the batch (and inside the material structure). This problem is even more important for a possible scale up of the reaction, where huge amounts of solvent to dispose of are involved. Moreover, organic solvents are expensive and DMSO and DMF are hard to recycle because of the high boiling point.
According to the Green Chemistry Principles, published in 1998[95], processes have to be designed in order to "minimize the quantity of final waste and to avoid hazardous or toxic solvents". Nanosponges themselves, nevertheless, are synthesized from starch derivatives and are biodegradable, so are a very promising material from this point of view.
Here a new, green, synthesis of nanosponges through mechanochemistry is proposed.
We synthetized NS via mechanochemistry testing different crosslinkers: 1,1-Carbonyldiimidazole (CDI) and diphenylcarbonate for CD based carbonate NS, hexamethylene diisocianate (HMDI) and toluene-2,4-diisocyanate (TDI) for carbamate NS, Sodium trimetaphosphate for phosphate NS and Bisphenol A diglycidyl ether (BADGE) for ether NS.
Then, among the many type of cyclodextrin nanosponges we focused on the carbonate NS, synthetized with 1,1-Carbonyldiimidazole as crosslinker, for many reasons: the reaction is usually driven at 90°C, so the heating of the system

related to the ball friction (against the wall of the milling jar and between the spheres themselves) is not only acceptable but useful for the kinetic of the reaction, and the solvent for solubilizing reactants is DMF.
So, we are here reporting a new green synthesis of biodegradable polymers, with wide application in many different fields, obtainable from renewable raw materials with a synthesis free of any solvent.
After the synthesis was detected the presence of a significant amount of still reactive imidazolyl carbonyl groups within the NS structure.
The presence of a "tunable" quantity of still reactive groups can be used for further easy functionalization and permitted us to easily obtain a covalent bond between the already synthetized cyclodextrin nanosponges and different organic dyes, with different structure (Methyl Red, Rhodamine B and Fluorescein), used as probe molecules. The possibility to easy-functionalize cyclodextrins NS, in this case via reactive imidazole moieties, is particularly interesting for many possible applications. Dye modified Cyclodextrins and CD derivatives are widely used for the preparation of chemical sensors [96][97]. Moreover, the possibility to easy obtain CD, and consequently CD-Nanosponges, marked with fluorophores could open many applications in the pharmacologic area, for example for biological markers and image guided therapies [98]–[100] or conjugated drugs delivery.
Because of the procedure, other active molecules can be grafted on the NS, obtaining a conjugate nanocarrier, liming or in certain cases avoiding the use of organic solvents.

In my research work, moreover, the possibility to easy functionalize directly in synthesis, with a "one step" reaction, was tested with different compounds.
For example, we tried, successfully, to attach PEG chains directly on CD Nanosponges.
Coating the surface of nanoparticles with polyethylene glycol (PEG), (the so called "PEGylation), is a commonly used approach for improving the efficiency of drug and gene delivery. PEG coatings on nanoparticles shield the surface from aggregation, opsonization, and phagocytosis, and can help to prolong the systemic circulation time, indeed.
Polyethylene glycol is one of the most used "stealth" polymers in the wide drug delivery field, classified by the FDA as Generally Regarded as Safe (GRAS).
In 1990, the FDA approved the first PEGylated protein product, a PEGylated adenosine deaminase enzyme for severe combined immunodeficiency disease [101]. The great success of protein PEGylation as a method for producing longer circulating intravenous therapies led, in the early 80's and 90's, to the application

of nanoparticle PEGylation for systemic applications. Moreover, thanks to the EPR effect, NPs can preferentially accumulate inside the tumor tissue [102].
Since PEGylated NPs are capable of stably circulating in the blood, they can be potentially utilized to similarly target other diseases characterized by abnormal neovascularization, including several ocular disorders, diabetes, obesity, asthma and multiple sclerosis [103].
There are many parameters that can influence the final result such as PEG molecular weight and its surface density and the repeated administration impact circulation time [104]. This will be partially investigated also in this dissertation. The main goal in my work is anyway a new synthetic pathway for the obtaining of PEGylated NPs, in this case CD-NSs, via mechanochemistry and without the use of any solvents in the whole process (except the water for the suspensions). The "one step" procedure for the functionalization of NSs was carried out also with Folic Acid (FA). As seen for PEGylation, also for FA the final aim is to target cancer cells. FA is one of the most common compounds that has been used to target overexpressed-folic acid receptor on the surface of cancer cells. Therefore, conjugation of FA to nanoparticles permits to enhance the delivery of therapeutic agents [105][106].

It is worth to say that that synthesis and characterization on this compound are still ongoing and further investigations are needed for confirming the formation of a covalent bond (e.g. Solid State Nuclear Magnetic Resonance, SS-NMR).

In vitro and *in vivo* tests, moreover, are now ongoing on all functionalized NSs, to prove, respectively, an effective stealth and tumor targeting effect.

3.1 Experimental

3.1.1 Materials

α-cyclodextrin (α-CD), β-cyclodextrins (β-CD) and γ-cyclodextrins (γ-CD), linear Maltodextrins (GLUCIDEX®2 and KLEPTOSE® Linecaps Maltodextrin from Roquette) were kindly provided by Roquette Italia SpA (Cassano Spinola, Italy) and purchased from Wacker Chemie. 1,1-Carbonyldiimidazole (CDI), Diphenylcarbonate (DPC), Hexamethylene diisocianate (HMDI), Toluene-2,4-diisocyanate (TDI), Bisphenol A diglycidyl ether (BADGE), 1,4-Diazabicyclo [2.2.2] octane (DABCO), Methyl Red, Rhodamine B, Fluorescein, Folic Acid, dimethylformamide (DMF), Choline Chloride, acetone and ethanol were purchased from Sigma Aldrich (Munich, Germany) and used with no further purification. Dextrins were dried before use, in oven until constant weight.
Poly (ethylene glycol) (PEG) at different Mw (750, 1000, 2000, 6000) was purchased from Sigma and freeze dried before used (for removing absorbed water).
Elemental Analysis: performed on a Thermo Scientific FlashEA 1112, using Vanadium Pentoxide purchased from Sigma.
Ball Mill: Retsch PM200 High Speed Planetary Ball Mill, 20 sintered zirconium oxide balls of 10 mm diameter; 16 mL (volume) of sintered zirconium oxide balls of 3 mm diameter; 2 jars of 50 mL (with 10 balls or 16 mL, for having the same weight, 60g, in each jar), also in zirconium oxide.
Thermogravimetric Analysis were carried out on a Hi-Res TGA 2050 Thermogravimetric Analyzer from TA Instruments.
IR spectra on dried powders were recorded on a PerkinElmer Spectrum 100 FT-IR Spectrometer with 16 scans.
Zeta Potential and DLS measure were performed on Zetasizer Nano ZS from Malvern Panalytical
Solvent extraction for purifying samples is carried out with a Pressurized Solvent Extractor (PSE) SpeedExtractor E-914 from Buchi.

3.1.2 Solvent synthesis of Dextrins Nanosponges (for comparison tests)

The reported procedures refer to the "classic" or "solvent" synthesis, so the procedure is the one described in most of NSs literature and, here, in the section dedicated to Photoactivated therapies. Synthesis described herein, anyway, refers to the samples freshly synthetized for a comparison with samples from ball mill synthesis: the scale of the reaction is similar, and the conditions are the most "common" (conditions can be tuned according to the final application).

3.1.2.1 Solvent synthesis of Cyclodextrins Carbonate Nanosponges

The procedure for the batch preparation of βNS-CDI is the following: 7.87 grams of β-CD (desiccated in oven at 120°C for at least 2-3 days) are dissolved in 47.0 ml of anhydrous dimethylformamide (DMF) under vigorous stirring, then 4.49 grams of CDI are added. Then, after complete solubilization of reactants, the solution is heated, under reflux, to 80-90°C. After 30 minutes the gelation process occurs.
The already formed NS is then milled and cleaned with an excess of deionized water in order to remove the DMF and unreacted monomers and imidazole.
A further purification is performed by Soxhlet extraction with ethanol and/or acetone (at least a week of Soxhlet).

For the Carbonate Nanosponges with Diphenil carbonate as crosslinker: 6,00 grams of β-CD (desiccated in oven at 120°C for at least 2-3 days) are dissolved in 47.0 ml of anhydrous dimethylformamide (DMF), then 5.10 grams of DPC are added. Then, after complete solubilization of reactants, the solution is sonicated for 3-4h and heated at 80°C. The crosslinked polymer precipitates as a white powder. The NS is cleaned with an excess of deionized water in order to remove the DMF and unreacted monomers and residual phenol. A further purification is performed by Soxhlet extraction with ethanol and/or acetone.

3.1.2.2 Solvent synthesis of Cyclodextrins Carbamate Nanosponges

The procedure for the preparation is the following: 3.75 grams of β-CD (desiccated in oven) are dissolved in 13 ml of DMSO under vigorous stirring.

After complete solubilization 1.85 grams of HMDI are added. The gelation process occurs immediately.
The already formed NS is then milled and cleaned with an excess of deionized water, ethanol and/or acetone.

The preparation using TDI, follows the same experimental conditions.
3.75 grams of β-CD are dissolved in 13 ml of DMSO under vigorous stirring. After complete solubilization of the dextrins 2.00 grams of TDI are added. The gelation process occurs immediately and already formed NS is then milled and cleaned with an excess of deionized water, ethanol and/or acetone.

3.1.2.3 Solvent synthesis of Cyclodextrins Ether Nanosponges

The procedure is the following: 4.0 grams of β-CD (desiccated in oven for at least 2-3 days) are dissolved in 30 ml of DMSO under vigorous stirring. After complete solubilization of the dextrins 4.20 grams of BADGE are added. The gelation process occurs immediately.
The already formed NS is then milled and cleaned with an excess of deionized water, ethanol and/or acetone.

3.1.2.4 Solvent synthesis of Linear Dextrins based Phosphate Nanosponges

4.0 grams of β-CD (desiccated in oven) are dissolved in 9.5 ml of water solution of NaOH 1.5 M, then 4.04 grams of STMP are added.
After complete solubilization of reactants, 15 minutes and the gelation process occur. The already formed NS is then milled and cleaned with an excess of deionized water, ethanol and/or acetone.

3.1.3 Ball Mill synthesis of Dextrins Nanosponges

Different Dextrin cross-linked polymers were prepared using the ball mill, all through a one-step reaction without solvent. Conditions and parameters of Ball Milling for are different and described in detail for each synthesis. The Milling conditions are reported in **Table 1-2**.

3.1.4 Ball Mill synthesis of Cyclodextrins Carbonate Nanosponges

α, β, γ CD Carbonate Nanosponges made in ball mill respect a 1:2, 1:4 and 1:8 molar ratio of anhydrous cyclodextrin and carbonyl diimidazole. For example, for the 1:4 ratio synthesis: 3.38 g of α-CD, 3.75 g of β-CD and 4.56 g γ-CD, respectively, were inserted inside the 50 mL jar with 10 zirconia balls. The added amount of CDI in each batch for maintaining the 1:4 molar ratio is 2.25 g.
After 3h of sun wheel rotation at 600 rpm, with clockwise to anticlockwise change of direction every 15 min, the reaction is completed and the external temperature is between 50-60°C (temperature from previous studies in literature is indicated as always lower than 72°C in different conditions [85]). The finely ground powder is then dispersed in water and ashed several times with deionized water and acetone. After the washing, all samples are extracted with Pressurized Solvent Extraction (PSE), with acetone, for removing the residual imidazole in the NS the structure

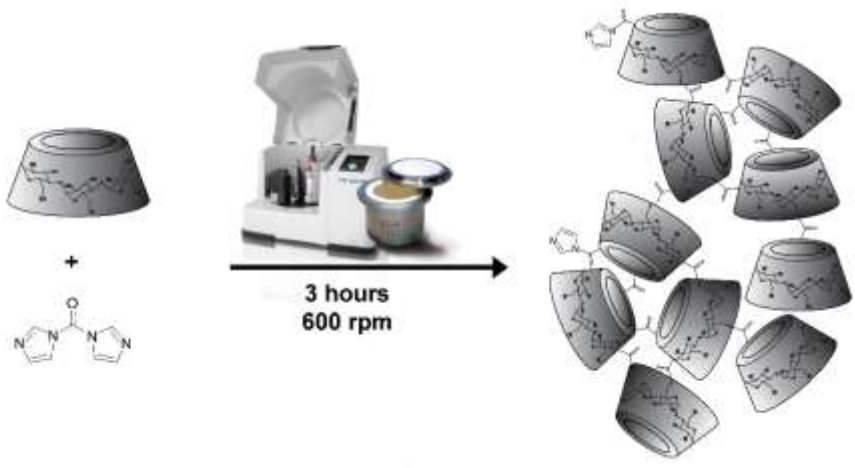

Figure 1-47 Simplified representation of a Ball Mill synthesis, using CDI as cross-linker

β-CD Carbonate Nanosponges 1:4 using diphenylcarbonate as cross-linker were prepared with the following procedure: 3.00 g of β-CD and 2.26 g of diphenilcarbonate were inserted inside the 50 mL jar with 16 mL (60 g) of zirconia balls with 3mm of diameter. After 4h of sun wheel rotation at 600 rpm, with clockwise to anticlockwise change of direction every 10 min, the finely ground powder is dispersed in water and washed several times with deionized water and acetone, and, dried at air. Mass balance is around 57%.

3.1.5 Ball Mill synthesis of Cyclodextrins Carbamate Nanosponges

β-CD Carbamate Nanosponges 1:4 using TDI and HMDI as cross-linkers were prepared with the following method: 3.75 g of β-CD and 2.00 g of TDI and 1.85 g of HMDI were inserted inside two different 50 mL jars with 16 mL (60 g) of zirconia balls with 3mm of diameter. We used 300 mg of DABCO as a catalyst. After 1h of sun wheel rotation at 600 rpm, with clockwise to anticlockwise change of direction every 10 min, the finely ground powder is dispersed in water and washed with deionized water and acetone, dried at air.
Mass balance is around 60% for HMDI Nanosponges and about 75% for TDI

3.1.6 Ball Mill synthesis of Cyclodextrins Ether Nanosponges

β-CD Ether Nanosponges 1:4 using BADGE as cross-linker were prepared with the following procedure: 3.75 g of β-CD and 4.50 g of Bisphenol A diglycidyl ether were inserted inside the 50 mL jar with 16 mL (60 g) of zirconia balls with 3 mm of diameter and 300 mg of DABCO. After 1h of sun wheel rotation at 600 rpm, with clockwise to anticlockwise change of direction every 10 min, the obtained bulk is ground in mortar and the powder is ball milled again for 30 min with water. The dispersion is centrifuged and washed several times with deionized water and acetone, and, eventually dried at air. Mass balance is around 55%.

3.1.7 Functionalization of Carbonate cyclodextrins Nanosponges

The functionalization is driven with the same procedure for all samples: 500 mg of Carbonate (CDI) βNS 1:2, 1:4, 1:8 (molar ratio between β-CD and cross-linker, as said before) are dispersed in anhydrous DMSO. An excess of organic dye (50 mg of dye, a 10% wt of the NS), respectively Methyl Red, Rhodamine B and Fluorescein is then added to the dispersion. The dispersion is heated for 4h at 85°C in an oil bath. The final product is washed with an excess of water and then extracted with acetone using a PSE for removing the unreacted dyes.

3.1.8 Ball Mill synthesis of Positively Charged Ether Dextrins Nanosponges

Positively Charged Linecaps and β-CD based Ether Nanosponges 1:4 using BADGE as cross-linker and Choline Cl as positive functionality were prepared with the following procedure: 3.75 g of dextrins (β-CD and LC, respectively) and 4.50 g of Bisphenol A diglycidyl ether were inserted inside the 50 mL jar with 16 mL (60 g) of zirconia balls with 3mm of diameter and 300mg of DABCO and 1g of Choline Cl. After 1h of sun wheel rotation at 600 rpm, with clockwise to anticlockwise change of direction every 10 min, the two obtained bulks are ground in mortar and the powder is ball milled again for 30 min with water. The dispersion is centrifuged and washed several times with deionized water and acetone, and, eventually dried at air. Mass balance is around 36%. The presence of choline and positive charge is confirmed by elemental analysis and zeta-potential: zeta potential is, respectively, +19 mV for βCD NS and +12 mV for LCNS. The amount of Nitrogen is around 1,50% wt. for both samples.

3.1.9 Ball Mill synthesis of PEGylated NS

PEGylated βCD based Carbonate Nanosponges 1:8 using PEG with different Mw were prepared (Figure 1-48, route a). The same molar ratio between CD, crosslinker and PEG was maintained for all samples: 1: 8: 0.25.
For all synthesis: 3,75 g of β-cyclodextrins, respectively, were inserted inside the 50 mL jar with 10 zirconia balls and the appropriate amount of PEG. The added amount of CDI in each batch for maintaining the 1:8 molar ratio is 4.50 g.
After 3h of sun wheel rotation at 600 rpm, with clockwise to anticlockwise change of direction every 15 min the finely ground obtained powder is then

dispersed in water and washed several times with deionized water and acetone. After the washing, all samples are extracted with Pressurized Solvent Extraction (PSE), with ethanol, for removing the residual imidazole in the NS the structure and, more importantly, the unreacted PEG.
This procedure was repeated for each sample.
Details about the particle size reduction steps and procedures are reported in section 3.2.

3.1.10 Ball Mill synthesis of FOLIC ACID NS

Folic Acid functionalized βCD based Carbonate Nanosponges 1:8 were prepared with 1 : 8 : 1 molar ratio between CD, crosslinker and folic acid, respectively (Figure 1-48, route b).
After 3h of planetary rotation at 600 rpm, clockwise to anticlockwise change of direction every 15 min, a yellow, finely ground powder is obtained.
The product is dispersed in water and washed several times with deionized water and acetone. After the washing, Nanosponges are extracted with Pressurized Solvent Extraction (PSE), for removing the encapsulated and non-bonded folic acid, byproduct and unreacted. The exaction steps were carried out with different solvents: acetone, water and acetone again after washing 2 times at 80°C with DMSO (Folic Acid is soluble in DMSO, and DMSO is miscible with Acetone). A simplified reaction scheme of the expected (but still to be confirmed) final structure is reported below:

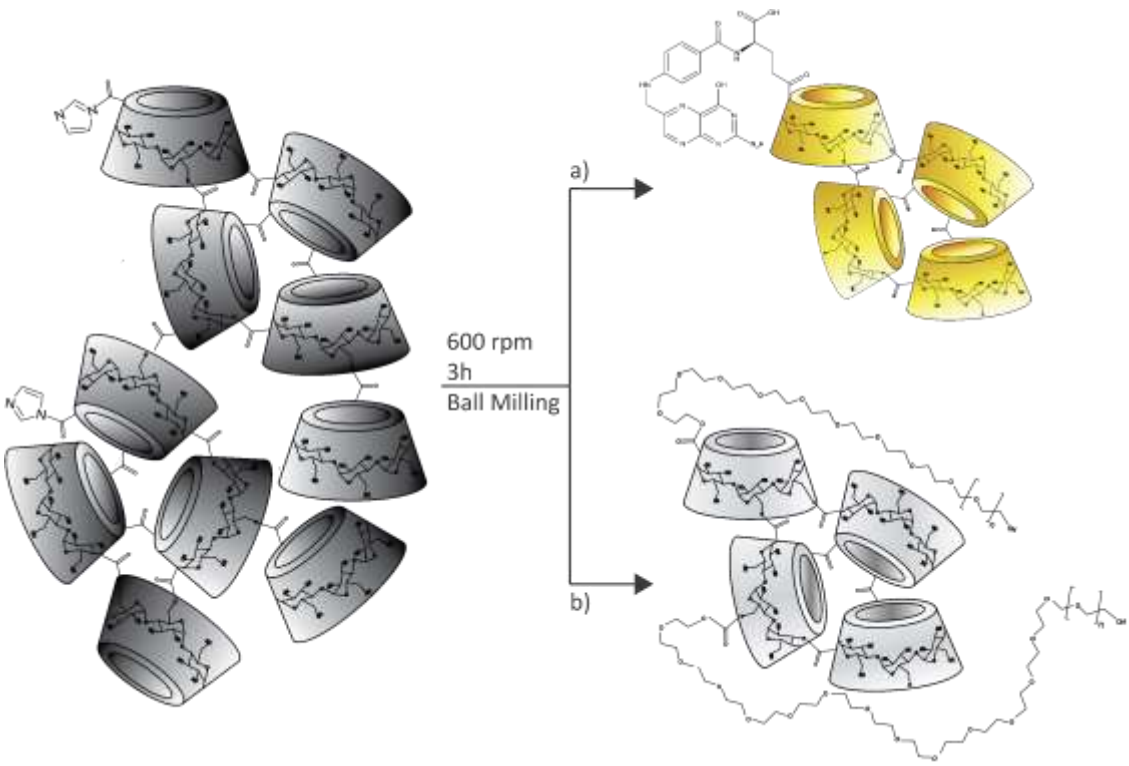

Figure 1-48 Simplified representation of the syntheses of a Folic Acid a) and PEGylated b) NS Ball Mill, using CDI as cross-linker, and plausible structure of the final product. Time and conditions are the same for both syntheses, except for the active compound added. Route b) Mw=750, 1000, 2000, 6000

3.2 Results and discussion

3.2.1 Comparison with Solvent Synthesis

We performed various synthesis, using different cyclodextrins and linear dextrins and changing the molar ratio between cyclodextrin and crosslinker, time and synthesis parameters. All the synthetized polymers are reported in Table 1-2. The abbreviation β-NS-CDI bm will refer to a cross-linked cyclodextrin polymer, NS, based on β-cyclodextrins and obtained by crosslinking with CDI, in ball mill (bm). For linear dextrins we will refer to Linecaps by using LC and to Glucydex by using GLU. The same abbreviation is used for α and γ cyclodextrins. The number following the crosslinker in the abbreviation refers to the molar ratio between cyclodextrins and crosslinker.
Three different ratios, 1:2, 1:4 and 1:8, were tested using the βcyclodextrin.
The mass balance for all samples is between 50-60%, higher, around 68% for βCD Carbonate, Carbamate Nanosponges, with γ yields over 90%, lower (30-60 %) for Phosphate NS.
It is worth to say that the reproducibility for all syntheses is very high since the operator has very few operations to do (just weighting the reactants) and most of parameter are set in the instrument.

Reaction conditions need to be further investigated for obtaining higher yields with all crosslinkers.
Dealing with synthesis totally conducted in a ball mill device (and with a one-step reaction) the parameters that can have an influence are the diameter of balls, the time of milling, the rotation speed and the direction reversal time. The diameter of the balls influences the contact surface of the milling process and consequently the internal temperature (smaller balls lead higher surface exposed and higher friction) and the impact force (related of course to the weight of the balls). Rotation speed and the reversal time also influence the temperature (with reversal time we refer to the possibility to set the instrument to change the rotation from clockwise to anticlockwise direction, and backward, for obtaining a better mixing and heating control).

Table 1-2 – Ball Mill set up and parameters

Nanosponge	Ball Mill Parameters			
	Balls diameter	Time [min]	rpm	Dir. Rev. Time [min]
αNS-CDI – 1:4 bm	10mm	180	600	15
βNS-CDI – 1:4 bm	10mm	180	600	15
γNS-CDI – 1:4 bm	10mm	180	600	15
βNS-CDI – 1:2 bm	10mm	180	600	15
βNS-CDI – 1:8 bm	10mm	180	600	15
βNS-DPC – 1:4 bm	3mm	240	600	10
βNS-HMDI – 1:4 bm	3mm	60	600	10
βNS-TDI – 1:4 bm	3mm	60	600	10
βNS-BADGE – 1:4 bm	3mm	60	600	10

The first step in characterization, since a new synthesis is proposed, is a comparison with the cross-linked polymer from the solvent synthesis, that will be always be referred to by "DMF synthesis". The solubility in various common solvents of the new nanosponges was tested (Table 1-3).

Table 1-3 – Ball Mill Synthesis of Cyclodextrin NS and relative solubility in tested solvents

Nanosponge	Solvent						
	Water	Ethanol	Acetone	Dimethyl formamide	Dimethyl sulfoxide	Diethyl ether	Petroleum ether
αNS-CDI – 1:4 bm	-	-	-	-	-	-	-
βNS-CDI – 1:4 bm	-	-	-	-	-	-	-
γNS-CDI – 1:4 bm	-	-	-	-	-	-	-
βNS-CDI – 1:2 bm	-	-	-	-	-	-	-
βNS-CDI – 1:8 bm	-	-	-	-	-	-	-
βNS-DPC – 1:4 bm	-	-	-	-	-	-	-
βNS-HMDI – 1:4 bm	-	-	-	-	-	-	-
βNS-TDI – 1:4 bm	-	-	-	-	-	-	-
βNS-BADGE – 1:4 bm	-	-	-	-	-	-	-

Cyclodextrins NS from ball mill synthesis are insoluble in the tested solvents, in accordance to the formation of a crosslinked network and with data from previous literature [37].
In the following pictures (Fig. 3-3 to 3-8) a FTIR qualitative analysis is reported, for all synthetized polymers divided by cross-linker (on the left ball mill NS, bm, on the right classic solvent synthesis).

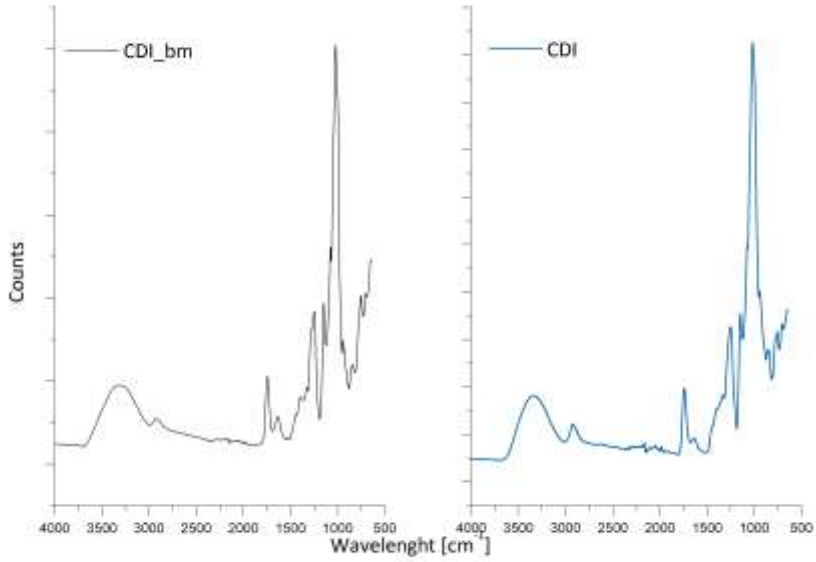

Figure 1-49 FTIR Analysis of Carbonate Nanosponges βNS-CDI 1:4, with 1,1-Carbonyldiimidazole as a cross-linker. On the left mechanochemical synthesis, on the right classic solvent synthesis

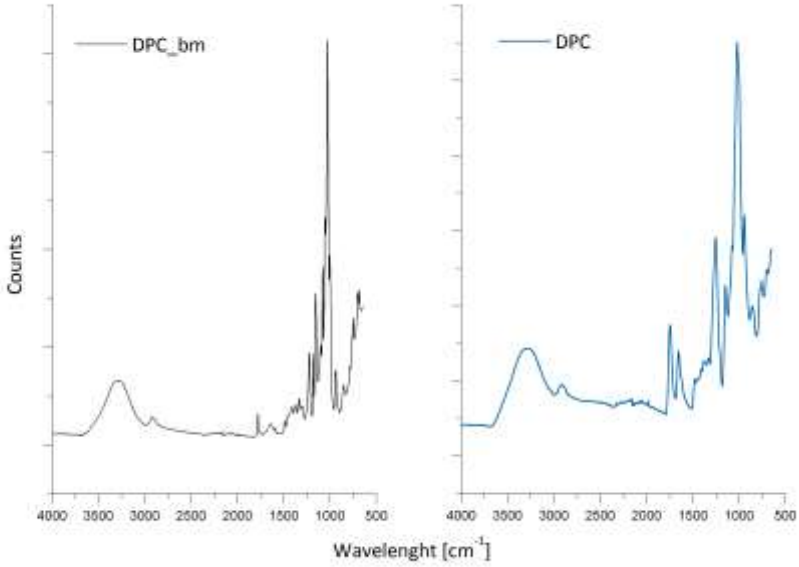

Figure 1-50 FTIR Analysis of Carbonate Nanosponges βNS-DPC 1:4, with Diphenyl carbonate as a cross-linker. On the left mechanochemical synthesis, on the right classic solvent synthesis

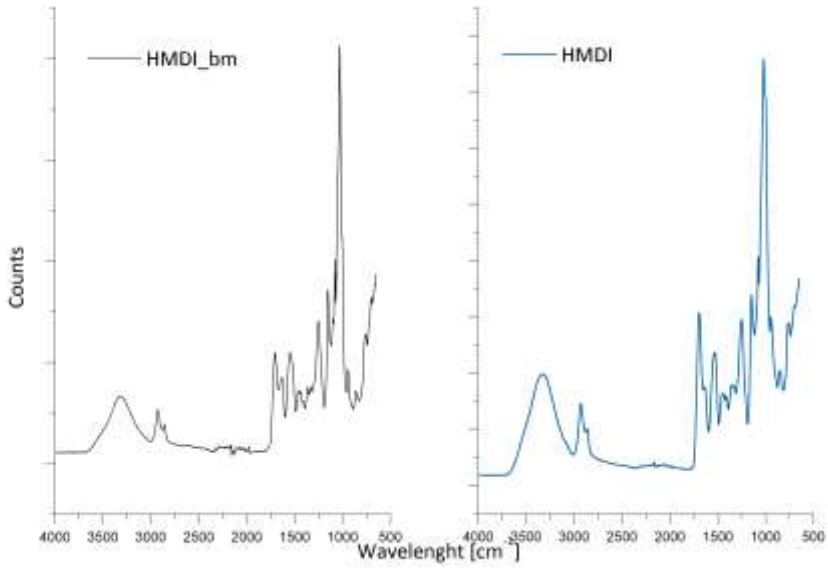

Figure 1-51 FTIR Analysis of Carbamate Nanosponges βNS-HMDI 1:4, with Hexamethylene diisocianate as a cross-linker. On the left mechanochemical synthesis, on the right classic solvent synthesis

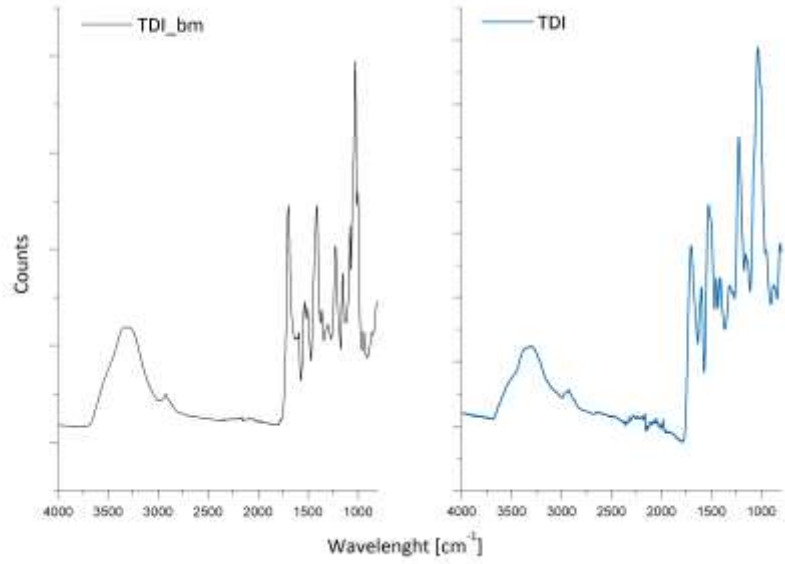

Figure 1-52 FTIR Analysis of Carbamate Nanosponges βNS-TDI 1:4, with Toluen diisocianate as a cross-linker. On the left mechanochemical synthesis, on the right classic solvent synthesis

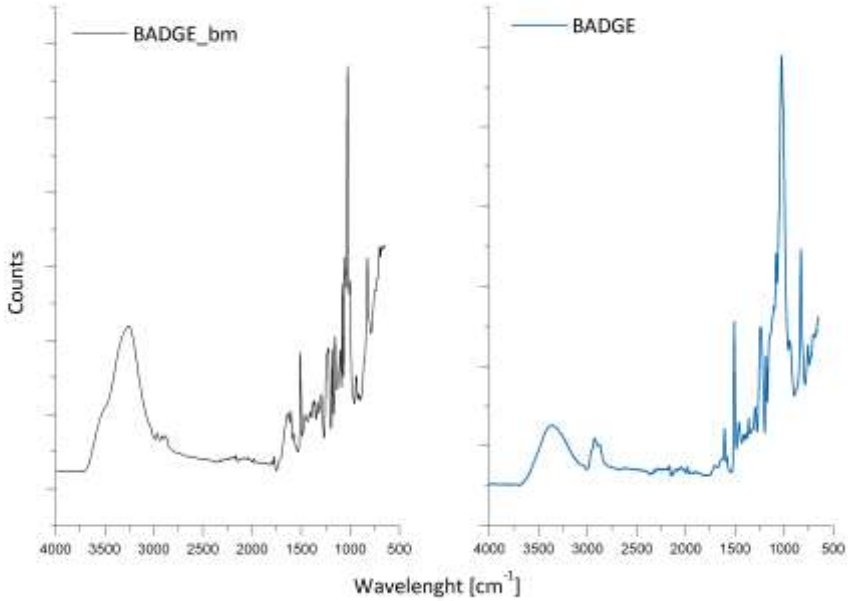

Figure 1-53 - FTIR Analysis of Ether Nanosponges βNS-BADGE 1:4, with Bisphenol A diglycidyl ether as a cross-linker. On the left mechanochemical synthesis, on the right classic solvent synthesis

3.2.2 Characterization and Functionalization of CDI Nanosponges

Following characterization are referred to ball mill CDI Nanosponges, since we performed many different tests and functionalization.
In the following pictures are reported FTIR Analyis and Thermogravimetric Analysis of cyclodextrins NS, with a comparison between βNS-CDI – 1:4 from ball mill synthesis and βNS-CDI – 1:4 from DMF synthesis. Figure 1-54 is reported a comparison of FTIR spectra after 4h in water at 40°C, confirming the insolubility of the system.

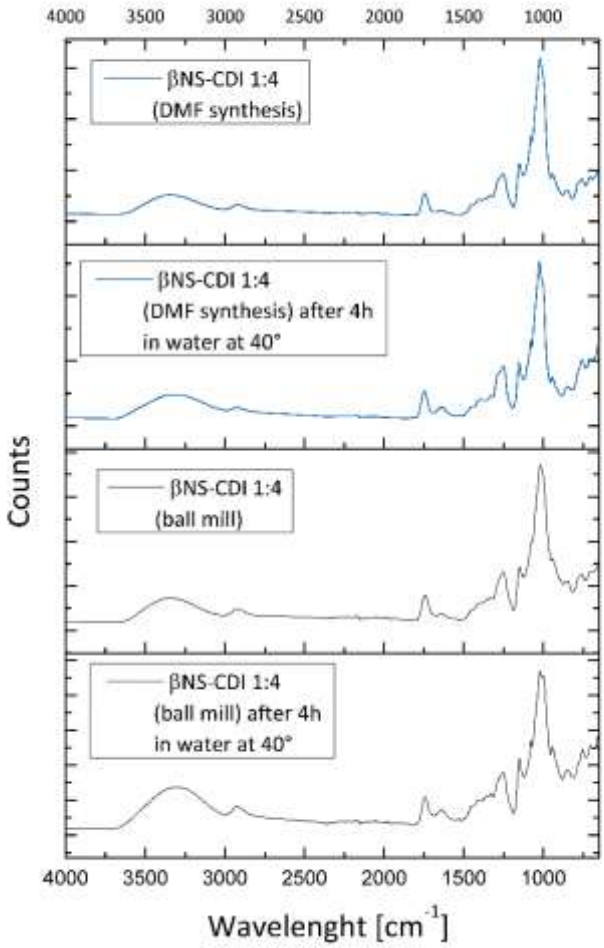

Figure 1-54 FTIR Analysis of βNS-CDI 1:4, before and after 4h in H2O at 40°C, from different synthesis. The band of interest at about 1750 cm-1 due to the carbonyl group of the carbonate bond, visible in all samples, even after hours in H2O at 40°C

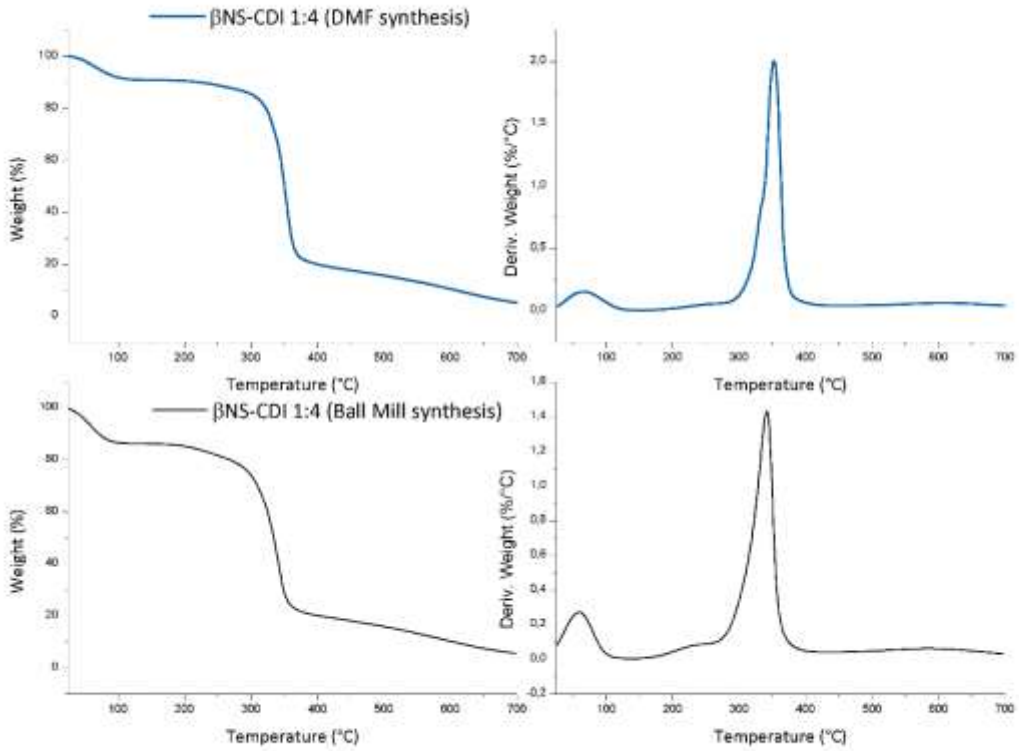

Figure 1-55 Thermogravimetric analysis of β-CD-based carbonate nanosponges, from BM and DMF synthesis. Nitrogen flow, ramp rate 10°C/min

It is evident from the TG mass loss curves and the corresponding derivate curves, Figure 1-55, that both cross-linked polymers exhibit a very close degradation path and, consequently, the same molecular structure is expected. The biggest mass loss starts above 300°C for both βNS; the relative maximum rate peak is located at around 345°C for both the βNS-CDI – 1:4 from DMF and for the βNS-CDI – 1:4 from ball mill. The initial mass loss present in both βNS-CDI – 1:4 is due to the adsorbed environmental water, always present when dealing with hygroscopic cyclodextrin based nanoparticles. In addition to this, particle size plays a key role: smaller the particles are and more extended is the surface exposed to environmental humidity.

In Figure 1-56, below, it is reported a different comparison, between Ball Mill synthetized αNS, βNS, γNS:

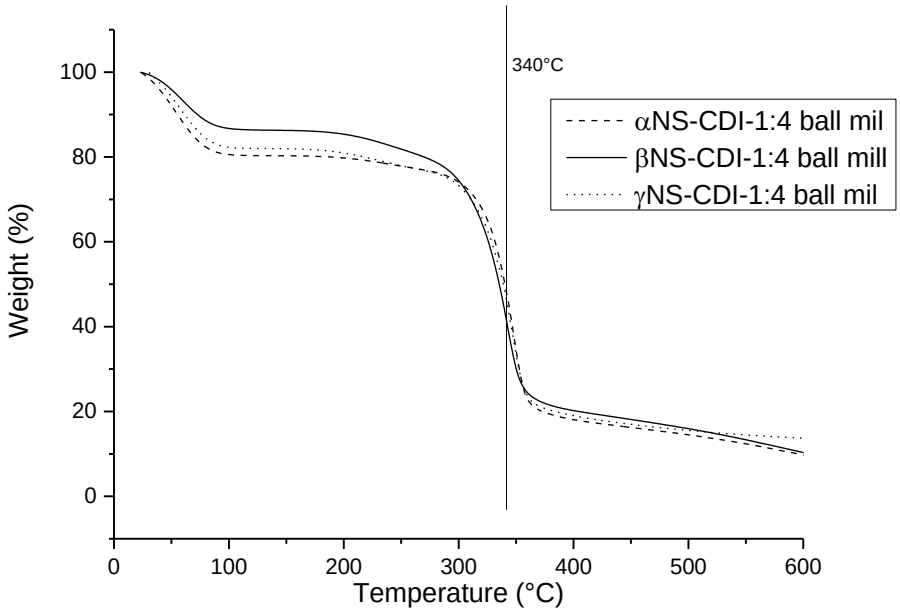

Figure 1-56 Thermogravimetric analysis of α, β and γ-CD-based carbonate nanosponges, from BM synthesis. Nitrogen flow, ramp rate 10°C/min

The degradation path is similar, with an interesting difference in the initial water loss, related to the different water affinity of the different CDs, leading to a different hygroscopicity of the final material.

In Figure 1-57 a test on the ability of carbonate nanosponges coming from Ball Mill synthesis to remove organic compounds from water solutions, compared to that of the classical solvent based NS [26] is reported. Methyl red is completely removed from its water solution by adding a small amount of carbonate nanosponges (50 mg for 10 mL aqueous solution of methyl red, 50 ppm) coming from ball mill synthesis.

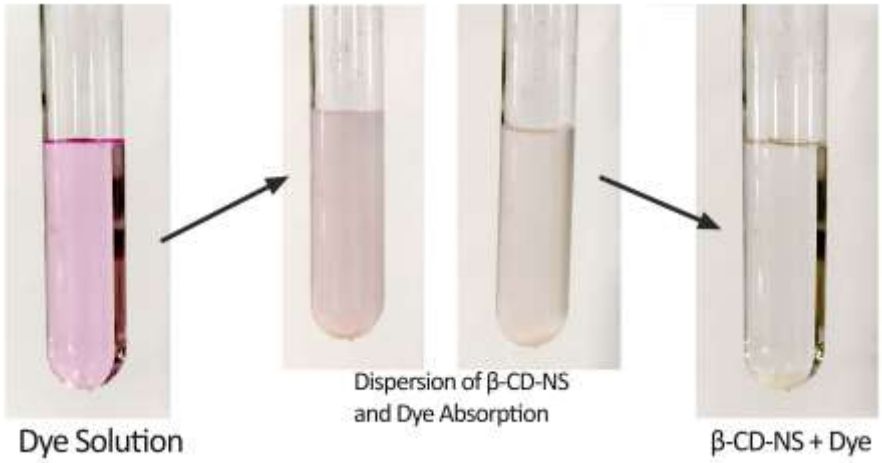

Figure 1-57 Absorption of organic dye in β-CD-based carbonate nanosponges, from a ball-mill synthesis.

The particle size of the βNS-CDI obtained through ball milling, measured using DLS, is less than a micron (800-900 nm) immediately after the synthesis; moreover stable suspensions (also in time) with a particle size of around 200 nm for all βNS-CDI were obtained using a *top-down* approach consisting of a short cycle of ball milling with smaller spheres.

The zeta-potential, Figure 1-58, of colloidal suspensions of βNS-CDI from ball mill was tested for all of the nanomaterials. In general, the stronger the charge, the better the colloidal stability of the particles: βNS-CDI synthesized in the ball mill showed an interesting negative ζ-potential, which can explain the stability of the dispersion.

As shown in Figure 1-58 all CD Nanosponges exhibit a negative ζ-potential. The negative charge seems to be related to the amount of crosslinker: the larger the amount, the more negative the ζ-potential detected. Elemental analysis showed the presence of nitrogen even after PSE extraction. This is attributable to the presence of reactive imidazolyl carbonyl groups (IM). In an ideal reaction, the carbonyl diimidazole should react completely with two hydroxyls of CDs, forming a carbonate bond between two monomers and therefore releasing two imidazoles soluble in water, which can be removed after synthesis.

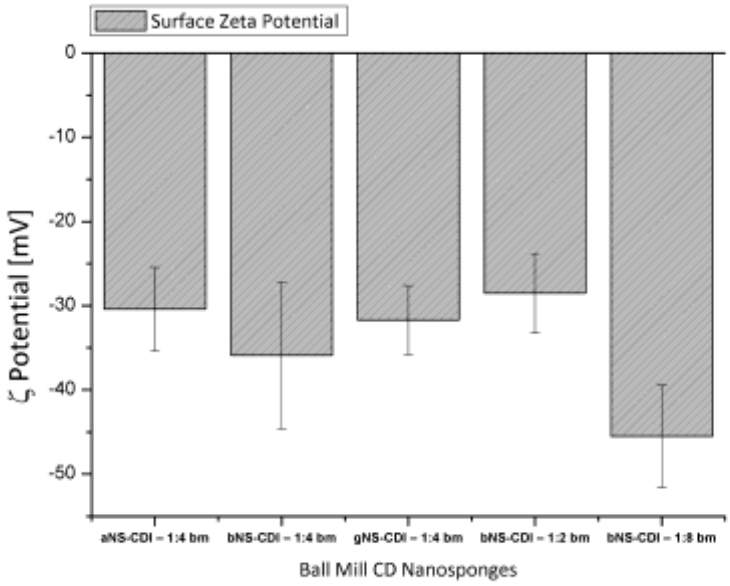

Figure 1-58 ζ-potential of Ball Mill Cyclodextrin Nanosponges with relative STDev (mV)

CDI, however, may react asymmetrically forming only a bond with a cyclodextrin but still maintaining one of the two moieties reactive. This is coherent with what is reported in the literature: the first activation of an alcohol by carbonyl imidazole has faster kinetics than the second one, which needs more time and/or a temperature from 60° to 80°C to obtain a significant yield [107], [108].
To distinguish between free imidazole by-product (IMH) and IM still able to form bonds (for example, with nucleophilic groups of active molecules) βNS-CDI were treated in two different ways: the first one entailed "hard" washing the samples using acetone and PSE. Acetone does not react by hydrolyzing the bond between the NS and the IM, and the high pressure (120 bar) in PSE made the removal of the encapsulated IMH possible. The second treatment was longer and entailed maintaining a small amount of material in water at 40°C for 8h, in order to conduct hydrolysis (Figure 1-59):

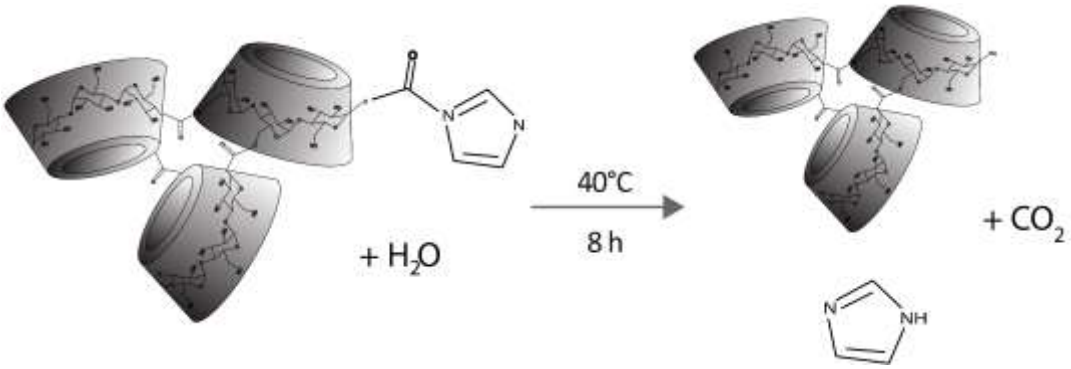

Figure 1-59 Hydrolysis reaction of the imidazoyl carbonyl group, water at 40°C

$$\boldsymbol{NS}(CO\text{-}IM)_n + nH_2O \rightarrow \boldsymbol{NS}(H)_n + nIMH + nCO_2$$

Every 2h part of the aliquot was withdrawn, washed in water to remove the IMH, freeze dried and checked with the elemental analyzer. Table 1-4 shows all of the results and Figure 1-60 shows a comparison between different βNS-CDI. Inset A in Figure 1-60 reports a comparison between different monomers with same CD/CDI ratio while inset B a comparison between same CD crosslinked with different ratios. In Figure 1-54, there is a comparison between DMF and BM βNS-CDI – 1:4 after 4h in water, which confirms what was stated in the previous paragraphs and Table 1-3, such as the solubility and especially the consistency as far as the properties are concerned between βNS-CDI obtained from the two different kinds of synthesis.

Table 1-4 - Elemental Analysis of βNS-CDI in Ball Mill and after PSE and 2,4 and 8 hours at 40°C in water. The presence of Nitrogen was tested starting from t0, plain NS, washed only with water and acetone at RT and on the same material but after a PSE extraction in acetone (that only remove the IMH) and after 2,4 and 8h of hydrolysis in water at 40°C in order to remove the residual covalently bonded imidazolyl carbonyl group.

Type of Nanosponge	Conditions	%wt N	STD
αNS-CDI 1:4 bm	t0 (plain NS)	1,33	0,07
	after 2h in H2O 40°C	0,53	0,02
	after 4h in H2O 40°C	0,25	0,00
	after 8h in H2O 40°C	0,20	0,01
βNS-CDI 1:4 bm	t0 (plain NS)	2,69	0,12
	after 2h in H2O 40°C	0,63	0,01
	after 4h in H2O 40°C	0,31	0,01
	after 8h in H2O 40°C	0,23	0,02
γNS-CDI 1:4 bm	t0 (plain NS)	2,21	0,16
	after 2h in H2O 40°C	0,61	0,02
	after 4h in H2O 40°C	0,11	0,10
	after 8h in H2O 40°C	0,00	0,00
βNS-CDI 1:8 bm	t0 (plain NS)	6,39	0,05
	after 2h in H2O 40°C	2,56	0,03
	after 4h in H2O 40°C	1,31	0,03
	after 8h in H2O 40°C	0,40	0,03
βNS-CDI 1:2 bm	t0 (plain NS)	1,27	0,01
	after 2h in H2O 40°C	0,77	0,01
	after 4h in H2O 40°C	0,52	0,01
	after 8h in H2O 40°C	0,17	0,01
	After Pressurized Solvent Extraction		
βNS-CDI 1:2 bm	after PSE (Acetone)	0,79	0,02
βNS-CDI 1:4 bm	after PSE (Acetone)	1,19	0,07
βNS-CDI 1:8 bm	after PSE (Acetone)	3,28	0,09

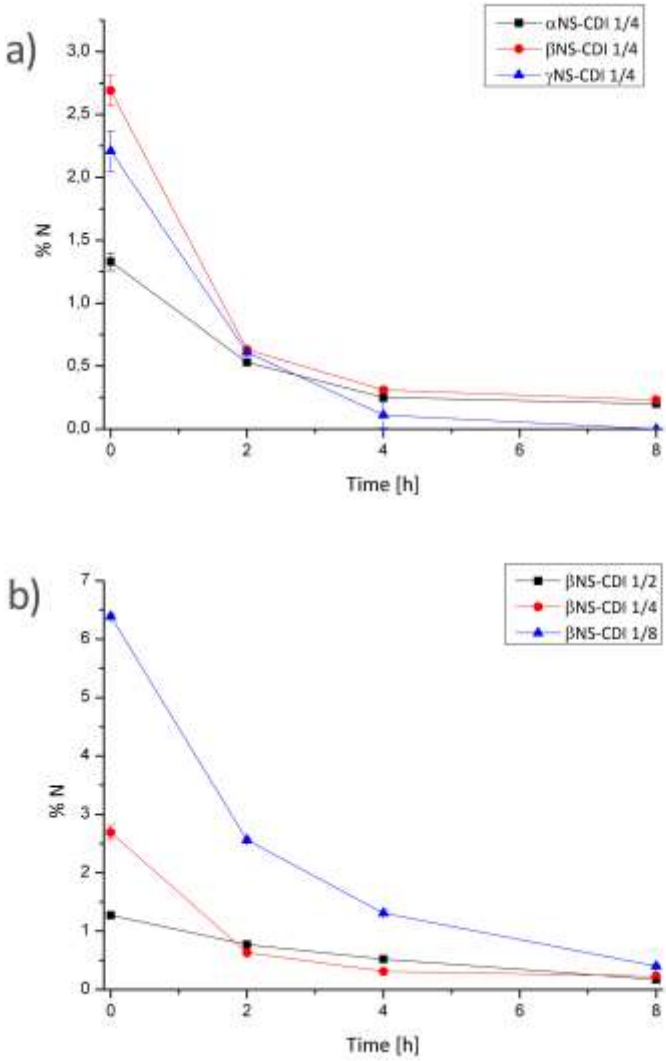

Figure 1-60 Nitrogen content, %wt, in Cyclodextrins NS-CDI. Comparison between different monomers with same CD/CDI ratio (a) and between same CD crosslinked with different ratios (b).

The results of the elemental analysis agree with what could be expected from the reaction conditions and molar ratios: the βNS-CDI 1:8 exhibited the highest nitrogen content, around 6% wt, before any further steps of purification. This result is consistent with the quantity of CDI involved in this nanosponge as it is 2-4 times as higher as the other βNS-CDI, assuming that the kinetics and reactivity were the same in all batches. In conclusion, the IMH and unreacted

IM contents are higher. Worthy of note is that most of the CDI reacts in the cross-linking step, as the amount of nitrogen after PSE Acetone extraction dramatically decreases due to release of the IMH byproduct entrapped in the NS network.
Furthermore, it can be stated that after about 8 hours, it is possible to eliminate almost completely both IMH and IM, using only water, from all nanomaterials.
The solubility and physicochemical properties of NS-CDI are not depleted by these two different processes: all NS-CDI, with different molar ratios and different CD, were still not soluble in all the solvents tested previously (therefore, as shown in Figure 1-54, for βNS-CDI 1:4 the FTIR spectra are comparable).
Hydrolysis in fact affected only imidazolyl carbonyl groups and not carbonate bond of CD-NSs.
In order to confirm the presence of reactive imidazolyl groups, which would make the functionalization of NS possible, an attempt was made on βNS-CDI – 1:8 purified with PSE (and so, with only reactive IM left) by using different organic dyes. The functionalization, as described in the Experimental section, was driven in DMSO, an organic solvent in which the material is insoluble but that is suitable for reactions in an anhydrous environment as in this case with organic dyes.
The choice fell on three common, well known and widely investigated organic dyes, i.e. Fluorescein, Methyl Red and Rhodamine B. They have a slightly different structure (and color) and different surface charge but have a reactive nucleophilic carboxylic group.
The simplified schematic reaction (previously reported by Staab [107] and more recently by Jadhav *et al.* [109]), with the relative ζ-pot of nanoparticles after functionalization, is present in Figure 1-61. Through a simple reaction in closed vials with an excess of organic dye, a covalent bond with the still reactive NS was obtained. As shown by the elemental analysis, after the PSE extraction, the amount of nitrogen and therefore of reactive IM is very low. The experiment was conducted on nanosponges having 1:2, 1:4, 1:8 βCD/CDI ratios, and good results were obtained only with βNS-CDI – 1:8. Even βNS-CDI – 1:8, if treated for 8h in H_2O 40°C (0,40 % N), presents a low amount (≈0) of reactive IM, therefore the reaction does not occur at all, leading only to an physical entrapment of dyes (which can be easily removed through a PS Extraction with acetone).
Moreover, this could be explained considering the fact that not all the reactive groups are freely accessible within the NS structure.

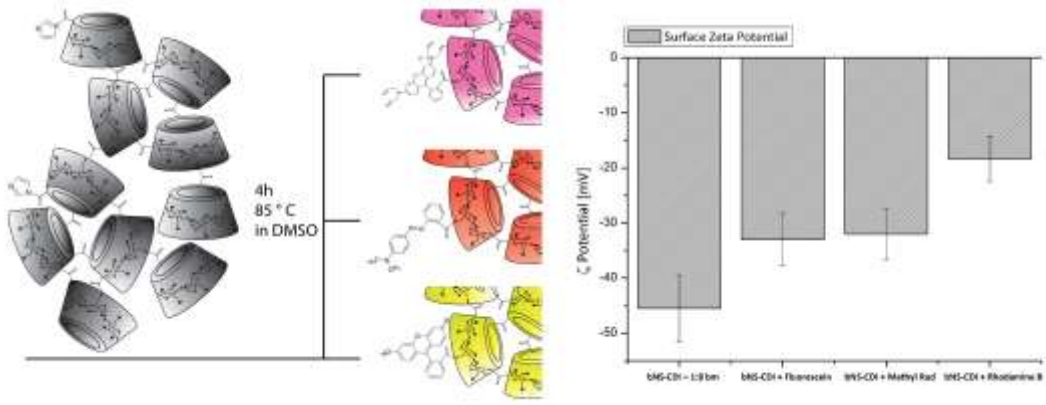

Figure 1-61 Simplified reaction scheme and procedure for the obtaining of dye functionalized βNS-CDI

What is particularly interesting is the difference in the Surface Zeta Potential: it ranged from a very negative ζ-potential of around -45 mV (due to carbonate bonds and IM groups) to 33 mV, -32 mV and -18,4 mV after reaction with Fluorescein, Methyl Red and Rhodamine B, respectively .
The variation of the ζ-potential is consistent with the Rhodamine B structure, as it exhibits a positive charge. The elemental analysis of the samples containing Rod B, confirms the presence of the organic compound within the structure (≈1 % wt. N).

3.2.3 Characterization of PEGylated CDI Nanosponges

The present section is dedicated to an ongoing project, so only preliminary results will be reported. *In vitro* and *in vivo* tests are, indeed, still to be carried out so the chapter will be more focused on the "chemical" aspect rather than on pharmaceutical applications

This section will also include a systematic study of the particle size reduction and measurement. The main goal was to obtain a stable dispersion using only the ball mill. Essentially, we tried to use the same instrument for both syntheses and all further modifications of the materials, to demonstrate that a very common lab equipment, if used with very different but precise operational conditions, shows great versatility.

We chose PEGylated NS as probe for particle size reduction tests because the final application of PEG NPs is specifically in the pharmaceutical field.

It is worth to say that the formation on a covalent bond is not easy to confirm; as seen for other compounds we tried to remove the entrapped PEG, inside the NS network, as a polyrotaxane or simply partially included in the CDs cavity, by washing using a PS Extractor. In this case the solvent was ethanol, at 80°C, 120 Bar, for 2 cycles. All characterizations had been carried out after this step.

As seen in the previous paragraphs via FTIR it is possible to make initial assessments of the probable structure (Figure 1-62).

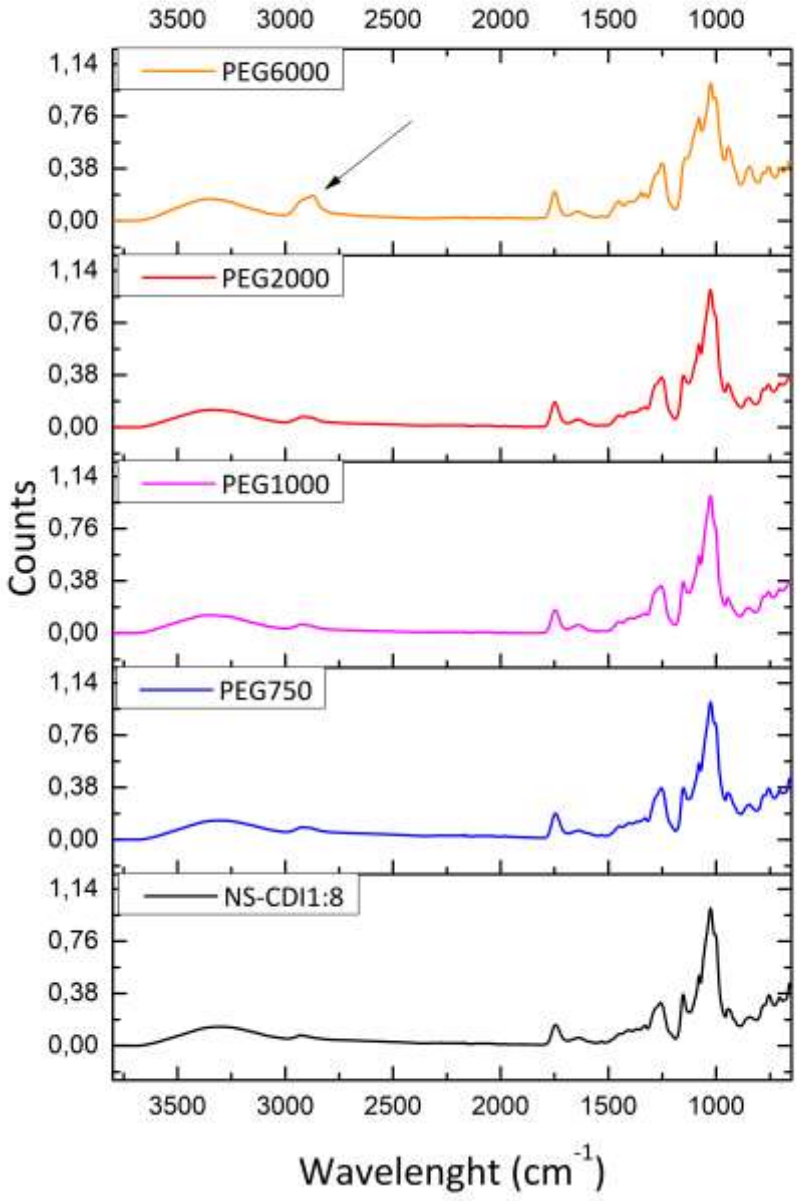

Figure 1-62 FTIR Spectra of PEGylated βCD CDI Nanosponges.

The formation of an insoluble polyester is confirmed by the almost superimposable spectra, with same characteristic peaks seen for plain NS (for CDI, Figure 1-54) presenting a strong absorption at 1750 cm^{-1} due to the carbonyl group of the carbonate bond, visible in all samples. A small, but

noticeable difference in the spectra, can be spotted at around 2870 cm^{-1} (Figure 1-63 for the detail).

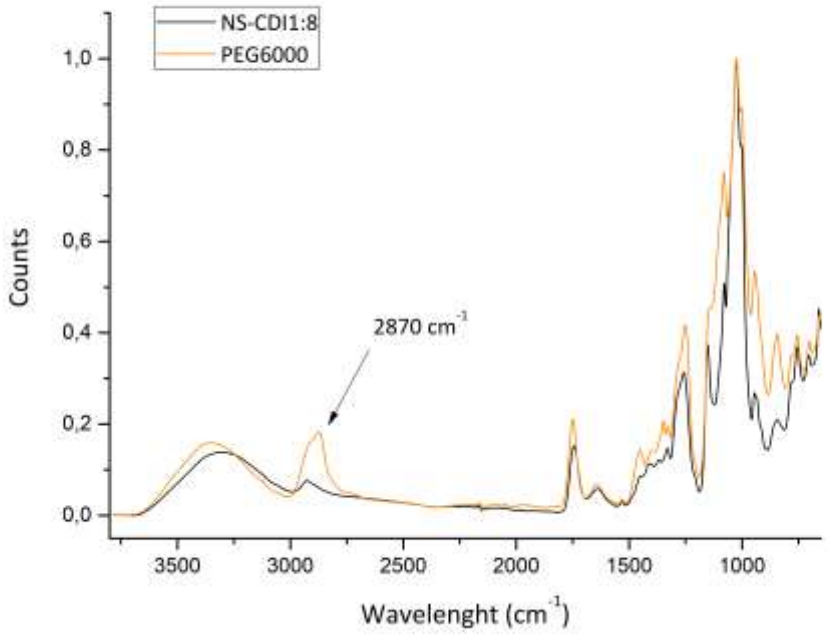

Figure 1-63 FTIR Spectra of PEGylated βCD CDI Nanosponges: comparison between βCD-NS CDI (plain) and βCD-NS CDI + PEG6000. Detail of the peak at 2870 cm^{-1}

The band is attributable to the stretching of the C-H, so is related to the presence of PEG and this can be the reason why is so evident only with the PEG6000. A small shoulder can be, anyway, be noticed also for lower molecular weight.

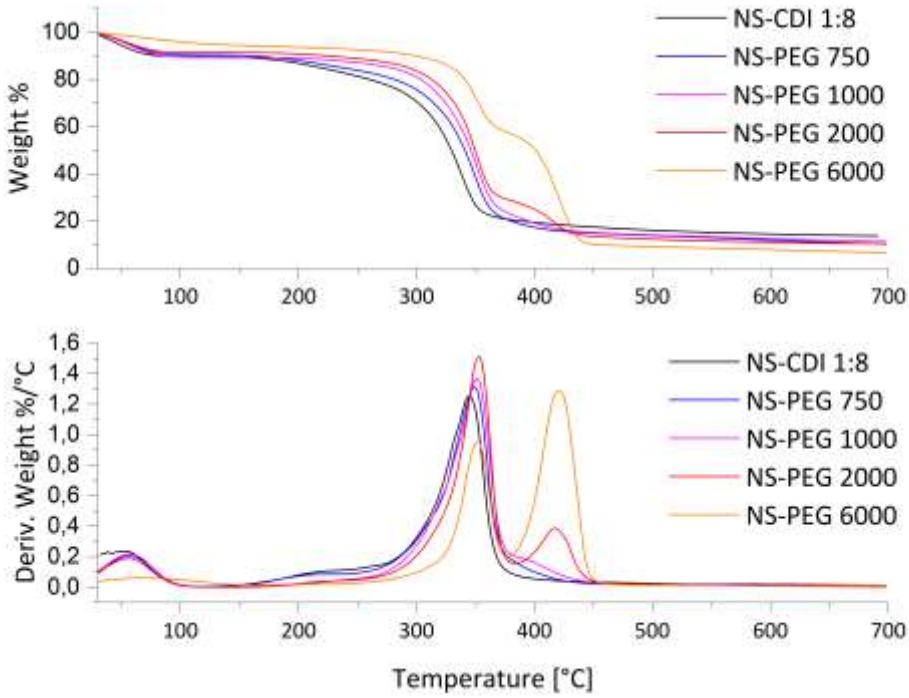

Figure 1-64 Thermogravimetric analysis of βCD-NS CDI, from ball mill syntheses. Black curve, plain βCD-NS CDI 1-8, colored curves PEGYlated βCD-NS CDI 1-8. Nitrogen flow, ramp rate 10°C/min

It is evident from the TG curves a difference in the first part: the lower content of water in the PEG6000 sample is manly related to the different granulometry. The presence of polyethylene glycol is confirmed by the presence of an additional degradative step in all NSs from syntheses in presence of PEG.
The percentage of weight loss seems to be proportional to the PEG chain length.

All samples dispersions, except PEG600, measured at the DLS immediately after the synthesis exhibited a dimension around 1 micron. Contrariwise, βCD-NS CDI + PEG6000 particles were 5-6 times larger preventing also the possibility of obtaining a stable dispersion in water.
So, Figure 1-65 reports ζ Potential measurements on dispersions obtained with PEGylated NS immediately after the synthesis.
As said, since the impossibility of obtaining a stable dispersion with PEG6000, this sample will be reported later, needing further modifications.

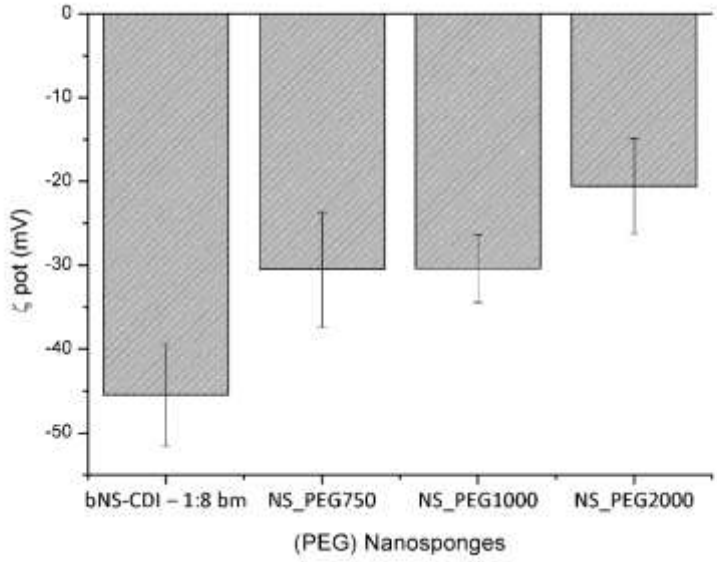

Figure 1-65 - ζ Potential: comparison of PEGylated NS, with different Mw. Particle size ≈1 µm

It is immediately noticeable the difference in ζ Potential, that seems to be related to the Mw of PEG, since the synthetic condition are the same for all samples. Apparently, a longer polyethylene glycol chain, leads to a less negative ζ potential. This results is coherent with what reported in literature [110], [111].
For a more precise measurement, and as already mentioned, a severe reduction of the particle size was carried out on all samples, allowing the ζ Potential measurements of PEG6000 NS.
The intent was to obtain particles with sizes between 150-200 nm, with all PEGylated NS, for a better comparison. For achieving this, the procedure of top-down size reduction (common for all samples) is the following: wet ball milling (WBM), using water as dispersant. The use of water permits to obtain directly a dispersion and allows a better control the temperature.
The WBM process was driven on a 15 mL dispersion, containing 150 mg of NSs powder; the milling process takes about 90 minutes, at 600 rpm.
Figures from Figure 1-66 to Figure 1-70, show the results.
Each reported picture contains a) DLS Measurent, with relative Average dimension b) I and II, Nanoparticle tracking analysis characterizations with relative dimensional distribution and concentration of different sizes. On top right the mean value.

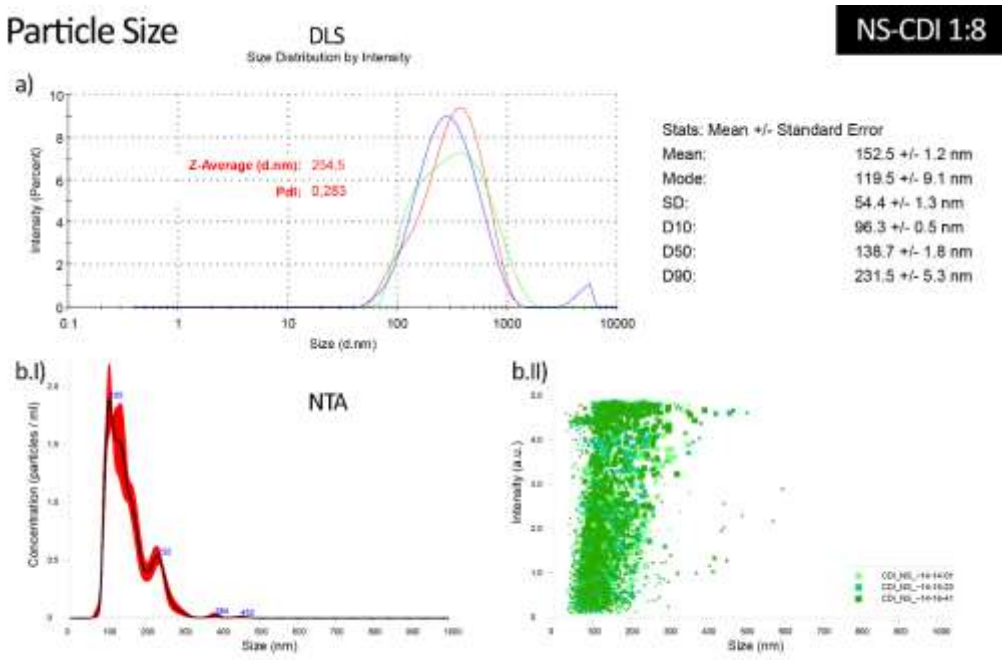

Figure 1-66 Particle Size of βCD-NS CDI: a) DLS Size distribution, average: 254 nm b) NTA Characterization b.I) Concentration (part/mL)/Size (nm) distribution. Mean Particle size distribution from NTA: 152.5 ± 1.2 nm

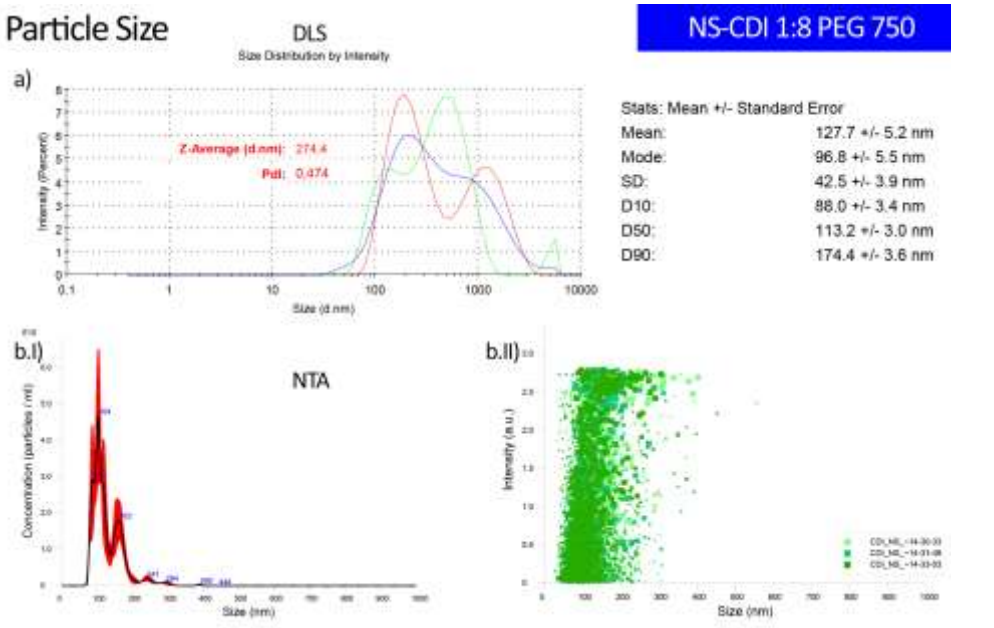

Figure 1-67 Particle Size of βCD-NS CDI PEG750: a) DLS Size distribution, average: 274 nm b) NTA Characterization b.I) Concentration (part/mL)/Size (nm) distribution. Mean Particle size distribution from NTA: 127.7 ± 5.2 nm

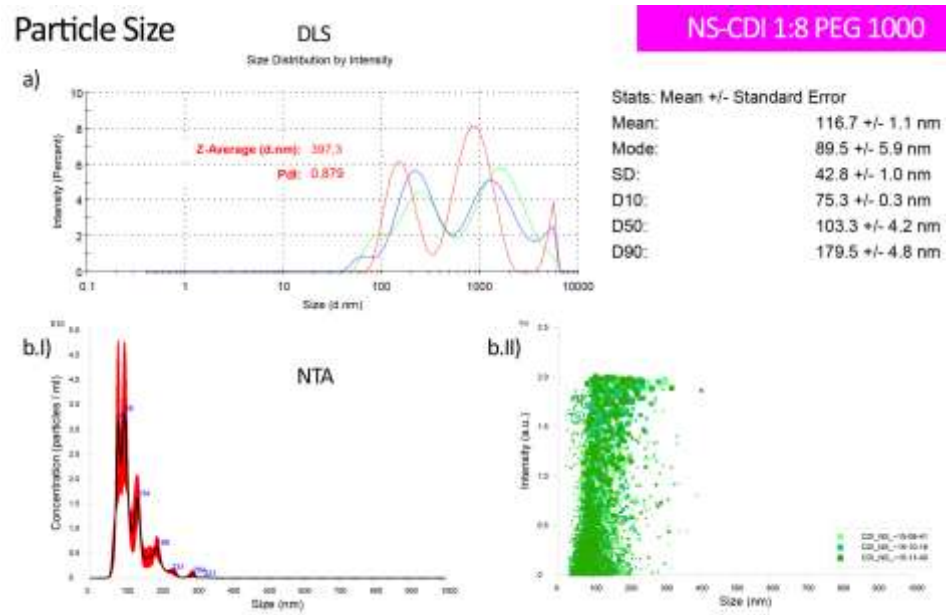

Figure 1-68 Particle Size of βCD-NS CDI PEG1000: a) DLS Size distribution, average: 397 nm b) NTA Characterization b.I) Concentration (part/mL)/Size (nm) distribution. Mean Particle size distribution from NTA: 116.7 ± 1.1 nm

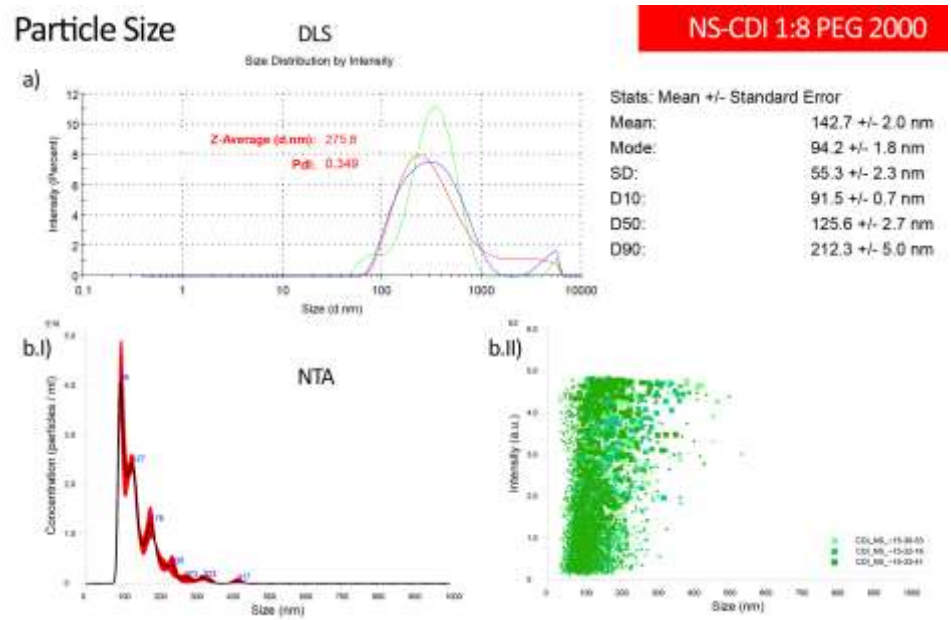

Figure 1-69 Particle Size of βCD-NS CDI PEG2000: a) DLS Size distribution, average: 275 nm b) NTA Characterization b.I) Concentration (part/mL)/Size (nm) distribution. Mean Particle size distribution from NTA: 142.7 ± 2.0 nm

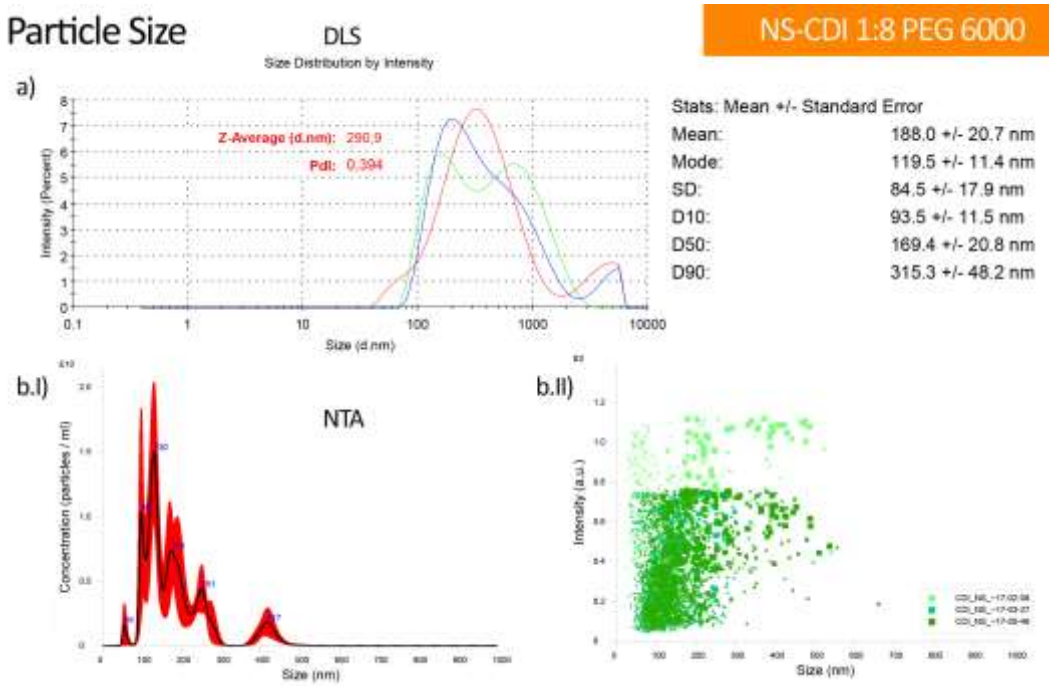

Figure 1-70 Particle Size of βCD-NS CDI PEG750: a) DLS Size distribution, average: 290 nm b) NTA Characterization b.I) Concentration (part/mL)/Size (nm) distribution. Mean Particle size distribution from NTA: 188.0 ± 20.7 nm

The measurements lead to very different results, but coherent among the various samples. It is worth too say that we performed also NTA analyses because was evident from DLS a heterogeneous size distribution.

Both Dynamic light scattering and Nanoparticle tracking analysis measure the Brownian motion of nanoparticles, but DLS does not visualize the particles individually but analyzes time dependent scattering intensity fluctuations.

Larger particles, that obviously have the greatest influence in the calculation on an average, with DLS, are not excluded.

It's therefore evident from NTA that in all samples half of the particle are even smaller than 200 nm.

Once obtained stable and comparable dispersions, new ζ potential measurements were performed. Results are shown in the following picture (Figure 1-71):

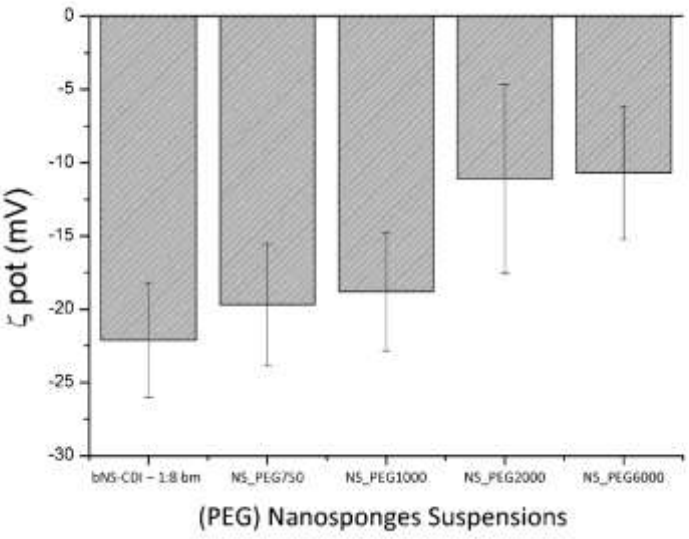

Figure 1-71 ζ Potential: comparison of PEGylated NS, with different Mw. Particle size ≥ 200 nm, dispersion after WBM

The zeta potential is negative for all nanoparticles and the correlation between surface charge and length of PEG chain seems to be maintained.
Nevertheless, it is immediately noticeable the fact that all samples exhibit a less negative ζ Potential. This can be attributable to the fact to the fact that smaller particles expose a greater surface and consequently a greater number of PEG chains. PEGylation, as seen, lead to more positive ζ Potential.

Characterizations on these promising nanomaterials are still ongoing.
In vitro and *in vivo* tests are now necessary for demonstrating the presence of an effective stealth effect.

3.2.4 Characterization of Folic Acid conjugated CDI Nanosponges (FA βNS-CDI 1:8)

This section will essentially follow the same scheme seen for the previous one.
In this case to the main aim is to demonstrate the actual formation of a covalent bond between the NS and the one of the Folic Acid (FA) carboxylic groups.
As seen before for dye-bonded ND, the aim is the formation of a chemical bond and not the formation of supramolecular complexes.
In this case the extraction of byproducts and unreacted CDs and Folic acid is particularly complicated.
Folic acid is nearly insoluble is all common solvents, PEG was easily removable by using ethanol. The preparative method of this functionalized NS is particularly interesting for this reason, too: since Folic Acid is only slight soluble in DMSO, a common synthesis using solvent is an issue. The obstacle of looking for the best solvent for conducting the reaction can be simply solved by using no solvents.
The poor solubility is also a drawback for the removal of the unreacted FA, that remains inside the NS crosslinked network.
We have solved this problem by subsequent washes (using PS Extraction) with different solvents, exploiting the insolubility of the NSs.
After each extraction, the nitrogen content was checked. Nitrogen is present in the FA structure and in the Imidazole group of the carbonyl diimidazole.
Figure 1-72 reports a probable structure of the NS, before PSE extractions, with all species.

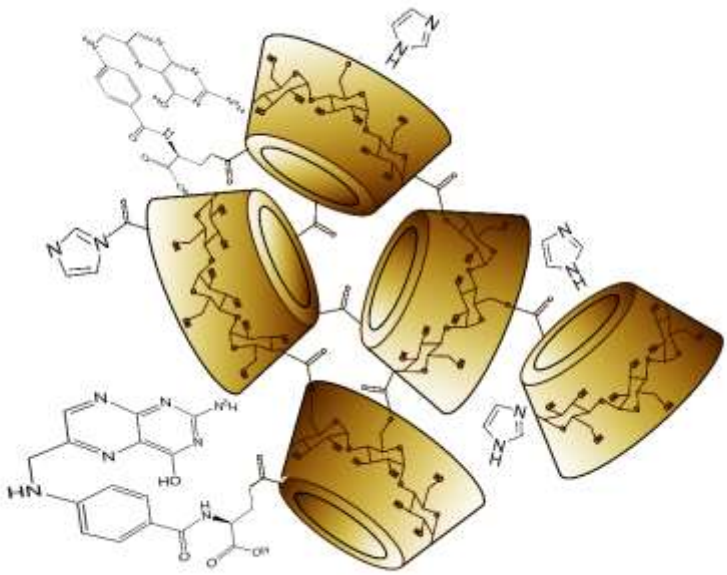

Figure 1-72 FA βNS-CDI 1:8**, structure and chemical compounds containing Nitrogen contained by the material**

The procedure already used for removing PEG in the previous part and Organic Dyes in part 3.2.2, converges in these successive PSE extractions.
The first extraction with acetone removes imidazolides and (if present) unreacted CDI.
The second one is driven with water at 120°C, 120 bar. We know from 3.2.2 that even with mild conditions it is possible to remove using water, by hydrolysis, the carbonyl imydazoil groups. It is evident from Table 1-5 that the nitrogen content drops mostly by the first extraction with acetone, but there is no big difference after extraction with water.
This is related to the poor solubility in water and acetone, even at high temperature. So, we stirred in DMSO at 80°C a suspension of FA βNS-CDI 1:8, then we extracted again with acetone in PSE. Acetone and DMSO are miscible and FA is soluble in DMSO at high temperature. Results are shown in Table 1-5, below.

Table 1-5 – Extraction Procedure on FA βNS-CDI 1:8

Nanosponge		Weight % of Nitrogen	STD
βNS-CDI 1:8 bm Folic Acid	After Ball Mill Synthesis	5,40	0,09
	After Pressurized Solvent Extraction with Acetone	4,70	0,02
	After Pressurized Solvent Extraction with Water	4,10	0,08
	After washing with DMSO and PSE Extraction with Acetone	3,78	0,30

The content of Sulphur, from DMSO, after the last step was checked via elemental analysis and is under the detection limit of the instrument.
Moreover, the nitrogen remains around 3.80 %wt; the theoretical (and maximum) content of N, from stoichiometry, is 5.4% wt, so the results are consistent.
All further characterizations, reported herein, were driven on this last, accurately cleaned sample.
In the comparisons of IR Spectra, Figure 1-73 and Figure 1-74, is clearly visible a peak at around 1600 cm^{-1}. Reported spectra are normalized from 0 to 1.

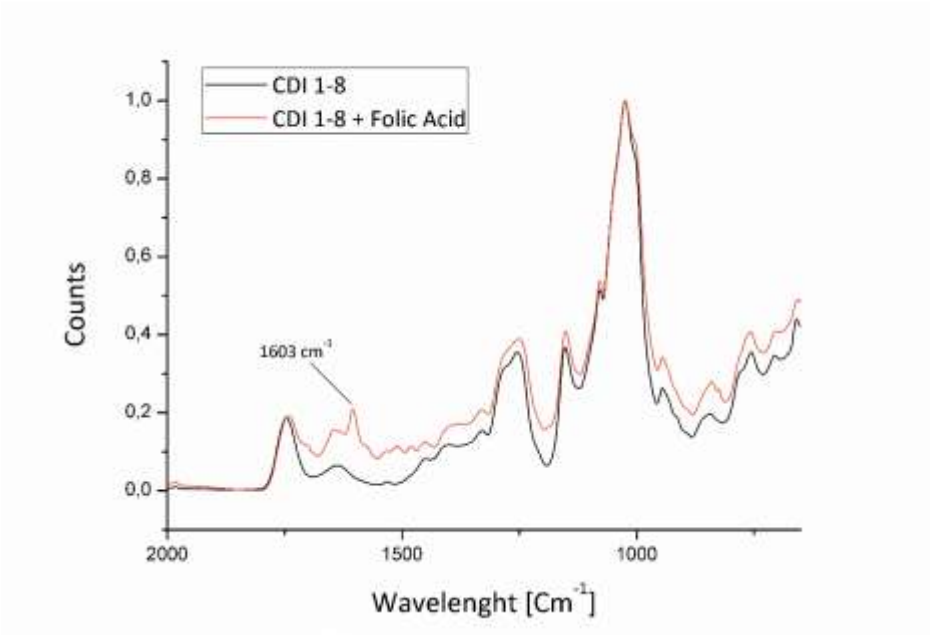

Figure 1-73 IR pattern of FA βNS-CDI 1:8 and plain βNS-CDI 1:8 bm. At 1603 cm^{-1} peak relative to aromatic group in FA

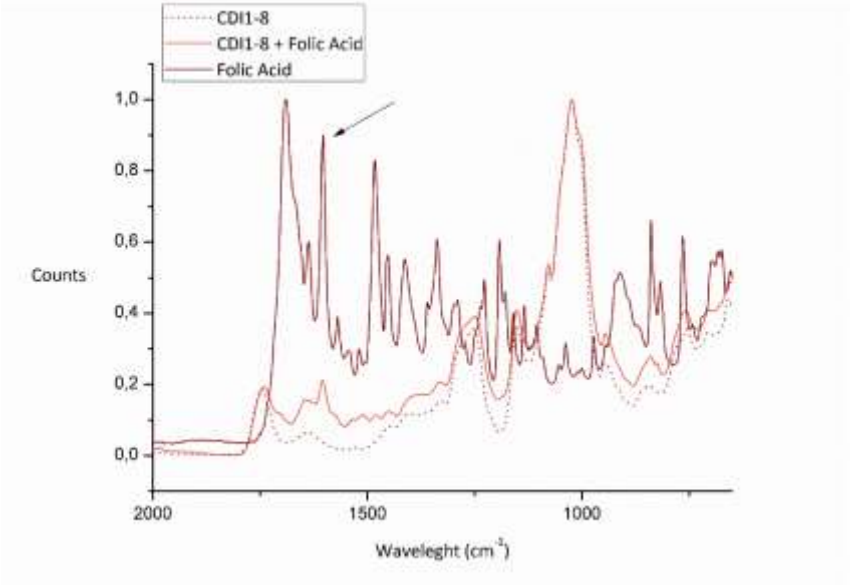

Figure 1-74 IR pattern of FA βNS-CDI 1:8, plain βNS-CDI 1:8 bm and Folic Acid

Except from the peak at 1600 cm^{-1} , attributable to the aromatic ring of folic acid, the spectra of the two different NSs are almost superimposable.
Unfortunately, it is impossible to confirm the presence of covalent bonded FA inside the structure and even less to quantify the Folic Acid.
This measurement anyway permits to confirm the presence of FA inside the structure. Only by crossing the results with those to follow it will be possible to make any assumptions.
In Figure 1-75 a comparison of the thermal degradation between free Folic Acid and NSs synthetized in Ball Mill.

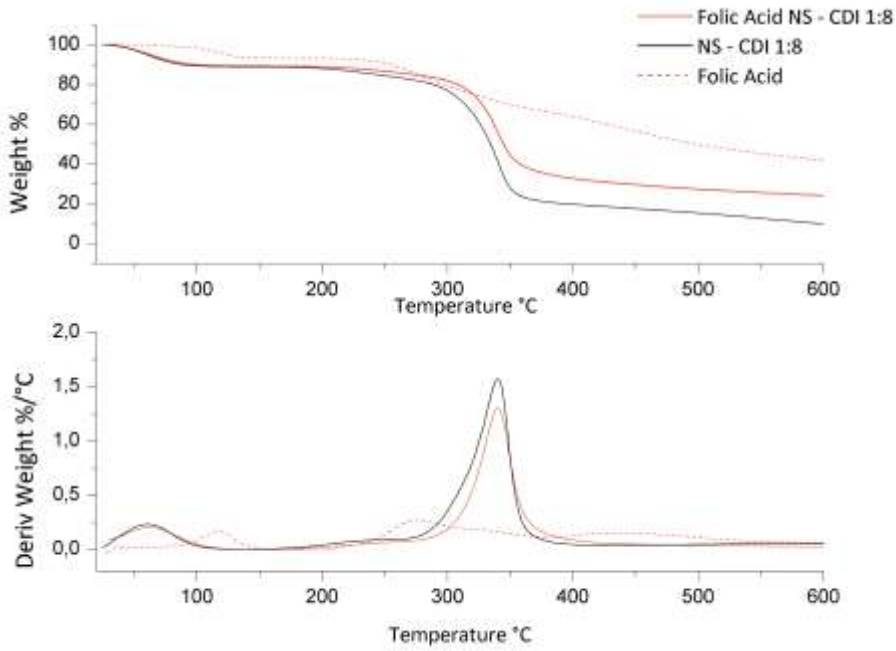

Figure 1-75 Thermogravimetric analysis, TG/DTG, from Folic Acid BM synthesis. Nitrogen flow, ramp rate 10°C/min

Thermal Stability of Folic Acid was investigated in 2002 by Vora et al. [112] evidencing two peculiar weight loss at around 108°C and before 270°C (mostly noticeable in the deriv. weight %/°C). They identified the decomposition products using various analytical techniques such as infrared (IR) spectroscopy, mass spectroscopy (MS) and X-ray diffraction (XRD).
They attributed, via IR analysis, this first weight loss to glutamic acid present in the FA structure. This weight loss is noticeable, as expected, in the folic acid thermogram, but is not present in the FA βNS-CDI 1:8.

This permit in a simple way to assume the actual formation of a covalent bond: using the CDI, cross-linking presumably occurs with a reaction between one of the hydroxyl groups of the CD and one of the carboxylic groups, as widely reported in literature [107]–[109], of the glutamic acid inside FA structure.
If the reaction occurs there is no more glutamic acid but an ester covalent bond, so the peak clearly visible in the folic acid thermogram is not present anymore.
A confirmation can be found in Figure 1-76.
The thermal degradation of FA βNS-CDI 1:8 is now compared to the TG curve of a physical mixture of βNS-CDI 1:8 bm, plain, and folic acid (only grinded in mortar for 15 minutes).

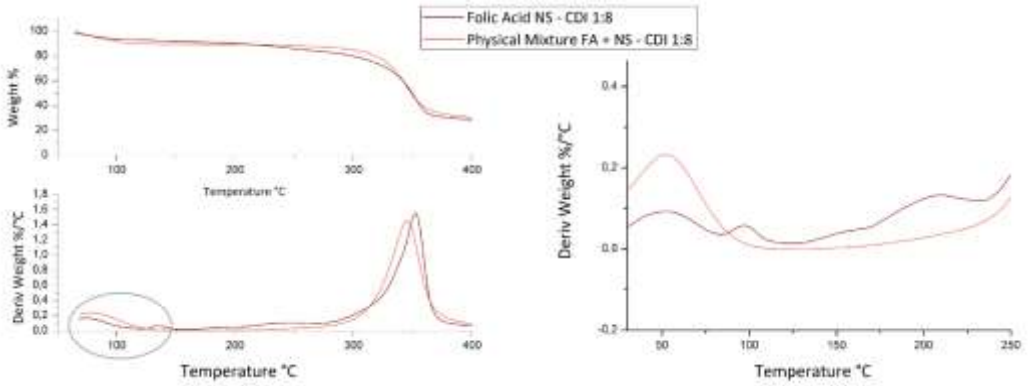

Figure 1-76 Thermogravimetric analysis, TG/DTG, from Folic Acid BM synthesis. Comparison with physical mixture of FA and βNS-CDI 1:8 bm Nitrogen flow, ramp rate 10°C/min

Curves reported in Figure 1-76 support and verify what assumed from the first comparison. It is evident (especially from the derivative %/°C between 30°C and 250°C) the presence of the two characteristic signals of the FA. This weight loss, again, is not present in the curve of FA βNS-CDI 1:8. Noteworthy, is the difference in the curve shape and temperature shift of about 10°C in the physical mixtures. NSs are known for the protective effect, even from thermal degradation, and since the preparation of the mixture is very similar to a kneading process, it is assumable a protective effect (from thermal degradation) of NSs.

As stated before for PEGylated NSs, these results thus need to be confirmed by *in vitro* and *in vivo* tests, for a complete characterization and for testing the effective efficacy.

3.3 Conclusions

In summary, different synthesis have been carried out, using different dextrins (α, β, γ, LC and GLU) and Crosslinkers and trying different molar ratios between dextrin and crosslinker for CDI NS (1:2, 1:4, 1:8).
Cross-linked cyclodextrin polymer were prepared via a new synthetic route based on only on mechanochemistry.
The green synthetic route here proposed permits a biodegradable polymer, having the same characteristics as cyclodextrin-based polymers synthesized in a solvent to be obtained without using any solvent.
The polymer obtained using the Ball Mill method exhibited the same characteristics as a CD-based carbonate NS synthesized in a solvent and insolubility in water and organic solvents. FTIR and TG analyses were performed on the new material, confirming the structure with a carbonate bond.
Nanoparticles, after cycles of ball milling had a mean diameter of less than 200 nm, measured with DLS, and exhibited a negative ζ-potential (the most negative being around -45 mV, measured for βNS at a 1:8 ratio carbonyl diimidazole/β-cyclodextrin). Reproducibility of all syntheses is very high, with constant yield.
The elemental analysis was conducted on all the synthesized nanosponges in order to detect the presence of nitrogen deriving from probably still reactive Imidazole moieties deriving, in turn, from carbonyl diimidazole.
This was confirmed by the reaction between the nanoparticle obtained and the nucleophilic carboxylic group of three different organic dyes, Fluorescein, Methyl Red and Rhodamine B, leading to a coloured (even after a PSE extraction) functionalized material, with a less negative ζ potential.
Moreover, one step syntheses, with the aim of covalently bond to NS different chemical compounds, were carried out with the same mechanochemical approach, using as pendant groups respectively Folic Acid and Polyethylene glycol leading to functionalized βNS-CDI.

4 Overall Conclusions and Perspectives

The two reported macro-projects both involve synthesis and application of cyclodextrins and dextrin-based biopolymers.
As seen Nanosponges are a versatile material that, starting from the same building block (this work as manly focused on β-cyclodextrins, but also examples with other dextrins are reported) permitted us to achieve interesting results.
In all projects, many characterization and measurement are now ongoing.

In vitro and *in vivo* tests, especially for what concern polymers specifically designed for pharmaceutical applications are now in due course, for demonstrating the efficacy of these new nanomaterials.
Future perspectives are of course aimed to a continuation of these two projects, but also, and above all, to future projects that will both solvent free synthesis and photoactivated therapies.
The possibility to achieve an easy functionalization of insoluble compounds via mechanosynthesis will allow us to test different insoluble photosensitizers, for example.
Then, encapsulation and release tests need to be performed an all these new nanomaterials, for confirming the good performances of NSs in the nano-drug delivery field.
Finally, we are now testing different approaches without solvent, using different crosslinkers and methods, to expand the possibilities of application of solvent free NSs.

5 References

[1] G. Crini, "Review: A history of cyclodextrins," *Chem. Rev.*, vol. 114, no. 21, pp. 10940–10975, 2014.

[2] J. Szejtli, "Introduction and General Overview of Cyclodextrin Chemistry," *Chem. Rev.*, vol. 98, no. 5, pp. 1743–1754, 1998.

[3] T. L. Sergey V. Kurkov, "Cyclodextrins," *Handb. Anal. Act. Compd. Funct. Foods*, vol. 453, pp. 167–180, 2013.

[4] T. Loftsson and D. Duchêne, "Cyclodextrins and their pharmaceutical applications," *Int. J. Pharm.*, vol. 329, no. 1–2, pp. 1–11, 2007.

[5] D. French, "The Schardinger Dextrins," *Adv. Carbohydr. Chem.*, vol. 12, no. C, pp. 189–260, 1957.

[6] J. Szejtli, "Utilization of cyclodextrins in industrial products and processes," *J. Mater. Chem.*, vol. 7, no. 4, pp. 575–587, 1997.

[7] D. Duchêne, "Cyclodextrins and Their Inclusion Complexes," *Cyclodextrins Pharm. Cosmet. Biomed. Curr. Futur. Ind. Appl.*, pp. 1–18, 2011.

[8] L. Szente and J. Szejtli, "Cyclodextrins as food ingredients," *Trends Food Sci. Technol.*, vol. 15, no. 3–4, pp. 137–142, 2004.

[9] A. Biwer, G. Antranikian, and E. Heinzle, "Enzymatic production of cyclodextrins," *Appl. Microbiol. Biotechnol.*, vol. 59, no. 6, pp. 609–617, 2002.

[10] M. L. Bender and Komiyama, *Cyclodextrin chemistry*. New York: Springer-Verlag, 1978.

[11] S. Brochsztain and M. J. Politi, "Solubilization of 1,4,5,8-naphthalenediimides and 1, 8-naphthalimides through the formation of novel host–guest complexes with a-cyclodextrin," *Langmuir*, vol. 15, pp. 486–4494, 1999.

[12] A. A. Elbashir, N. F. A. Dsugi, T. O. M. Mohmed, and H. Y. Aboul-Enein, "Spectrofluorometric analytical applications of cyclodextrins," *Luminescence*, vol. 29, no. 1, pp. 1–7, 2014.

[13] P. Mura, "Analytical techniques for characterization of cyclodextrin complexes in aqueous solution: A review," *J. Pharm. Biomed. Anal.*, vol. 101, pp. 238–250, 2014.

[14] K. Lang, J. Mosinger, and D. M. Wagnerová, "Photophysical properties of porphyrinoid sensitizers non-covalently bound to host molecules; models for photodynamic therapy," *Coord. Chem. Rev.*, vol. 248, no. 3–4, pp. 321–350, 2004.

[15] G. Wenz, "Angew. Chem Inl. Ed Engl. 1994, 33, 803-822.pdf," 1994.

[16] M. Raynal, P. Ballester, A. Vidal-Ferran, and P. W. N. M. Van Leeuwen, "Supramolecular catalysis. Part 2: Artificial enzyme mimics," *Chem. Soc. Rev.*, vol. 43, no. 5, pp. 1734–1787, 2014.

[17] G. Crini, "Recent developments in polysaccharide-based materials used as adsorbents in wastewater treatment," *Prog. Polym. Sci.*, vol. 30, no. 1, pp. 38–70, 2005.
[18] T. Loftsson, P. Saokham, and A. R. Sá Couto, "Self-association of cyclodextrins and cyclodextrin complexes in aqueous solutions," *Int. J. Pharm.*, vol. 560, no. 5, pp. 228–234, 2019.
[19] T. Loftsson, A. Magnúsdóttir, M. Másson, and J. F. Sigurjónsdóttir, "Self-Association and Cyclodextrin Solubilization of Drugs," *J. Pharm. Sci.*, vol. 91, no. 11, pp. 2307–2316, 2002.
[20] A. Mazzaglia, M. T. Sciortino, N. Kandoth, and S. Sortino, "Cyclodextrin-based nanoconstructs for photoactivated therapies," *J. Drug Deliv. Sci. Technol.*, vol. 22, no. 3, pp. 235–242, 2012.
[21] J. Zhang and P. X. Ma, "Cyclodextrin-based supramolecular systems for drug delivery: Recent progress and future perspective," *Adv. Drug Deliv. Rev.*, vol. 65, no. 9, pp. 1215–1233, 2013.
[22] S. Farrell, D., Limaye, S.Y., Subramanian, "Silicon nanosponge particles," U. S. patent 0,251,561A1, 2006.
[23] L. Guo, G. Gao, X. Liu, and F. Liu, "Preparation and characterization of TiO2 nanosponge," *Mater. Chem. Phys.,* no. 111, pp. 322–325, 2008.
[24] G. I. Dakankov, V.A., Llyin, M.M., Tsyurupa, M.P., Timofeeva and L. V. Dubronina, "From a dissolved polystyrene coil to intramolecularly hyper cross linked nanosponges. ," *Macromo- lecules*, vol. 29, 1998.
[25] Erem Bilensoy, *Cyclodextrins in Pharmaceutics, Cosmetics, and Biomedicine: Current and Future Industrial Applications*. 2011.
[26] F. Trotta, "Cyclodextrin Nanosponges and their Applications," *Cyclodextrins Pharm. Cosmet. Biomed. Curr. Futur. Ind. Appl.*, pp. 323–342, 2011.
[27] J. Szejtli, *Cyclodextrin Technology*. s.l.:Springer Netherlands, 1988.
[28] F. Caldera, M. Tannous, R. Cavalli, M. Zanetti, and F. Trotta, "Evolution of Cyclodextrin Nanosponges," *Int. J. Pharm.*, 2017.
[29] J. Alongi, M. Pošković, A. Frache, and F. Trotta, "Novel flame retardants containing cyclodextrin nanosponges and phosphorus compounds to enhance EVA combustion properties," *Polym. Degrad. Stab.*, vol. 95, no. 10, pp. 2093–2100, 2010.
[30] S. Swaminathan, R. Cavalli, and F. Trotta, "Cyclodextrin-based nanosponges: a versatile platform for cancer nanotherapeutics development," *Wiley Interdiscip. Rev. Nanomedicine Nanobiotechnology*, vol. 8, no. 4, pp. 579–601, 2016.
[31] F. Trotta and R. Cavalli, "Characterization and application of new hyper-cross-linked cyclodextrins," *Compos. Interf.*, vol. 16, pp. 39–48, 2009.
[32] F. Trotta, C. Dianzani, F. Caldera, B. Mognetti, and R. Cavalli, "The application of nanosponges to cancer drug delivery," pp. 931–941, 2014.
[33] B. Sellergren and C. J. Allender, "Molecularly imprinted polymers: A bridge

to advanced drug delivery," *Adv. Drug Deliv. Rev.*, vol. 57, no. 12, pp. 1733–1741, 2005.
[34] G. Vasapollo *et al.*, "Molecularly imprinted polymers: Present and future prospective," *Int. J. Mol. Sci.*, vol. 12, no. 9, pp. 5908–5945, 2011.
[35] D. Bitas and V. Samanidou, "Molecularly imprinted polymers as extracting media for the chromatographic determination of antibiotics in milk," *Molecules*, vol. 23, no. 2, pp. 4–6, 2018.
[36] F. Trotta *et al.*, "Molecularly imprinted cyclodextrin nanosponges for the controlled delivery of L-DOPA: perspectives for the treatment of Parkinson's disease," *Expert Opin. Drug Deliv.*, vol. 13, no. 12, pp. 1671–1680, 2016.
[37] F. Trotta, P. Shende, and M. Biasizzo, "METHOD FOR PREPARING DEXTRIN NANOSPONGES," WO 2012/147069 Al, 2012.
[38] B. B. Mamba, R. W. Krause, T. J. Malefetse, G. Gericke, and S. P. Sithole, "Nanosponges for water purification. Clean Products and Processes 2," vol. 2, pp. 112–116, 2000.
[39] G. G. e S. P. S. B. B. Mamba, R. W. Krause, T. J. Malefetse, "Cyclodextrin nanosponges in the removal of organic matter to produce water for power generation," vol. 34, no. 5, pp. 657–660, 2008.
[40] C. Zheng, X. Huang, L. Kong, X. Li, and H. Zou, "Cross-linked beta-cyclodextrin polymer used for bilirubin removal," *Chinese J. Chromatogr.*, vol. 22, no. 2, pp. 128–130, 2004.
[41] F. Castiglione *et al.*, "Inside new materials: An experimental numerical approach for the structural elucidation of nanoporous cross-linked polymers," *J. Phys. Chem. B*, vol. 116, no. 43, pp. 13133–13140, 2012.
[42] B. Rossi *et al.*, "Networking properties of cyclodextrin-based cross-linked polymers probed by inelastic light-scattering experiments," *J. Phys. Chem. B*, vol. 116, no. 17, pp. 5323–5327, 2012.
[43] S. Berto *et al.*, "Synthesis of new ionic β-cyclodextrin polymers and characterization of their heavy metals retention," *J. Incl. Phenom. Macrocycl. Chem.*, vol. 57, no. 1–4, pp. 631–636, 2007.
[44] A. Rubin Pedrazzo *et al.*, "Eco-Friendly β -cyclodextrin and Linecaps Polymers for the Removal of Heavy Metals," *Polymers (Basel).*, pp. 1–15, 2019.
[45] V. Crupi *et al.*, "Connection between the vibrational dynamics and the cross-linking properties in cyclodextrins-based polymers," *J. Raman Spectrosc.*, vol. 44, no. 10, pp. 1457–1462, 2013.
[46] F. Trotta *et al.*, "Synthesis and characterization of a hyper-branched water-soluble β-cyclodextrin polymer," *Beilstein J. Org. Chem.*, vol. 10, pp. 2586–2593, 2014.
[47] R. K. Dolmans, D.E.; Fukumura, D.; Jain, "Photodynamic therapy for cancer," vol. 3, no. May, pp. 380–387, 2003.
[48] D. Van Straten, V. Mashayekhi, H. S. De Bruijn, S. Oliveira, and D. J.

Robinson, "Oncologic Photodynamic Therapy : Basic Principles , Current Clinical Status and Future Directions," pp. 1–54, 2017.
[49] R. Diamond, I.; Granelli, S.G.; McDonagh, A.F.; Nielsen, S.; Wilson, C.B.; Jaenicke, "Photodynamic therapy of malignant tumours," *Lancet*, pp. 1175–1177, 1972.
[50] T. J. Dougherty, G. B. Grindey, R. Fiel, K. R. Weishaupt, and D. G. Boyle, "Photoradiation Therapy . II . Cure of Animal Tumors With Hematoporphyrin and Light," vol. 55, no. I, 1974.
[51] W. Henderson and J. Dougherty, "HOW DOES PHOTODYNAMIC THERAPY WORK ?," vol. 55, no. 1, pp. 145–157, 1992.
[52] C. S. FOOT, "Definition of Type I and Type I1," vol. 54, no. 5, p. 8655191, 1991.
[53] J. MOAN and K. BERG, "the Photodegradation of Porphyrins in Cells Can Be Used To Estimate the Lifetime of Singlet Oxygen," *Photochem. Photobiol.*, vol. 53, no. 4, pp. 549–553, 1991.
[54] et al. Agostinis P, Berg K, Cengel K., "Photodynamic Therapy of Cancer: An Update," *Ca Cancer J Clin*, vol. 61, no. April, pp. 250–281, 2017.
[55] Z. Meng, W. Hou, H. Zhou, L. Zhou, H. Chen, and C. Wu, "Therapeutic Considerations and Conjugated Polymer-Based Photosensitizers for Photodynamic Therapy," *Macromol. Rapid Commun.*, vol. 39, no. 5, pp. 1–15, 2018.
[56] S. Mallidi, S. Anbil, A. L. Bulin, G. Obaid, M. Ichikawa, and T. Hasan, "Beyond the barriers of light penetration: Strategies, perspectives and possibilities for photodynamic therapy," *Theranostics*, vol. 6, no. 13, pp. 2458–2487, 2016.
[57] J. M. Dąbrowski *et al.*, *Engineering of relevant photodynamic processes through structural modifications of metallotetrapyrrolic photosensitizers*, vol. 325, no. September. 2016.
[58] A. Kamkaew, F. Chen, Y. Zhan, R. L. Majewski, and W. Cai, "Scintillating Nanoparticles as Energy Mediators for Enhanced Photodynamic Therapy," *ACS Nano*, vol. 10, no. 4, pp. 3918–3935, 2016.
[59] A. B. Ormond and H. S. Freeman, "Dye sensitizers for photodynamic therapy," *Materials (Basel).*, vol. 6, no. 3, pp. 817–840, 2013.
[60] T. J. Dougherty *et al.*, "Photodynamic therapy," *Natl. Cancer Inst.*, vol. 90, no. 1, p. 889, 1998.
[61] T. Nann, "Nanoparticles in photodynamic therapy," *Nano Biomed. Eng.*, vol. 3, no. 2, pp. 137–143, 2011.
[62] G. Blasse, "Scintillator Materials," *Chem. Mater*, vol. 6, p. 1465– 1475, 1994.
[63] M. Nikl, "Scintillation detectors for x-rays," *Meas. Sci. Technol.*, vol. 17, no. 4, 2006.
[64] L. Serpe *et al.*, "Squaraines bearing halogenated moieties as anticancer photosensitizers: Synthesis, characterization and biological evaluation,"

Eur. J. Med. Chem., vol. 113, pp. 187–197, 2016.
[65] W. Ziegenbein and H. -E Sprenger, "Condensation Products of Squaric Acid and Azulenic Hydrocarbons," *Angew. Chemie Int. Ed. English*, vol. 5, no. 10, pp. 893–894, 1966.
[66] D. Ramaiah, I. Eckert, K. T. Arun, L. Weidenfeller, and B. Epe, "Squaraine Dyes for Photodynamic Therapy : Study of Their Cytotoxicity and Genotoxicity in Bacteria and Mammalian Cells { à," vol. 76, no. 6, pp. 672–677, 2002.
[67] V. Monge-Fuentes, L. A. Muehlmann, and R. B. de Azevedo, "Perspectives on the application of nanotechnology in photodynamic therapy for the treatment of melanoma.," *Nano Rev.*, vol. 5, p. 24381, 2014.
[68] J. M. Burns *et al.*, "Methods for reactive oxygen species (ROS) detection in aqueous environments," *Aquat. Sci.*, vol. 74, no. 4, pp. 683–734, 2012.
[69] L. Takacs, "The historical development of mechanochemistry," *Chem. Soc. Rev.*, vol. 42, no. 18, pp. 7649–7659, 2013.
[70] S. L. James *et al.*, "Mechanochemistry: opportunities for new and cleaner synthesis," *Chem. Soc. Rev.*, vol. 41, no. 1, pp. 413–447, 2012.
[71] A. D. McNaught and A. Wilkinson, *IUPAC Compendium of Chemical Terminology*, 2nd ed. (t. Oxford: Blackwell Scientific Publications, 1997.
[72] A. J. Lynch and C. A. Rowland, *The History of Grinding*. Society of Mining, Metallurgy and Exploration, Inc., 2005.
[73] M. Faraday, "Arts," *Q. J. Sci., Lit.*, vol. 8, p. 374, 1820.
[74] J. Johnston and L. H. Adams, ".," *Am. J. Sci.*, vol. 4, no. 35, p. 205, 1913.
[75] A. Ling and J. L. Baker, "Tran.," *J. Chem. Soc.*, vol. 63, p. 1814, 1893.
[76] W. Spring, "Fr.," *Bull. Soc. Chim.*, vol. 44, p. 166, 1885.
[77] L. Takacs, "The historical development of mechanochemistry," *Chem. Soc. Rev.*, vol. 42, no. 18, pp. 7649–7659, 2013.
[78] N. Willis-Fox, E. Rognin, T. A. Aljohani, and R. Daly, "Polymer Mechanochemistry: Manufacturing Is Now a Force to Be Reckoned With," *Chem*, pp. 1–39, 2018.
[79] A. Gilet *et al.*, "Unconventional media and technologies for starch etherification and esterification," *Green Chem.*, vol. 20, no. 6, pp. 1152–1168, 2018.
[80] T. Gan *et al.*, "Esterification of bagasse cellulose with metal salts as efficient catalyst in mechanical activation-assisted solid phase reaction system," *Cellulose*, vol. 24, no. 12, pp. 5371–5387, 2017.
[81] C. F. Burmeister and A. Kwade, "Process engineering with planetary ball millss," *Chem. Soc. Rev.*, vol. 42, no. 18, pp. 7660–7667, 2013.
[82] J. Andersen and J. Mack, "Mechanochemistry and organic synthesis: From mystical to practical," *Green Chem.*, vol. 20, no. 7, pp. 1435–1443, 2018.
[83] F. Fischer, K. J. Wenzel, K. Rademann, and F. Emmerling, "Quantitative determination of activation energies in mechanochemical reactions," *Phys. Chem. Chem. Phys.*, vol. 18, no. 33, pp. 23320–23325, 2016.

[84] L. Jicsinszky, M. Caporaso, E. C. Gaudino, C. Giovannoli, G. Cravotto, and B. Martel, "Synthesis of randomly substituted anionic cyclodextrins in ball milling," *Molecules*, vol. 22, no. 3, pp. 1–16, 2017.
[85] L. Jicsinszky, K. Tuza, G. Cravotto, A. Porcheddu, F. Delogu, and E. Colacino, "Influence of the milling parameters on the nucleophilic substitution reaction of activated β -cyclodextrins," pp. 1893–1899, 2017.
[86] G. Cravotto, M. Caporaso, L. Jicsinszky, and K. Martina, "Enabling technologies and green processes in cyclodextrin chemistry," *Beilstein J. Org. Chem.*, vol. 12, pp. 278–294, 2016.
[87] M. A. Castriciano *et al.*, "Poly(carboxylic acid)-Cyclodextrin/Anionic Porphyrin Finished Fabrics as Photosensitizer Releasers for Antimicrobial Photodynamic Therapy," *Biomacromolecules*, vol. 18, no. 4, pp. 1134–1144, 2017.
[88] A. Scala, A. Piperno, G. Grassi, L. M. Scolaro, and A. Mazzaglia, "Nanoconstructs Based on Cyclodextrins for Antimicrobial Applications," *RSC Adv.*, no. 1, pp. 229–244, 2017.
[89] F. Trotta, M. Zanetti, and R. Cavalli, "Cyclodextrin-based nanosponges as drug carriers," *Beilstein J. Org. Chem.*, vol. 8, pp. 2091–2099, 2012.
[90] N. Barbero *et al.*, "Microwave-Assisted Synthesis of Near-Infrared Fluorescent Indole- Based Squaraines," 2015.
[91] N. Barbero, S. Visentin, and G. Viscardi, "Journal of Photochemistry and Photobiology A : Chemistry The different kinetic behavior of two potential photosensitizers for PDT," *"Journal Photochem. Photobiol. A Chem.*, vol. 299, pp. 38–43, 2015.
[92] M. Zanetti *et al.*, "Microporous and Mesoporous Materials Micro porous carbon spheres from cyclodextrin nanosponges," *Microporous Mesoporous Mater.*, vol. 235, pp. 178–184, 2016.
[93] R. W. O'Brien, B. R. Midmore, A. Lamb, and R. J. Hunter, "Electroacoustic studies of moderately concentrated colloidal suspensions," *Faraday Discuss. Chem. Soc.*, vol. 90, pp. 301–312, 1990.
[94] F. A. Villamena and J. L. Zweier, "Detection of Reactive Oxygen and Nitrogen Species by EPR Spin Trapping," *Antioxid. Redox Signal.*, vol. 6, no. 3, pp. 619–629, 2004.
[95] J. W. Paul Anastas, *Green Chemistry: Theory and Practice*. 1998.
[96] T. Ogoshi and A. Harada, "Chemical sensors based on cyclodextrin derivatives," *Sensors*, vol. 8, no. 8, pp. 4961–4982, 2008.
[97] T. Kuwabara, H. Nakajima, M. Nanasawa, and A. Ueno, "Color change indicators for molecules using methyl red-modified cyclodextrins," *Anal. Chem.*, vol. 71, no. 14, pp. 2844–2849, 1999.
[98] Z. A. Fayad *et al.*, "Synthesis of Polymer–Lipid Nanoparticles for Image-Guided Delivery of Dual Modality Therapy," *Bioconjug. Chem.*, vol. 24, no. 9, pp. 1429–1434, 2013.
[99] M. Becuwe, D. Landy, F. Delattre, F. Cazier, and S. Fourmentin,

"Fluorescent indolizine-β-cyclodextrin derivatives for the detection of Volatile Organic Compounds," *Sensors*, vol. 8, no. 6, pp. 3689–3705, 2008.

[100] J. Huang *et al.*, "Fluorescently Labeled Cyclodextrin Derivatives as Exogenous Markers for Real-Time Transcutaneous Measurement of Renal Function," *Bioconjug. Chem.*, vol. 27, no. 10, pp. 2513–2526, 2016.

[101] W. V., P. TK, and M. N., "Nanopharmaceuticals (part 1): products on the market," *Int. J. nanomedicine.*, vol. 9, pp. 4357–4373, 2014.

[102] S. K. Hobbs *et al.*, "Regulation of transport pathways in tumor vessels: Role of tumor type and microenvironment," *Proc. Natl. Acad. Sci. U. S. A.*, vol. 95, no. 8, pp. 4607–4612, 1998.

[103] F. Alexis, E. Pridgen, L. K. Molnar, and O. C. Farokhzad, "Factors affecting the clearance and biodistribution of polymeric nanoparticles," *Mol. Pharm.*, vol. 5, no. 4, pp. 505–515, 2008.

[104] J. S. Suka, Q. Xua, N. Kima, J. Hanesa, and L. M. Ensign, "PEGylation as a strategy for improving nanoparticle-based drug and gene delivery," *Adv Drug Deliv Rev.*, no. 399, pp. 28–51, 2017.

[105] A. Narmani *et al.*, "Folic acid functionalized nanoparticles as pharmaceutical carriers in drug delivery systems," *Drug Dev. Res.*, vol. 80, no. 4, pp. 404–424, 2019.

[106] H. S. Yoo and T. G. Park, "Folate receptor targeted biodegradable polymeric doxorubicin micelles," *J. Control. Release*, vol. 96, no. 2, pp. 273–283, 2004.

[107] H. A. Staab, "New Methods of Preparative Organic Chemistry IV. Syntheses Using Heterocyclic Amides (Azolides)," vol. 1, no. 7, pp. 351–367, 1962.

[108] F. Trotta, G. Moraglio, M. Marzona, and S. Maritano, "Acylic carbonates of beta-cyclodextrin," *Gazz. Chim. Ital.*, vol. 123, 1993.

[109] S. A. Jadhav, S. D. Karande, and S. H. Burungale, "Facile synthesis of β-cyclodextrin-grafted solid silica nanoparticles," *Mater. Des. Process. Commun.*, vol. 1, no. 4, pp. 1–5, 2019.

[110] Q. Xu *et al.*, "Impact of Surface Polyethylene Glycol (PEG) Density on Biodegradable Nanoparticle Transport in Mucus ex Vivo and Distribution in Vivo," *ACS Nano*, vol. 9, no. 9, pp. 9217–9227, 2015.

[111] Y. Song, A. Feng, Z. Liu, and D. Li, "Zeta potentials of PDMS surfaces modified with poly(ethylene glycol) by physisorption," *Electrophoresis*, pp. 1–8, 2019.

[112] A. Vora, A. Riga, D. Dollimore, and K. S. Alexander, "Thermal stability of folic acid," *Thermochim. Acta*, vol. 392–393, pp. 209–220, 2002.

Appendix

Publications

Fioravanti, A.; Morandi, S.; RUBIN PEDRAZZO, A.; Bracco, P.; Zanetti, M.; Manzoli, M.; Mazzocchi, M.; Carotta, M.C. Ultrasensitive Gas Sensors Based on Electrospun TiO_2 and ZnO. *Proceedings* 2017, 1, 485

Caldera F., RUBIN PEDRAZZO A., Anceschi A., Zanetti M., Trotta F. "Nanospugne di ciclodestrine" *LA CHIMICA E L'INDUSTRIA* 2017, N° 6

Shohreh P, Fabrizio C, ALBERTO RUBIN PEDRAZZO, Nilesh Kumar D. Smart Cyclodextrin-Based Drug Delivery Systems: StimuliResponsiveness and Controlled Release. *Biomed J Sci&Tech* Res 9(5)-2018. BJSTR. MS.ID.001850. DOI:10.26717/ BJSTR.2018.09.001850.

Francesco Trotta, ALBERTO RUBIN PEDRAZZO, et al. "Metal Organic Frameworks in Medicine". *Acta Scientific Pharmaceutical Sciences* 3.4 (2019): 107-109.

Dhakar, N.K., Caldera, F., Bessone, F., Cecone, C., RUBIN PEDRAZZO A., Cavalli, R., Dianzani, C., Trotta, F. "Evaluation of solubility enhancement, antioxidant activity, and cytotoxicity studies of kynurenic acid loaded cyclodextrin nanosponge" *Carbohydrate Polymers*, 224,(2019),115168. DOI:/10.1016/j.carbpol.2019.115168

RUBIN PEDRAZZO A., Smarra, A., Caldera, F., Musso, G., Dhakar, N.K., Cecone, C., Corsi, I., Trotta, F. "Eco-friendly β-cyclodextrin and linecaps polymers for the removal of heavy metals". *Polymers* 2019

Patent

ALBERTO RUBIN PEDRAZZO, Francesco Trotta– "Processo per la preparazione di una Nanospugna" – P021499IT-01

Posters

"*Dextrin-based nanosponges for the removal of metal contaminants in wastewaters*" – Alessandra Smarra, ALBERTO RUBIN PEDRAZZO, Fabrizio Caldera, Claudio Cecone, Francesco Trotta – MIPOL2017– Milano, Italy 15-16th February 2017

"*Influence of the polymer on both morphology and microstructure of nanosized SnO_2 prepared by electrospinning*" – ALBERTO RUBIN PEDRAZZO, Claudio Cecone, Sara Morandi, Maela Manzoli, Marco Zanetti, Pierangiola Bracco – EUPOC 2019 – COMO (ITALY), 12-16 May 2019

"*Mechanochemical synthesis of hyper-crosslinked Cyclodextrin Polymers* " – ALBERTO RUBIN PEDRAZZO, Fabrizio Caldera, Claudio Cecone and Francesco Trotta – 6*th European Conference on Cyclodextrins* – Santiago de Compostela – 2 – 4 Ottobre 2019

"*NADES as a suitable reactive media for the synthesis of βcyclodextrin based polymers*" – Claudio Cecone, Gjylije Hoti, ALBERTO RUBIN PEDRAZZO, Fabrizio Caldera, Marco Zanetti, Pierangiola Bracco, Francesco Trotta– 6*th European Conference on Cyclodextrins* – Santiago de Compostela – 2 – 4 Ottobre 2019

"*Novel Photosensitizers based on cyclodextrin nanosponges and cationic porphyrins*" – Roberto Zagami, ALBERTO RUBIN PEDRAZZO, Fabrizio Caldera, Francesco Trotta, Antonino Mazzaglia – 6*th European Conference on Cyclodextrins* – Santiago de Compostela – 2 – 4 Ottobre 2019

Conferences

[Poster Presenter] MiPOL - Milano Polymer Days – Milano, Italia 15-16th Febbraio 2017

Il Trasferimento Tecnologico: un'opportunità per l'evoluzione della propria ricerca - Cavallerizza Reale, Torino, Italia – 23 Novembre 2017

5th European Conference on Cyclodextrins – Lisbona, Portogallo – 3 - 6 Ottobre 2017

2nd International Congress "Advances in the Packaging Industry - Product and Process" - Ottobre 26 - 27, 2017

International workshop NO-CANCER 2017 - Novara (Italia) Ottobre 29-30, 2017

UNITO-POLITO CONFERENCE SERIES IN CANCER Imaging of Cancer Dynamics – Torino, Italia - Marzo 7-9, 2018

Giornate Italo-Francesi di Chimica – Genova, Italia - 16 – 18 Aprile 2018

NIS Colloquium - Torino, Italia – 20 Luglio 2018

[Poster Presenter] EUPOC 2019 – Como, Italy, 12-16 May 2019

[Poster Presenter] 6*th European Conference on Cyclodextrins* – Santiago de Compostela – 2 – 4 Ottobre 2019

I did the right thing, didn't I? It all worked out in the end.

"In the end"? Nothing ends. Nothing ever ends.